The Effective Communication of Brain Network Dynamics Under Different States

Josefina Cruzat Grand

DOCTORAL THESIS UPF / 2020

Thesis Supervisors

Prof. Dr. Gustavo Deco & Assoc. Prof. Rodrigo Rocamora

Department of Information and Communication Technologies

AGRADECIMIENTOS

"If I have seen further it is by standing on the shoulders of giants"

—Isaac Newton, The Correspondence of Isaac Newton (1643–1727)

El doctorado me cambió la vida—y juro que no exagero.

Esta tesis es el fruto de casi cinco años de trabajo y dedicación. Probablemente sean los años más felices que he vivido, y soy consciente de que fue así sólo gracias al amor y al apoyo que recibí de parte de la maravillosa gente que me rodea.

Dicen que el que da, no debe acordarse; pero el que recibe nunca debe olvidar. A ti Gustavo Deco, jamás te olvidaré. No sólo has sido un tremendo supervisor, sino también un gran amigo y sin duda mi mejor ejemplo. Para ti sólo tengo palabras de elogio, gratitud y admiración. Gracias por creer en mí, por todo lo que me has enseñado y ayudado, gracias por tu entrega, por tu voluntad de oro, por cada conversación y porque si soy mejor persona, también te lo debo a ti.

Gracias Morten L. Kringelbach por ser un magnífico supervisor, colaborador y amigo. Gracias por tu cariño, cuidado, preocupación, lealtad, paciencia y entrega. Jamás olvidaré cada una de las

conversaciones que tuvimos respecto del amor y aquellas en que junto a Gustavo resolvían el cerebro una vez más. Gracias por darme la oportunidad de realizar una estancia en tu laboratorio en Oxford y regalarme la maravillosa experiencia de vivir ahí.

Agradezco de corazón a Albert Costa, quien fue también un gran supervisor, colaborador y amigo. Me siento tremendamente honrada de haberlo conocido y de haber tenido la suerte de aprender de él. Lamentamos profundamente su partida en 2018, pero atesoro en el alma los lindos recuerdos que nos dejó, en especial las conversaciones post-pádel que compartimos junto con Gustavo y Andrea Polo ¡Que manera de aprender y disfrutar!

Muchas gracias, Salvador Soto-Faraco, has sido un gran supervisor y cercano amigo. Gracias por dejarme explorar contigo el maravilloso y enigmático mundo de la memoria. Al final, eso es lo que somos, un conjunto de memorias. Que sepas que en la mía—aunque cambiante, quimérica, imprecisa e infiel—siempre vas a estar.

Gracias Rodrigo Rocamora por supervisar mi trabajo y por abrirme las puertas de la Unidad de Epilepsia del Hospital del Mar. Gracias a ti, a tu equipo y a los pacientes de la unidad, pude llevar a cabo con éxito mi primer estudio.

Infinita gratitud a Cristina Cuadrado, Pamela Miller, Silvia Blanch y Xavier Mayoral, por su cuidado trabajo y ayuda. Gracias por siempre mostrar buena disposición y por dejarme ganar—poquito a poquito—un espacio en su corazón.

Con profunda admiración y cariño agradezco a Adrià Tauste-Campo, Manuela Ruzzoli y Mireia Torralba. Gracias por las discusiones, orientación, su tiempo y dedicación por el trabajo que llevamos adelante juntos. Con su ayuda todo parecía más fácil.

A los grandes amigos que me regaló la ciencia, quienes diluyeron la frontera entre la vida personal y la profesional. Gracias Alexandre Hyafil, Ana Martín, Ramón Nogueira, Joao Barbosa, Heike Stein, Marc Lluis Vives, Vicente Pallarés, Joana Cabral, Tobias Hauser, Teresa Zapata y Myriel Lopez ¡Con ustedes cerca, todo es mucho mejor! Gracias por el sin fin de conversaciones, risas y asados. Por la complicidad, cariño y apoyo. Los admiro con el alma, los quiero infinito y espero tenerlos cerca siempre.

A mis queridos Silvana Silva, Ernest Montbrió, Gabriela Mochol, David Liley, Klaus Wimmer, Carlos Gaudari, Patricio Donnelly, Alice Fourcat, Miguel Burgaleta e Iñigo Arandia por su amistad y por que su ejemplo ha quedado marcado en mi hoja de ruta. Gracias también a todos quienes forman o han formado parte del grupo CNS: Adrian Ponce, Selen Atasoy, Gorka Zamora, Mathieu Gilson, Nikos Kouvaris, Andrea Insabato, Mario Pannunzi, Ignasi Cos, Raphael Kaplan, Ana Sanjuan, Ruggero Bettinardi, Katharina Glomb, Beatriz Jobst, Victor Saenger, Jessica de Santiago, Katerina Capouskova, Eleonora de Filippi, Anira Escrichs, Ane Lopez, Laura Ulysse, David Blair, Manel Vila-Vidal, Federico Devalle y José María Esnaola.

Agradezco a quienes conforman la maravillosa comunidad BARCCSYN, en especial a Rubén Moreno-Bote, Alex Roxin, Jaime de la Rocha, Albert Compte, Genis Prat, Maria Alemany y Ainhoa Hermoso, entre otros. Por impulsar, apoyar y brindar un espacio a todos quienes nos dedicamos a la neurociencia computacional en Barcelona. Gracias por la posibilidad de participar en el retreat de los años 2015, 2016 y 2017.

Gracias a todos quienes hicieron posible mi asistencia al Cognitive and Computational Neuroscience Summer School, 2016; Brain, Minds and Machines Summer School, 2017; Radboud Summer School, 2019; Barcelona Summer School for Advanced Modeling of

Behavior, 2019; y a los intercambios realizados en Oxford University, Harvard University y University California Los Angeles.

Quiero agradecer a mis amigas de corazón Paula Délano, Trinidad Hagemann, Isabel Ruiz, María Paz Ramírez, Elisa García de la Huerta, Carola Vergara y María José Albarrán por compartir esta aventura conmigo y hacerse presente en todo momento a pesar de la distancia.

A mis amigos Beatriz Fabres y Martín Fruns quienes sin terminar de entender del todo a que me dedicaba, siempre tuve cerca como hermanos y fueron parte fundamental de este maravilloso viaje.

A ti Laura Greene, mi amiga del alma. Gracias por tu cariño y lealtad. Por tu entrega y bondad que superan todos los límites imaginables. Gracias porque has estado muy cerca en todo momento. Gracias por acompañarme, escucharme, no juzgarme, siempre intentar entender y empatizar con lo que me pasa. Gracias por alegrarte con mis logros y por alentarme en la dificultad. No imagino cómo sería la vida sin una amiga como tú.

Agradezco a mis hermanos Francisca y Tomás, a quienes quiero y admiro profundamente, porque con el ímpetu con que han buscado sus sueños, han inspirado también la búsqueda de los míos. Y agradezco a la preciosa Vinka que llegó para unirnos en su amor.

Finalmente—y con especial dedicación—agradezco a mis padres, Nicole y Gastón, por darme la vida, por la dedicación y esfuerzo que pusieron en mi educación, por darme siempre total libertad, por apoyarme en todo, por creer en mí, y por favorecer por todos los medios que haga todo lo que me hace feliz.

Por que es de buen nacido, ser agradecido—infinitas gracias a todos.

To Nicole, Gastón, Gustavo

and in loving memory of Albert

ABSTRACT

Cognitive processing requires to flexibly combine information from functionally specialized neural processes that are widely distributed throughout the brain. Neuroimaging studies have consistently reported that functional network configurations are governed by two fundamental principles of brain organization: functional segregation and integration. Yet, the mechanisms underlying the dynamic network reorganization are not well understood. In this work, we present evidence for two mechanisms through which the dynamic system-level integration is modulated. On the one hand, the large-scale brain organization is mediated by transient changes in phase-synchronization, facilitating global information flow between distant cortical areas as proposed by the "Communication Through Coherence" (CTC) theory. And in the other, it is mediated by the ascending neuromodulatory system. Neuromodulators constrain local processes by selectively changing the balance of the excitation and inhibition of individual brain regions.

RESUMEN

El procesamiento cognitivo requiere combinar de manera flexible la información de procesos neuronales funcionalmente especializados que están ampliamente distribuidos por todo el cerebro. Los estudios de neuroimagen han informado consistentemente que las configuraciones de red funcional se rigen por dos principios fundamentales de la organización del cerebro: segregación funcional e integración. Sin embargo, los mecanismos subyacentes a la reorganización dinámica de la red aún no son bien comprendidos. En este trabajo, presentamos evidencia en soporte de dos mecanismos a través de los cuales se modula la integración dinámica a nivel de sistema. Por un lado, la organización del cerebro a gran escala está mediada por cambios transitorios en la sincronización de fases, lo que facilita el flujo de información global entre áreas corticales distantes como lo propone la teoría de "comunicación a través de la coherencia" (CTC). Y por otro, está mediada por el sistema neuromodulador ascendente. Los neuromoduladores restringen los procesos locales al cambiar selectivamente el equilibrio de la excitación e inhibición de las regiones cerebrales individuales.

PREFACE

"If the brain were simple enough for us to understand it, we would be too simple to understand it".

—Emerson M. Pugh (1938)

Understanding how the human mind emerges from the functional organization of the brain remains one of the greatest intellectual challenges of our times. The brain is arguably the most complex system in the universe. It contains around 100 billion neurons—*more than the number of stars in the Milky Way*—which are connected by ~100 trillion synapses anatomically organized over multiple scales. Despite having a fixed anatomy characterized by its connectome[1], the

[1] The complete map of the neural connections within a brain.

brain network structure has the ability to dynamically and adaptively reconfigure giving rise to complex cognition and a wide range of behavior. Over the last decades, the dynamical system approach to the brain has become a crucial tool for explaining how cognition emerges from the intricate interaction between multiple structural and functional levels. Dynamical systems exhibit emergent behavior in that their collective behavior has novel properties that differ quantitatively and qualitatively from their simplest components and, therefore, represent more than the sum of their parts at all possible levels. In virtue of understanding cognitive processes as an emergent property of neurons and their connections, this thesis brings new insights into the brain's underlying organizational principles and mechanisms governing the interaction of cortical regions.

This dissertation comprises five chapters: In Chapter 1, we will introduce the two principles governing brain function, namely integration and segregation, in support of the view of brain function as a global rather than a local phenomenon. We will provide insights into phase synchronization as a mechanism responsible for large-scale integration, and we will further review current research regarding the influence of the neuromodulatory system on the functional level. Additionally, we will argue in favor of whole-brain computational modeling as a remarkable tool for mechanistically explaining the properties of brain structure and neuronal dynamics observed from neuroimaging data. In Chapters 2 and 3, we will show new insights into the neural activity patterns and functional network architecture associated with cognitive processing. In Chapter 4, we will introduce a whole-brain model of the dynamic brain activity under the effects of LSD—which integrates a receptor map of serotonin distribution—as a new approach to understand experimental manipulations of the neuromodulatory system. Finally, in Chapter 5, we will present a general overview of the main results, recognize some limitations of the studies, and address future perspectives.

The study presented in **Chapter 2** is published in:

Cruzat, J., Deco, G., Tauste-Campo, A., Principe, A., Costa, A., Kringelbach, M. L., & Rocamora, R. (2018). The dynamics of human cognition: Increasing global integration coupled with decreasing segregation found using iEEG. *NeuroImage*, *172*, 492-505.

Link: https://doi.org/10.1016/j.neuroimage.2018.01.064

Work presented in **Chapter 3** is published in:

Deco, G., Cruzat, J., Cabral, J., Knudsen, G. M., Carhart-Harris, R. L., Whybrow, P. C., Logothetis, N. K., & Kringelbach, M. L. (2018). Whole-brain multimodal neuroimaging model using serotonin receptor maps explains non-linear functional effects of LSD. *Current biology*, *28*(19), 3065-3074.

Link: https://doi.org/10.1016/j.cub.2018.07.083

The contents of **Chapter 4** reflect a paper currently under review in *Neuropsychology* under:

Cruzat, J., Torralba, M., Ruzzoli, M., Fernández, A., Deco, G., Soto-Faraco, S. (2020) The phase of Theta oscillations modulates successful memory formation at encoding.

The main results of two additional studies conducted in the context of this dissertation are presented in **Chapter 5**, and have been published as detailed below:

Deco, G., Cruzat, J., Cabral, J., Tagliazucchi, E., Laufs, H., Logothetis, N. K., & Kringelbach, M. L. (2019). Awakening:

Predicting external stimulation to force transitions between different brain states. *Proceedings of the National Academy of Sciences*, *116*(36), 18088-18097.

Link: https://doi.org/10.1073/pnas.1905534116

Deco, G., Cruzat, J., & Kringelbach, M. L. (2019). Brain songs framework used for discovering the relevant timescale of the human brain. *Nature communications*, *10*(1), 1-13.

Link: https://doi.org/10.1038/s41467-018-08186-7

Kringelbach, M. L., Cruzat, J., Cabral, J., Knudsen, G. M., Carhart-Harris, R. L., Whybrow, P. C., Logothetis, N. K., & Deco, G. (2020) Dynamic coupling of Whole-Brain Neuronal and Neurotransmitter Systems. *Proceedings of the National Academy of Sciences*.

Link: https://doi.org/10.1073/pnas.1921475117

CONTENTS

LIST OF FIGURES

CHAPTER 1

Introduction

"The essence of knowledge is, having it, to apply it"

—Confucius (551–478 BC)

For more than a century, there was a tendency to attribute cognitive functions to the remote operations of individual brain areas. However, the weight of evidence shifted in favor of the view that cognition emerges from the dynamic interaction of broadly distributed brain regions operating collectively on large-scale networks (Mountcastle, 1978; Mesulam, 1990; Bressler, 1995; McIntosh, 2000; Sporns et al., 2004). The historical roots of this view can be traced to the pioneering work done by Carl Wernicke in the 19th century. Wernicke first observed specific behavioral impairment following focal brain lesions and realized that the attribution of a brain function to a cortical area was related to its anatomical connectivity with distant brain regions (Wernicke, 1874).

As a result of the shift to this new paradigm, neuroscience has increasingly adopted tools and concepts from network science (i.e., graph theory, dynamical systems) to characterize the operation of sets of brain regions (Fox et al., 2005; Power et al., 2011). Essentially, all network models represent the brain as a set of nodes, which correspond to the brain areas, with edges or links representing the pairwise connectivity between nodes. Of particular challenge, is the fact that the brain is spatially organized in a multiscale level, meaning that networks can be validly defined at the microscale level of neurons and synapses, the mesoscale level of neuronal populations and axons, and the macroscale level of brain regions and neuronal fibers (see Figure 1.1). Within the context of this work, in the following, we will focus on networks at the macroscopic scale.

Large-scale brain networks can be defined based on their structural topology or functional dynamics. On the one hand, the *structural connectivity* (SC) refers to the white matter fiber tracts physically connecting different brain regions, the description of which has been coined as the human connectome (Sporns, Tononi and Kötter, 2005; Hagmann, 2005). In human neuroimaging studies, SC is commonly measured using diffusion-weighted imaging (DWI) methods, such as diffusion tensor imaging (DTI) and diffusion spectrum imaging (DSI). On the other hand, the *functional connectivity* (FC) indicates that a set of brain regions are functionally related to one another. Operationally, the FC is defined as the temporal pattern of statistical dependence among neuronal time series from different voxels or brain areas, determined by Pearson correlations, phase synchronization, covariance, mutual information or, causality measures (Friston, 1994; Stephan and Friston, 2009). In most current applications, brain activity is measured on several timescales and with varying degrees of spatial precision, using methods such as electroencephalography (EEG), magnetoencephalography (MEG), functional magnetic resonance imaging (fMRI) and positron emission tomography (PET). The whole set of functional connections

between all pairs of brain regions describes the functional brain network. It is reasonable to assume that if two separate brain regions show correlated activity, they are involved in the same functional processing and, therefore, integrate information. For this reason, analyzing the topological organization of the functional brain networks yields crucial insights into global brain function.

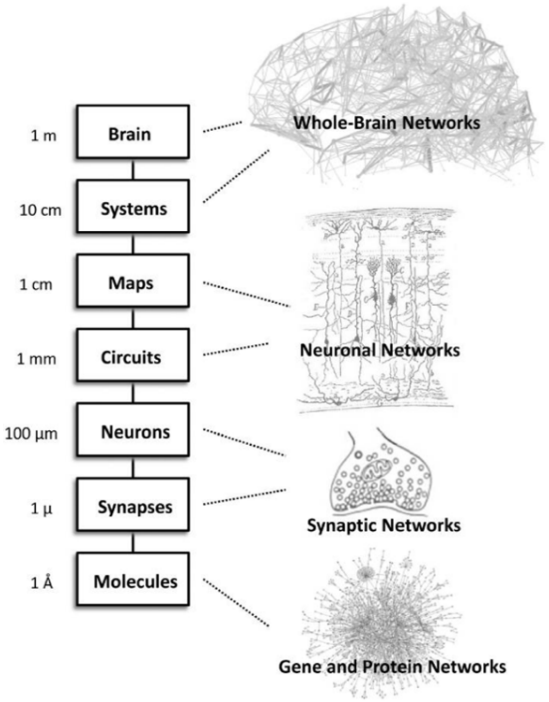

Figure 1.1 Schematic representation of the organization of the structural levels of the central nervous system (CNS).

The hierarchical structural organization of the CNS varies over many orders of magnitude, from molecular dimensions measured in angstroms to fiber tracts that span centimeters. In the context of this work, we focus on the levels of maps and systems. Illustration reproduced from (Petersen and Sporns, 2015).

Importantly, considerable efforts have been set to determine the complex synergy between the resulting (relatively stable) structural and (highly dynamic) functional networks (Bullmore and Sporns, 2009; Honey et al., 2009). In this regard, Hae-Jeong Park and Karl Friston (Park and Friston, 2013) wrote that,

> *"The human brain presents a puzzling and challenging paradox: Despite a fixed anatomy, characterized by its connectivity, its functional repertoire is vast, enabling action, perception, and cognition […] The resolution of this paradox may reside in the brain's network architecture, which organizes local interactions to cope with diverse environmental demands—ensuring adaptability, robustness, resilience to damage, efficient message passing, and diverse functionality from a fixed structure".*

The divergence between structure and function allows non-overlapping functional network configurations that are governed by two fundamental principles of brain organization: *functional segregation* and *integration* (Tononi, Sporns and Edelman, 1994; Fox and Friston, 2012; Bullmore and Sporns, 2009; Deco et al., 2015). The segregation principle refers to the functional processes that engage localized and specialized brain regions. By contrast, the integration principle highlights the relevance of the interactions among distributed brain regions in the emergence of brain function.

Natural questions then arise about, how cognitive processing modulates the level of integration and segregation of information in human brain networks? How networks dynamically reorganize to allow broad communication between many different brain regions in

order to integrate information? And, what are the underlying dynamics and possible mechanisms facilitating this information routing? The research work presented in this thesis will address these issues using novel methods combined with human iEEG, EEG, fMRI, and behavioral data, together with computational whole-brain modeling.

The upcoming sections provide a brief overview of four key concepts in the context of this work: 1) the segregation and integration principles, 2) insights into phase synchronization as a possible mechanism for integration, 3) the neuromodulatory influence on integration and 4) the potential of computational whole-brain modeling to provide possible mechanistic explanations on the modulation of whole-brain dynamics.

Integration and Segregation in the Brain

Complex cognition and adaptive behavior require combining incoming environmental information with internal representations from past experiences. How does the brain flexibly orchestrate information from functionally specialized neural processes that are widely distributed throughout the brain? The general hypothesis is that the two fundamental principles of large-scale brain organization, namely, integration and segregation, compensates for the distributed nature of its anatomical and functional organization (Dehaene, Kerszberg and Changeux, 1998; Bressler and Kelso, 2001; Deco et al., 2015; Cohen and D'Esposito, 2016).

The balance between integration and segregation in the brain is crucial for cognitive function. Recent modeling work has

demonstrated that the trade-off between functional specialization and global communication is manifested through transient changes in correlated patterns of neural activity that are constrained by the almost invariant structural connectome (Deco, Jirsa and McIntosh, 2013; Honey et al., 2007). This balance represents the interplay between the microscale dynamics that govern local neuronal activity, and the macroscale dynamics describing the interaction among distant neuronal populations (Varela et al., 2001; Bressler and Tognoli, 2006). Segregation refers to the process in which densely connected network communities are arranged within modules, with statistical dependence of neural signals among them, and statistical independence across them (Tononi, Sporns and Edelman, 1994; Sporns 2013). Conversely, by quantifying the connectivity level across the brain, the functional integration denotes the ability of the network to integrate distributed and functionally specialized submodules in order to facilitate global communication (Figure 1.2). Importantly, these principles are complementary: a global increase in integration will lead to a decrease in segregation.

Intrinsic and task-evoked interactions between different brain areas are crucial to understanding brain integration (Friston, 2011; Cole et al., 2014; Deco and Kringelbach, 2017). Existing research has proven that individual cognitive tasks drive specific transient reconfiguration of the brain network structure (Mennes et al., 2013; Davison et al., 2015; Cole et al., 2013) while preserving a nearly stable functional topology reminiscent of the resting state configuration (Power et al., 2011; Cole et al., 2014; Krienen, Yeo and Buckner, 2014). In fact, the functional network architecture during rest accounts for nearly 80% of the variance in task-evoked network configurations (Cole et al., 2014; Krienen, Yeo and Buckner, 2014).

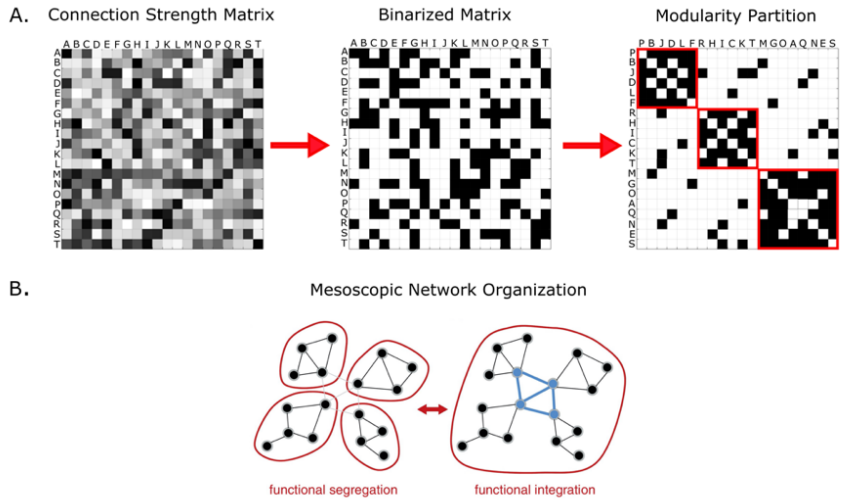

Figure 1.2 Integration and Segregation measures.

A) The direct functional connectivity (FC) between each pair of cortical regions are represented in the connection strength matrix. The binarized FC matrix is obtained after thresholding, and the size of the largest connected component extracted as a measure of integration. B) Nodes are arranged into mesoscopic networks that form communities. Functional segregation indicates dense connection within communities, with sparse connections across communities, whereas functional integration indicates strong connections across community boundaries. Figure adapted from (Sporns, 2013; Lord et al., 2017).

Previous research has shown that the configuration of the brain network structure during task performance exhibits higher integrated states facilitating global information flow as compared to the resting-state networks (Shine et al., 2016; Kitzbichler et al., 2011; Di et al., 2013; Cohen and D'Esposito, 2016). For instance, higher integrated states have been associated with a more accurate behavioral performance on a range of cognitive tasks (Kitzbichler et al., 2011; Shine et al., 2016; Ekman et al., 2012; Liang et al., 2015). Moreover, the extent of integration has been shown to fluctuate over time both

during single scanning neuroimaging sessions (Shine et al., 2016; Hutchison et al., 2013; Chang and Glover, 2010) and during the course of weeks and months (Shine, Koyejo, and Poldrack, 2016).

Beyond the mere increase in the strength of pairwise functional connections, the resulting integrated states of the network topology provide the substrate for the "global workspace" essential to cognition as postulated by the global workspace theory (Baars, 2002; 2005; Dehaene and Changeux, 2011). This theory suggests that after local operations within modules, the information processed is integrated within a global workspace and broadcasted to different areas. The observed changes in network topology are also congruent with the idea that the brain network organization is the result of an economic trade-off between the wiring cost of the network and the topological efficiency (Bullmore and Sporns, 2012). The main idea is that, since long-range connections are more costly to the system, the brain under resting-state operates in an energy-saving mode characterized by higher modularity, greater clustering, and a small proportion of long-range connections. Whereas, according to task demands, the brain exhibits a rapid network reconfiguration in which long-range connections are recruited to allow global information transmission.

Despite substantial evidence in support of the fact that cognitive processing relies on the flexible integration of information widely distributed across specialized regions of the brain, the mechanisms responsible for the coordination are still poorly understood. In the following sections, we will introduce two primary candidates underlying these interactions: large-scale phase synchronization and modulation from the neuromodulatory system.

Phase Synchronization as a Mechanism for Large-Scale Integration in the Brain

Synchronization is a fundamental phenomenon revealing the appearance of positive temporal correlations between the phases and frequencies of two, or more, neural populations. This notion is broadly used in experimental cognitive studies and computational models investigating coordinated oscillatory behavior.

Based on the idea that "what fires together, wires together" (Hebb, 1949; Shatz, 1992, p. 64), it is assumed that distant task-related brain regions will become co-activated in response to task demands. Among several mechanisms describing the reciprocal interaction between brain regions, measures of phase synchronization such as phase coherence and phase-locking values, are one of the most studied within the context of neurophysiology (Lachaux et al., 1999; Mormann et al., 2000; Fell and Axmacher, 2011).

The relevance of phase synchronization for sensory-cognitive processes has become increasingly evident (Buzsaki and Draguhn, 2004; Buzsáki, 2009). Large-scale neural synchronization in different frequencies establishes transient associations between anatomically distributed brain areas and appears to be responsible for information exchange across them. The main idea behind this phenomenon is that oscillatory neuronal activity reflects rhythmic fluctuations in membrane potential, which are associated with changes in neuronal excitability (Buzsaki and Draguhn, 2004; Lakatos et al., 2005; Fries, Nikolic and Singer, 2007). Consequently, these fluctuations may gate neural responses to incoming sensory information, producing peaks and troughs that correspond to optimal and suboptimal windows for communication. As we will see in the next section, the binding mechanism through phase synchronization

has been generalized to the communication through coherence theory (Varela et al., 2001; Deco and Kringelbach, 2016).

The Communication Through Coherence Theory

Oscillations at different frequency bands are commonly observed in neurons in the cortex, subcortex, and cerebellum (Buzsaki and Draguhn, 2004). It is widely accepted that they contribute to the processing of information in neural circuits by communicating distant neuronal populations, but how do they communicate?

In general terms, the "Communication Through Coherence" (CTC) theory states that the synchronization between different neuronal populations modulates the flexible communication between them, meaning that communication is mechanistically implemented by a pattern of coherence (Fries, 2005; 2015). Indeed, two populations of neurons may communicate most effectively when they are in phase, i.e., when their excitability level is coordinated in time (see Figure 1.3). The CTC theory suggests that effective connections in a network can be shaped through phase relations, more specifically through beta (13–30 Hz) and gamma band (30–100 Hz) synchronization, as reported experimentally (Fries, 2005; 2009; 2015). Thus, oscillations are proposed to dynamically shape the computational role of different neuronal groups linked through static structural connectivity.

Several empirical studies support task-induced changes in synchronization at the level of individual regions during selective attention (Womelsdorf et al., 2006), working memory (Howard et al., 2003), and motor control (Ball et al., 2008). Moreover, such task-induced changes in synchronization have been observed between distant cortical regions during working memory (Jones and Wilson,

2005; Sauseng et al., 2004), long-term memory encoding (Fell et al., 2001; Axmacher et al., 2008; Fell et al., 2008), visual attention (Gregoriou et al., 2009), motor control (MacKay, 1997) and sensorimotor integration (Roelfsema et al., 1997).

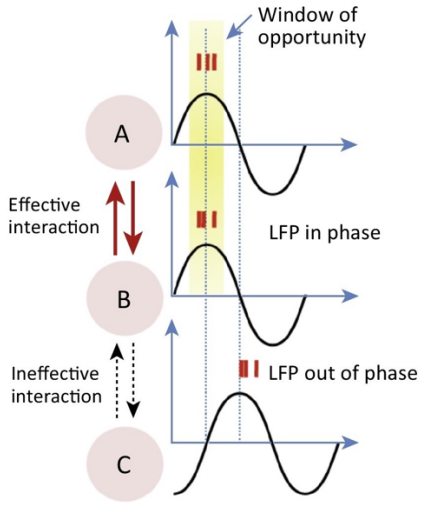

Figure 1.3 The Influence of Brain Oscillations and Synchronization in Neural Communication

A, B and C represent three synchronized neuronal populations. The black line represents the sinusoidal local field potential, and the red lines at the peak correspond to spikes. A and B are phase-aligned, meaning that their windows for input and output exchange invariantly occur at the same time, therefore, they can interact more efficiently. Conversely, B and C present a phase-lag, thus action potentials will arrive at a non-optimal phase likely restricting communication between them. Figure adapted from Fries, 2005; Deco and Kringelbach, 2016.

Importantly, to study the way in which the flexible effective connectivity repertoire of patterns is implemented within fixed whole-brain anatomical structural connectivity, Deco and

Kringelbach (Deco and Kringelbach, 2016) extended the CTC hypothesis to the whole-brain level and linked it to the concept of metastability. They proposed that the dynamics at the macroscale level of slow oscillations are shaped by the underlying microscopic CTC-mediated interactions and that the way to implement it is by maximizing the metastability, an essential sign of a healthy brain. As metastability, they refer to the variability of the phase configurations as a function of time, in other words, how the phase-based synchronization between the different brain regions fluctuates over time.

In chapter 2 we will exploit the high spatiotemporal resolution of intracranial EEG to further explore how cognitive processing modulates global functional measurements, i.e., the level of integration and segregation of information in the human brain networks during task performance, and how these modulations are related to the CTC theory.

The Relevance of Theta Phase for Memory Processes

As outlined in the previous section, the phase of brain oscillations is associated with the exact timing of neural activity. In particular, the phase determines the degree of excitability of the neurons and influences the timing of action potentials. For this reason, the oscillatory phase and phase synchronization have been primarily studied in the context of information transfer for several cognitive processes, including memory operations.

Considerably progress in elucidating how memory is accomplished has been made analyzing the role of phase synchronization-based mechanisms. Extensive research supports that memory-related oscillations are likely confined to theta (4–8 Hz) and alpha (8–13 Hz)

and that higher frequencies are only relevant when coupled to lower frequencies or in the context of a specific role for a high precision timing of neural events (like long-term potentiation or long-term depression) (Klimesch et al., 2008; Fell and Axmacher, 2011).

Enhanced spectral coherence and long-range phase synchronization in the theta range between prefrontal and posterior regions have been associated with the successful episodic encoding of visually presented stimuli (Weiss and Rappelsberger, 2000; Summerfield and Mangels, 2005; Sato and Yamaguchi, 2007). In fact, it has been observed that the strength of the synchronization increases as a function of task demands (Fell et al., 2003; Sauseng et al., 2007; Mizuhara and Yamaguchi, 2007). A plausible interpretation of these results is that phase synchronization might represent the link between prefrontal executive control areas exerting top-down influence over material-specific posterior regions. Based on iEEG recordings, other evidence highlights the role of phase synchronization in communicating medial temporal structures, particularly the hippocampus and rhinal cortex, for memory formation. Greater phase synchronization between those sites was observed for subsequently remembered stimuli, compared to forgotten ones (Fell et al., 2001; Fell et al., 2008).

The studies mentioned above have focused their analysis in the encoding period, i.e., the time-window just after the stimulus is presented. Alternatively, other studies have considered that oscillatory activity even before the stimulus is presented might also play a role in determining whether or not a stimulus will be later remembered (Park and Rugg, 2010; Haque et al., 2015; Otten et al., 2006; Otten, Quayle and Puvaneswaran, 2010; Guderian et al., 2009; Addante, de Chastelaine and Rugg, 2015).

In addition, the phase of ongoing low-frequency oscillations appears to reset at the moment of the presentation of behaviorally relevant

stimuli (Rizzuto et al., 2003; Haque et al., 2015). This shift in the dynamics of prestimulus ongoing oscillations might play a fundamental role in the synchronization of neuronal populations and the coordination of information transfer necessary for efficient encoding. In fact, some studies show that phase synchronization is more precise during encoding of information that is later remembered compared to later forgotten, most likely acting as the "gluing mechanism" for binding human memories (Buzsaki and Draguhn, 2004; Backus et al., 2016; Hanslmayr, Staresina and Bowman, 2016; Clouter, Shapiro and Hanslmayr, 2017; for review see Fell and Axmacher, 2011).

Despite our understanding that phase synchronization underlying memory processes has a binding role for communication and coordination of local processes and inter-region interaction, there remain many unresolved issues concerning the role of the prestimulus phase for memory formation. In the hope of progressing on these issues, Chapter 3 will explore whether ongoing fluctuations in prestimulus neural activity have an impact on memory formation. To do so, we will use a paired-associates memory task in two experiments performed by healthy participants.

o o o

Taken together, the evidence presented in this section highlights the relevance of long-range neural synchrony during the emergence of cognitive processes and shows that, beyond a simple epiphenomenon, it is causally related to human behavior. In view of this, phase synchronization appears as a key mechanism for global neuronal communication and large-scale integration within

frequency-specific, cortical networks. However, the neurobiological mechanisms responsible for the dynamic system-level integration are not restricted only to the synchronization between brain areas, the modulation of the global neuronal gain—mediated by the ascending neuromodulatory system—also plays a major role. The following section will briefly expand on some theoretical foundations and experimental findings that illustrate the influence that neuromodulators exert on shaping global brain dynamics.

Neuromodulatory Influences on Integration and Segregation in the Brain

It is widely accepted that the powerful ability of the brain to adapt its behavior flexibly is largely due to the ascending neuromodulatory systems. Neuromodulators constrain local processes by selectively changing the balance of the excitation and inhibition of individual brain regions—i.e., the neural gain—and, therefore, adjust inter-regional interactions (Cohen, Braver and Brown, 2002; Aston-Jones and Cohen, 2005; Shine et al., 2018). Extensive literature supports the fact that neuromodulatory systems have a strong influence on cognitive processing (Puig et al., 2015; Thiele and Bellgrove, 2018; Naish et al., 2018; Robbins and Arnsten, 2009; Moran et al., 2013); hence, there has been a growing interest in the link between neuromodulators and the emerging network topology at the system-level. For instance, recent computational work has demonstrated that neuromodulatory systems adjust the balance of integration and segregation within the whole-brain network by mediating communication between brain regions (Shine et al., 2018; Poldrack and Yarkoni, 2016). In particular, the results showed that selective increases in the neural gain of different brain regions transitioned the

network to higher integrated states, exhibiting a more complex organization and greater variability in the topological structure over time. Notably, the concentration of neurotransmitter receptors is quite heterogeneous throughout the cerebral cortex, which, in addition to reflecting the modular and hierarchical organization of the cortex, constitutes a significant source of variability and allows the transition between different brain states (Eickhoff et al., 2007; Pillai and Jirsa, 2017).

Selective pharmacological activation of specific neurotransmitter receptors has shed light upon the role of neuromodulatory systems in shaping global network dynamics. Psychedelic drugs such as lysergic acid diethylamide (LSD) and psilocybin, provide the opportunity to do so, offering a unique experimental framework for relating neuropharmacology to changes in global connectivity due to their profound effects in perception, thinking, and consciousness. First synthesized in 1938 by Albert Hofmann, LSD is a serotonin (5-HT) and dopamine (D1 and D2) receptor agonist with psychoactive properties. Some of the effects users experience include ego-dissolution, changes to the quality and attribution of thoughts, visual and sensory misperceptions, and increased awareness of repressed memories (Rucker, Iliff, and Nutt, 2018). Psilocybin is a natural psychedelic prodrug compound obtained from certain species of mushrooms—commonly known as "magic mushrooms"—which presumably has subjective effects very similar to those of LSD (Hollister and Hartman, 1962; Hollister and Sjoberg, 1964). It is also a serotonin receptor (5-HT) agonist with a particular affinity to the 5-HT_{2A}, but unlike LSD, it is selective, i.e., it does not have action at the D1–D2 dopamine receptors.

Over the last two decades, the interest in psychedelic drug research has significantly increased due to its promising therapeutic effect in neuropsychiatric disorders. Positive preliminary evidence on the safety, tolerability, and efficacy of psilocybin for medical use has

been found for obsessive-compulsive disorder (Moreno et al., 2006), alcohol and tobacco addictions (Bogenschutz et al., 2015; Johnson et al., 2014) and for major depression disorder (Carhart-Harris et al., 2016b; Carhart-Harris et al., 2018a), and of psilocybin and LSD for end-of-life psychological distress (Gasser et al., 2014; Griffiths et al., 2016; Grob et al., 2011; Ross et al., 2016).

The effects of LSD on the human brain at a resting state have now been revealed using modern neuroimaging techniques. Studies using this approach have shown decreases in connectivity between the brain regions composing the default mode network (DMN)—a collection of regions exhibiting correlated activations, especially during rest—allowing an increase in the connectivity between brain networks that are highly segregated (Carhart-Harris et al., 2016c; Müller et al., 2018). Notably, LSD enhances global and between-module integration while decreasing the integrity of individual modules, relative to placebo, particularly in frontal, parietal, and temporal regions (see *Figure 1.4*; Tagliazucchi et al., 2016), and in the thalamus and basal ganglia (Müller et al., 2017; Preller et al., 2018). Related findings on the effects of psilocybin reported increases in between-network resting-state functional connectivity under psilocybin (Roseman et al., 2014), implying that networks become less differentiated from each other in the psychedelic state. Moreover, the exploration of the brain's repertoire of functional networks states has been found to be characterized by an increase in the metastability (Lord et al., 2019).

The above results provide strong evidence for the impact of the neuromodulatory system in shaping global network dynamics and can be interpreted in terms of a global rearrangement of the balance between integration and segregation, offering valuable insights into how they can be used for therapeutic means. However, the mechanisms underlying these experimentally observed phenomena remain obscure. Building on these ideas, in chapter 4, we will use a

computational whole-brain model integrating multimodal neuroimaging data to explore mechanistic explanations for the effects of pharmacologic manipulations. For this purpose, in the following section, we will introduce the potential of computational whole-brain modeling.

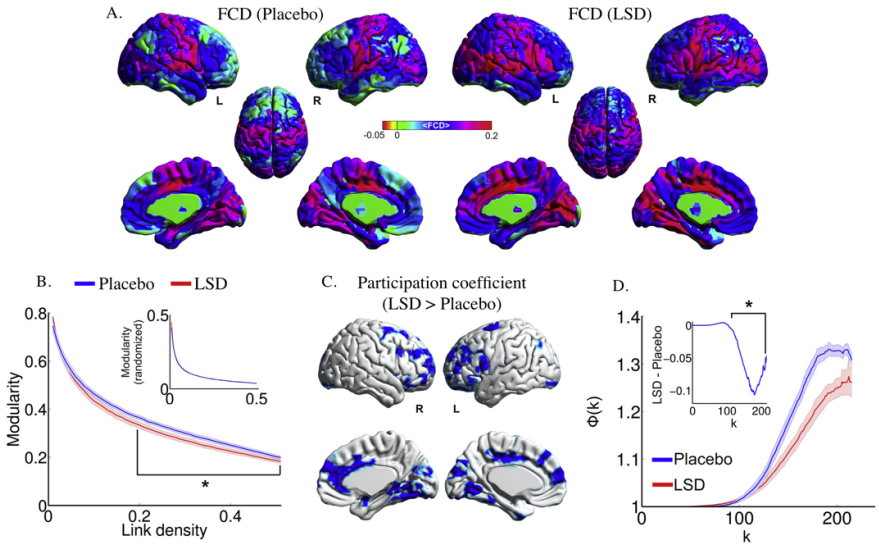

Figure 1.4 LSD Increases Global Integration

A) LSD selectively increases global functional connectivity as seen in the comparison of average functional connectivity dynamics (FCD) under placebo and LSD conditions, B) Decreases in brain modularity under LSD reveal a reduction in the separation of intrinsic brain networks, C) Brain regions showing increased participation coefficient in LSD versus placebo. The participation coefficient of each node was computed measuring how much each node communicates across modules, compared to how much they communicate within module, D) Changes in the level of integration between coupled regions by means of the rich-club coefficient Φ(k) *are higher for the placebo condition, meaning that LSD decreases the level of communication between the brain's dominant hub regions. Figure adapted from Tagliazucchi et al., 2016.*

The Advantage of Whole-Brain Computational Models

During the last decades, advances in neuroimaging techniques and data analysis methods have led to an excellent description of global brain dynamics and functional networks. However, empirical data solely only covers descriptive aspects of these phenomena while missing possible mechanistic explanations. Whole-brain computational modeling has significantly contributed to bridging this gap since it can be used to explore the intricate link between structure and function by considering the dynamics of interacting cortical regions (Deco and Corbetta, 2011; Nakagawa et al., 2013; Ponce-Alvarez et al., 2015; Honey et al., 2009).

An appropriate mathematical model allows a systematic parameter variation hardly feasible in experiments and data analysis and helps to formulate predictions and hypotheses that can serve as a basis for further experimental investigation. The large number of variables affecting the brain structure and function makes it nearly impossible for them to be considered in a single model. Therefore, whole-brain dynamical models go beyond the level of individual synapses and neurons and consider the mesoscopic behavior of neuronal populations instead (for a review see Deco et al., 2008).

Several models of different complexity have been suggested to simulate the activity of a neuronal population including detailed spiking neuron models (Deco and Jirsa, 2012), phase oscillators (Cabral et al., 2011; Ponce-Alvarez et al., 2015), limit-cycle oscillators (Deco et al., 2017a; Bettinardi et al., 2017), neural mass or mean-field models (Deco et al., 2014b), and others (Deco et al., 2008; Sanz-Leon et al., 2015; Haimovici et al., 2013; Marinazzo et al., 2014). These models reproduce the ongoing activity of large populations of neurons based on the assumption that their collective

macroscopic behavior is only weakly dependent on the behavior of individual neurons (Breakspear and Jirsa, 2007). This premise has taken its lead from statistical physics, which has shown that macroscopic physical systems obey laws independently of their micro- or mesoscopic constituents (Haken, 1975).

Modeling of resting-state dynamics represents the brain as a densely connected network of nodes, where each node denotes a brain region based on a neuroimaging parcellation template[2]. The inter-node connections are derived from empirical data, typically diffusion magnetic resonance (dMRI) and tractography techniques. According to the chosen model, the local dynamics of each node are mathematically described by a set of differential equations that can be constrained by known neurophysiology (Deco, Jirsa and McIntosh, 2011). The model constraints and couples the local dynamics between regions according to the empirical structural properties. Expressly, it assumes that the density of the white matter fibers connecting two brain areas corresponds to the strength of the reciprocal synaptic projections between those areas.

The model parameters can be systematically varied to find the optimum at which the simulated global network dynamics closely replicates the ones observed with current neuroimaging techniques

[2] A brain parcellation defines distinct partitions of the brain on the basis of specific anatomical or functional features, ranging from local properties of brain tissue to long-range connectivity patterns (for a review see Eickhoff, Yeo and Genon, 2018).

including fMRI (Ghosh et al., 2008; Honey et al., 2009; Deco et al., 2009; Cabral et al., 2011; Deco and Jirsa, 2012), MEG (Cabral et al., 2014b; Nakagawa et al., 2013), and EEG (Hindriks, van Putten and Deco, 2014). The optimal working point of the model is found for spatiotemporal patterns characterized by measures such as FC (Deco et al., 2013; 2014) and FCD (Hansen et al., 2015; Glomb et al., 2017).

Of particular interest, in the context of this work, is the dynamic mean-field (DMF) model, which has been successfully used to investigate how the physiological state of cortical circuits shapes FC (Deco et al., 2013; 2014). Interestingly, the maximum similarity between the model and the empirical data is mostly achieved when the model is close to the bifurcation (Deco et al., 2017b). This suggests that the resting brain operates at a critical point at which a sudden quantitative change of its dynamics, results in a transition between states (Deco, Jirsa and McIntosh, 2013; Golos, Jirsa and Daucé, 2015; Cocchi et al., 2017). In the following, we will review the mean-field model and describe how to transform a simulated neural activity into a hemodynamic signal that captures the changes in mean the firing rate (Brunel and Wang, 2003).

Whole-Brain Dynamic Mean-Field Model

The DMF model proposed by Deco et al. (Deco et al., 2014) approximates the average ensemble behavior of interconnected excitatory and inhibitory spiking neurons to a reduced set of dynamical equations describing the activity of coupled excitatory (*E*) and inhibitory (*I*) pools of neurons. Under resting-state conditions, each single brain node emulates spontaneous neuronal noise, i.e., reproducing the typical asynchronous low firing rate spontaneous activity observed empirically (around 3 Hz for the pyramidal neurons and 9 Hz for inhibitory neurons). We implement this neuronal noise

by a modified DMF model based on the original reduction of Wong and Wang (Wong and Wang, 2006). In this DMF reduction, the excitatory synaptic currents, $I^{(E)}$, are mediated by NMDA receptors, and the inhibitory currents, $I^{(I)}$, are mediated by $GABA_A$ receptors. Within each brain area n, the E and I neuronal pools are reciprocally connected, whereas inter-area coupling between two areas n and p occurs only at the E-to-E level and is scaled by the structural connectivity C_{np}.

More specifically, the DMF model at the whole-brain level is expressed by the following system of coupled differential equations:

$$I_n^{(E)} = W_E I_o + w_+ J_{NMDA} S_n^{(E)} + G J_{NMDA} \sum_p C_{np} S_p^{(E)} - J_n S_n^{(I)} \qquad (1)$$

$$I_n^{(I)} = W_I I_o + J_{NMDA} S_n^{(E)} - S_n^{(I)} \qquad (2)$$

$$r_n^{(E)} = H^{(E)}\left(I_n^{(E)}\right) = \frac{g_E\left(I_n^{(E)} - I_{thr}^{(E)}\right)}{1 - exp\left(-d_E g_E\left(I_n^{(E)} - I_{thr}^{(E)}\right)\right)} \qquad (3)$$

$$r_n^{(I)} = H^{(I)}\left(I_n^{(I)}\right) = \frac{g_I\left(I_n^{(I)} - I_{thr}^{(I)}\right)}{1 - exp\left(-d_I g_I\left(I_n^{(I)} - I_{thr}^{(I)}\right)\right)} \qquad (4)$$

$$\frac{dS_n^{(E)}(t)}{dt} = -\frac{S_n^{(E)}}{\tau_{NMDA}} + \left(1 - S_n^{(E)}\right)\gamma r_n^{(E)} + \sigma v_n(t) \qquad (5)$$

$$\frac{dS_n^{(I)}(t)}{dt} = -\frac{S_n^{(I)}}{\tau_{GABA}} + r_n^{(I)} + \sigma v_n(t) \qquad (6)$$

Here, for each excitatory *(E)* or inhibitory *(I)* pool of neurons in each brain area *n*, $I_n^{(E,I)}$ (in nA) represents the total input current, $r_n^{(E,I)}$ (in Hz) denotes the firing rate, and $S_i^{(E,I)}$ denotes the synaptic gating variable. The neuronal response functions, $H^{(E,I)}$, convert the total input currents received by the E and I pools into firing rates, $r_i^{(E,I)}$, following the input-output function of Abbott and Chance (Abbott and Chance, 2005), where $g_E = 310\, nC^{-1}$ and $g_I = 615\, nC^{-1}$ are gain factors determining the slope of H, $I_{thr}^{(E)} = 0.403\, nA$, and $I_{thr}^{(I)} = 0.288\, nA$ are the threshold currents above which the firing rates increase linearly with the input currents, and $d_E = 0.16$ and $d_I = 0.087$ are constants determining the shape of the curvature of H around I_{thr}. The synaptic gating variable of excitatory pools, $S_i^{(E)}$, is controlled by NMDA receptors with a decay time constant $t_{NMDA} = 0.1$s and $g = 0.641$, whereas the average synaptic gating in inhibitory pools depends on GABA receptors with $t_{GABA} = 0.01$s. The overall effective external input is $I_0 = 0.382\, nA$ with $W_E = 1$ and $W_I = 0.7$. Furthermore, $w_+ = 1.4$ is the weight of recurrent excitation, and $J_{NMDA} = 0.15\, nA$ weighs all excitatory synaptic couplings. In Equations 5 and 6 y_n is uncorrelated standard Gaussian noise with an amplitude of $s = 0.01\, nA$. All parameters were set as in Wong and Wang (Wong and Wang, 2006). The parameters of the DMF model were defined in Wong and Wang (Wong and Wang, 2006) to emulate resting-state conditions, such that each isolated node displays the typical noisy spontaneous activity with low firing rate $\left(r^{(E)} \sim 3Hz\right)$ observed in electrophysiology experiments (Burns and Webb, 1976; Koch and Fuster, 1989; Softky and Koch, 1993; Shadlen and Newsome, 1998). Moreover, following Deco et al. (Deco et al., 2014), the inhibition weight, j_n, was adjusted for each node *n* such that the firing rate of the excitatory pools $r_n^{(E)}$ remains clamped at 3Hz even when receiving excitatory input from connected areas. This regulation is known as Feedback Inhibition Control (FIC), and the algorithm to achieve it is described in Deco et al. (Deco et al.,

2014). It has been demonstrated that the FIC leads to a better prediction of the resting-state FC and to a more realistic evoked activity (Deco et al., 2014).

Following the parcellation applied to the structural and functional MRI data, we considered N = 90 brain areas in our whole-brain network model. Each area n receives excitatory input from all structurally connected areas p into its excitatory pool, weighted by the connectivity matrix, C_{np}, obtained from dMRI. Furthermore, all inter-area *E*-to-*E* connections are equally scaled by a global coupling factor G. This global scaling factor is the only control parameter that is adjusted to move the system to its optimal working point, where the simulated activity maximally fits the empirical resting-state activity of participants under placebo conditions.

Transforming Neuronal Activity into BOLD-fMRI Signal

Hemodynamic models estimate blood oxygen level-dependent signals from simulated neural activity, enabling a more direct comparison with fMRI measures (Razi et al., 2017).

The Balloon–Windkessel model (Friston, Harrison and Penny, 2003; Stephan et al., 2007) describes the coupling of perfusion to the BOLD signal, with a dynamical model of the transduction of neural activity into perfusion changes. The model assumes that the BOLD signal is a static nonlinear function of the normalized total deoxyhemoglobin voxel content, normalized venous volume, resting net oxygen extraction fraction by the capillary bed, and resting blood volume fraction. The BOLD-signal estimation for each brain area is computed by the level of neuronal activity summed over all neurons in both populations (excitatory and inhibitory populations) in that particular area. In all our simulations shown here, this level of

neuronal activity is given by the rate of spiking activity in windows of 1 ms. In brief, for the *i*-th region, neuronal activity z_i causes an increase in a vasodilatory signal s_i that is subject to autoregulatory feedback. Inflow f_i responds in proportion to this signal with concomitant changes in blood volume v_i and deoxyhemoglobin content q_i. The equations relating these biophysical variables are:

$$\frac{ds_n}{dt} = 0.5r_n^{(E)} + 3 - ks_n - \gamma(f_n - 1) \tag{7}$$

$$\frac{df_n}{dt} = s_n \tag{8}$$

$$\tau\frac{dv_n}{dt} = f_n - v_n^{\alpha^{-1}} \tag{9}$$

$$\tau\frac{dq_n}{dt} = \frac{f_n(1-p)^{f_n^{-1}}}{p - q_n v_n^{\alpha^{-1}}/v_n} \tag{10}$$

where p is the resting oxygen extraction fraction, t is a time constant, and α represents the resistance of the veins. Finally, the BOLD signal in each area n, B_n, is a static nonlinear function of volume, v_n, and deoxyhemoglobin content, q_n, that comprises a volume-weighted sum of extra- and intravascular signals:

$$B_n = V_0[k_1(1 - q_n) + k_2(1 - q_n/v_n) + k_3(1 - v_n)] \tag{11}$$

All biophysical parameters were taken from Stephan et al. (Stephan et al., 2007). To concentrate on the frequency range where resting-state activity appears the most functionally relevant, both empirical and simulated BOLD signals were band-pass filtered between 0.1 and 0.01 Hz (Biswal et al., 1995; Glerean et al., 2012; Buckner et al., 2009; Achard et al., 2006).

° ° °

To summarize, we have introduced the two fundamental principles of functional brain organization, namely, integration and segregation, and examined their implications for cognitive processing. In addition, we have discussed two possible mechanisms through which the dynamic system-level integration may be modulated. Finally, we have reviewed the potential value of computational whole-brain modeling—a unique framework—for providing insights into the mechanisms underlying the intricate functional architecture of human brain networks. In the following chapters, we will elaborate carefully on these topics aiming to marshal evidence and arguments that elucidate the mechanisms driving large-scale integration for cognitive processing.

CHAPTER 2

The Dynamics of Human Cognition Characterized by Integration and Segregation Measures

"The scientist is not a person who gives the right answers; is the one who asks the right questions"

Claude Lévi-Strauss (1908–2009)

Cognitive processing requires the ability to flexibly integrate and process information across large brain networks. How do brain networks dynamically reorganize to allow broad communication between many different brain regions in order to integrate information? In this chapter, we explore how cognitive processing modulates the level of integration and segregation of information in human brain networks (Deco et al., 2015), and how this is related to

CTC theory[3]. To do so, we recorded iEEG data from 12 patients with epilepsy using intracranial EEG while performing three different cognitive tasks. We show that the functional connectivity between different brain areas changes to facilitate communication across them. At the topological level, the facilitation is characterized by significant increases in integration and decreases in segregation during cognitive processing, especially in the gamma band (50–90 Hz). In addition, task execution drives an increase in the level of global synchronization and functional connectivity in the same frequency band. More importantly, functional connectivity modulations are not caused by changes in the level of the underlying oscillations. Instead, these modulations are caused by a rearrangement of the mutual synchronization between the different nodes as proposed by the "Communication Through Coherence" Theory.

[3] The results presented in this chapter are published in: Cruzat, J., Deco, G., Tauste-Campo, A., Principe, A., Costa, A., Kringelbach, M. L., & Rocamora, R. (2018). The dynamics of human cognition*:* Increasing global integration coupled with decreasing segregation found using iEEG. *NeuroImage,* 172, 492-505.

Human Cognitive Processing at the Whole-Brain Level

Intracranial electroencephalography (iEEG) recordings from the human brain provide a unique opportunity to study cognitive functions measuring neural activity at the mesoscopic level. Beyond the high temporal resolution intrinsic to iEEG measurements, this technique also allows higher levels of spatial resolution and enhanced signal-to-noise ratio (Engel et al. 2005; Lachaux et al. 2003). These advantages have led scientists to use the technique (Lachaux et al. 2012) to study several cognitive processes such as attention (Müsch et al., 2014), visual perception (Bertrand et al., 2014; Ossandón et al., 2012), language (Chan et al., 2011; Hamamé, Alario, Llorens, Liégeois-Chauvel, & Trébuchon-Da Fonseca, 2014; Sahin, Pinker, Cash, Schomer, & Halgren, 2009), memory (Greenberg, Burke, Haque, Kahana, & Zaghloul, 2015; Haque et al., 2015; Kucewicz et al., 2014), decision making (Perez et al., 2015), emotion (Murray et al. 2014; Boucher et al. 2015) and consciousness (Gaillard et al., 2009). Most of this research has attempted to assign functions to specific local brain areas by correlating task-performance with measurements of neural activity (but see also recent coherence network studies: Kingyon et al. 2015; Zheng et al. 2017; Mercier et al. 2015). Furthermore, most studies using iEEG have focused mainly on single-electrodes analysis, using predominantly event-related potentials (Lachaux et al. 2012) or spectral analysis (Kahana, 2006). Here, we take a different perspective. Instead of focusing on single electrodes, we assess changes in functional connectivity analyzing all the implanted electrodes.

In contrast to the regional view of brain function, growing evidence reveals that human cognition relies on the flexible integration of information widely distributed across different brain regions

(Bressler and Menon 2010; Deco et al. 2015; Fallani et al. 2008; Kitzbichler et al. 2011; Palva et al. 2010; Valencia et al. 2008; Bassett et al. 2011; Chai et al. 2016; Ekman et al. 2012; Kinnison et al. 2012; Wang et al. 2016). In these studies, cognitive processing increases the global integration of information across neural networks, while at the same time leads to a decrease in their modularity (Kitzbichler et al. 2011; Ekman et al. 2012; Kinnison et al. 2012; Bola and Sabel 2015; Vatansever et al. 2015; Godwin et at. 2015; Liang et al. 2015). Although some iEEG studies have observed increased synchronization by task demands (Axmacher et al., 2008; Becher et al., 2015; Gaillard et al., 2009), no one has assessed integration and segregation dynamics. Furthermore, limited knowledge is available regarding the mechanisms that underlie changes in integration and segregation associated with cognitive processing.

Experimental Setting and Participants

We explored how cognitive processing modulates the level of integration and segregation of information in human brain networks (Deco et al., 2015), and how these modulations are related to the communication through coherence (CTC) theory. To do so, we recorded iEEG data from depth electrodes stereotactically implanted for presurgical diagnosis in 12 patients with epilepsy (PWE) performing three different cognitive tasks. The iEEG electrodes used a stereo-electroencephalography (SEEG) implantation methodology and covered broad brain regions, including cortical as well as subcortical regions. Hence, we were able to assess global changes in a broad brain network. Furthermore, we also assessed how integration and segregation relate to synchronization rather than to the level of oscillations (amplitude). Finally, is important to

emphasize that our claims about the modulation of the integration/segregation and the validity of CTC theory are global since they are independent of the location of the electrodes (i.e., node location, which was different for each patient) and type of cognitive processing (three different cognitive tasks were used).

The Clinical Research Ethical Committee of the Municipal Institute of Health Care (CEIC-IMAS) approved this study. Following the Declaration of Helsinki, patients were informed about the procedure and they gave their written consent before the experiment.

Twelve subjects (N = 12) (3 women; all right-handed; mean age 36.4 ± 10.1 years-old), evaluated for presurgical diagnosis in the Epilepsy Monitoring Unit of the Hospital del Mar (Barcelona, Spain), participated in the study. All patients were stereotactically implanted with depth electrodes for invasive presurgical diagnosis using a stereotactic ROSA robotic device (Medtech, France). The location of the electrodes was established only for clinical reasons using an SEEG approach. The implantation schemas were similar between all patients, given that they were all under investigation for temporal lobe epilepsy. The number of electrodes used varied among 8 to 16 for a patient with 5–15 contacts each (diameter: 0.8 mm; contacts 2 mm long, 1.5 mm apart) (DixiMédical, France). All patients underwent an extensive neuropsychological evaluation and had a normal or corrected-to-normal vision. They were within the normal range of education, having completed from primary to high academic level. Supplement Table S2.1 summarizes personal data, pathological information, and an overview of implanted electrodes for each patient. Since we aim to study the network dynamics supporting cognitive processes under normal circumstances, patients were assessed in the absence of pharmacological treatment. They were tested at least three days after the last administration of the drug.

Picture-naming Task

Participants were asked to name aloud in Spanish, as fast and accurately as possible, 228 pictures presented in three different blocks. Pictures were black & white line drawings of familiar objects from a wide range of semantic categories selected from the Snodgrass and Vanderwart 1980 set. Each picture appeared once centrally and sequentially on the computer screen in a pseudo-random order for 2000 ms, followed by a fixation cross for 1000 ms (see Figure 2.1).

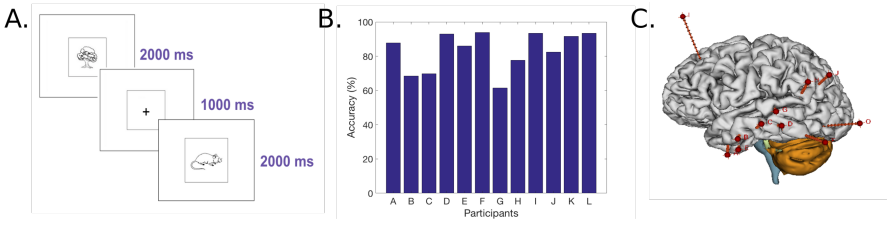

Figure 2.1 Paradigm, behavioral performance and implantation scheme

A) Schematic example of the experimental paradigm of the picture-naming task. After an interval of 1000 ms for preparation, each target picture was presented and remained on the screen for 2000 ms. B) Picture naming accuracy for each patient. On average, patients achieved 83.2 ± 11.3% accuracy on test items (N = 228). C) Example of the intracerebral implantation scheme for iEEG recordings in patient E. Eleven electrodes were implanted in the left hemisphere.

Size-judgement Task

Participants were instructed to indicate via button press if the presented Spanish word represented an object larger than a one-foot box in any dimension. Word stimuli were 68 items from two different categories: animals and human-made objects. Half of the words in each category represented objects larger than one foot. Words were auditorily presented through computer speakers. Each word was presented sequentially in a pseudo-random order followed by an inter-trial lapse of 3500 ms.

Lexical-decision Task

Participants were instructed to indicate whether the letter string presented in each trial written on a computer screen was a real word (e.g., run, table) or a pseudoword (e.g., lun, tible). We included four types of real words: motion verbs (e.g., run), static verbs (e.g., think), concrete nouns (e.g., table), and abstract nouns (e.g., theory). The task included a total of 150 trials. Each word was presented once centrally and sequentially on the computer screen in a pseudo-random order for 2000 ms followed by a fixation cross for 1000 ms.

The three tasks had different stimulus presentation modality. This allowed us to assess neural activity elicited when retrieving conceptual knowledge from a lexical form, from an object depicting a concept and from a written lexical form.

The stimuli were presented using the software Sketchbook Processing 2.2.1 (Programming Software, 2001 *https://processing.org/*) on a laptop computer at an approximate size

of 5 degrees of visual angle. For the picture-naming task, the experimenter transcribed the responses and provided an accuracy score. For the size-judgement and lexical-decision task, responses were collected through keyboard input and response times recorded and timed in milliseconds. An electronic processor, "Arduino, UNO" was used to connect and synchronize both hardware; the XLTEK system with the computer (MacBook Pro). The application interfaced with an Arduino board that, in turn, was connected to the EEG amplifier, and at each trial, a signal was sent through the Arduino to the EEG.

iEEG Data Acquisition and Pre-processing

Neurophysiological responses were registered by the iEEG system from deep multichannel electrodes (DIXI Microtechniques, Besançon, France). On average, each patient had 13 ± 2 electrodes implanted (range 8–16) with a total of 120±13 recording contacts (range 85–127). The data were acquired continuously by the Neuroworks XLTEK system (version 6.3.0, build 636) at 32 kHz with a headbox of 128 channels recorded at a sampling frequency of 500 Hz. For our analysis, we considered all channels placed in both cortex and subcortical structures. Channels placed in white matter or misplaced were disregarded. A bipolar montage was constituted offline to increase spatial resolution by removing any confounds from the common reference signal (Lachaux et al. 2003; Jerbi et al. 2009). Bipolar signals were derived by differentiating neighboring electrode pairs of recorded and not rejected consecutive channels within the same electrode array (Lachaux et al. 2012; Boucher et al. 2015; Gaillard et al. 2009; Burke et al. 2013). The continuous iEEG data was first high-pass filtered at 1 Hz and low-pass filtered at 150 Hz.

To remove common line contamination, an extra notch filter was applied at 50 and 100 Hz. In order to have specific spectral information, we analyzed the spatio-temporal correlations of the Band Limited Power (BLP) at a given carrier frequency. This is a standard approach introduced in the context of MEG analysis (Brookes et al. 2011a). For that, at a given carrier frequency $f_{carrier}$ (we consider here $f_{carrier} = 1 - 130\ Hz$ in steps of 4 Hz) we band-pass filtered the signal within the narrow band [$f_{carrier}$ – 2, $f_{carrier}$ + 2 Hz] (we used the second-order Butterworth filter) and computed the corresponding envelope using the Hilbert transform (Brookes et al. 2011b; Cabral et al. 2014b). The Hilbert transform yields the associated analytical signals. The analytic signal represents a narrowband signal, $s(t)$, in the time domain as a rotating vector with an instantaneous phase, $s(t)$, and an instantaneous amplitude, $A(t)$, i.e., $s(t) = A(t)cos(\varphi(t))$. The phase and the amplitude (the envelope of that carrier frequency) are given by the argument and the module, respectively, of the complex signal $z(t)$, given by $z(t) = s(t) + i.H[s(t)]$, where i is the imaginary unit, and $H[s(t)]$ is the Hilbert transform of $s(t)$. We further consider only the slow components of the envelope A(t) by filtering the amplitudes again below 12 Hz (Nir et al., 2008). Finally, the slow component of the envelope of each brain node—which corresponds to each bipolar channel—at a given carrier frequency was used to calculate the envelope FC (see subsection below).

To test another possible definition of integration, we also used the monopolar montage. Spatial resolution was increased by removing any confounds from the common reference signal for each time point. In this case, brain nodes correspond to each single monopolar channel. The full analysis pipeline is detailed in Figure 2.2.

Envelope Functional Connectivity (FC)

For the three tasks, all trials were considered. The data was segmented into two windows around stimulus presentation: the first one spanning from –500 ms to 0 from the stimulus presentation (pre-stimulus window), and the second one from 0 to 500 ms from stimulus onset (post-stimulus windows). We defined an Envelope FC matrix of the continuous bipolar iEEG data for pre- and post-stimulus windows as a matrix of Pearson's correlations of the corresponding amplitude envelopes, i.e., the slow components of the BLP of iEEG signals at a given carrier frequency between two brain areas over the whole-time window for a given window (pre- and post-stimulus). Thus, the mean FC is specific for each narrow-band frequency window.

Phase-lock Matrix

For each time point, we calculated the phase lock matrix describing the global state of synchronization across all network nodes using the bipolar montage. The elements of the phase-lock matrix are given by:

$$P_{ij}(t) = e^{-3|\varphi_i(t)-\varphi_i(t)|}$$

where $\varphi_i(t)$ is the extracted phase of node *i* at time *t* (at a given carrier frequency using the Hilbert transform as specified above). We used the phase-lock matrix at a specific single time point to calculate the integration, as specified below.

Integration

We used the measure of integration introduced by Deco et al. 2015 defined at the network level to characterize the level of the broadness of communication between regions across the whole brain. After filtering the data, we calculated the envelope FC for both the pre- and post-stimulus windows. Then, we define *integration* as the size of the largest connected component in the FC matrix. That is the number of nodes of the largest connected graph in the binarized FC matrix obtained after thresholding it. More specifically, for a given absolute threshold θ between 0 and 1 (scanning the whole range), the FC (using the criteria $\left|FC_{ij}\right| < \theta$, i. e a value of 0 and 1 otherwise) is binarized and the largest subcomponent (see definition below) extracted as a measure of integration. To get a measure that is independent of the threshold, this curve is integrated in the range of thresholds between 0 and 1. The integration measure is then normalized by the maximal number of connected brain areas (i.e., all N areas) for each integration step and by the number of integration steps such that the maximal integration is normalized to 1. Note, that the concept of integration is designed to account for the broadness of communication across the brain, and thus require considering positive and negative correlations as potentially establishing a communication link. Therefore, we took the absolute values of the FC correlations. In other words, we quantified the broadness of communication (measured by means of correlation) regardless of whether the correlation values were negative or positive.

In graph-theoretical terms, subcomponents are extracted from the undirected graph defined by the binarized matrix (which itself is considered as an adjacency matrix). More precisely, a subcomponent is a subgraph in which paths connect any two vertices to each other, and which connects to no additional vertices in the super-graph (Deco et al., 2015). A vertex *u* is said to be connected to a vertex *v* in a graph *G* if there is a path in *G* from *u* to *v*. The concepts of subgraph and super-graph are defined as follows: Let *H* be a graph with vertex set *V(H)* and edge set *E(H)* and similarly let *G* be a graph with vertex set *V(G)* and edge set *E(G)*. Then, we say that *H* is a subgraph of *G* if $V(H) \subseteq V(G)$ and $E(H) \subseteq E(G)$. In such a case, we also say that *G* is a super-graph of *H*.

Segregation

Complementary to the integration, we used the modularity (Rubinov & Sporns, 2011) as a measure of segregation. Following Rubinov and Sporns 2011, modularity is defined as a measure of the goodness with which a network is optimally partitioned into functional subgroups, i.e., a complete subdivision of the network into non-overlapping modules, and supported by densely connected network communities. We consider the modularity of our envelope FC matrix. This matrix contains positive and negative weights, namely the corresponding correlation between two nodes. The modularity measure we used is given by,

$$Q^{GJA} = \frac{1}{v^+ + v^-} \sum_{ij} \left[\left(w_{ij}^+ - e_{ij}^+ \right) - \left(w_{ij}^- - e_{ij}^- \right) \right] \delta_{M_i M_j}$$

Where the total weight, $V^{\pm} = \sum_{ij} W_{ij}^{\pm}$ is the sum of all positive or negative connection weights (counted twice for each connection), being $w_{ij}^{+} \in [0,1]$ the weighted connection between nodes *i* and *j*. The chance-expected within-module connection $e_{ij}^{\pm} = \frac{s_i^{\pm} s_j^{\pm}}{v^{\pm}}$, where the strength of node $i, s_i^{\pm} = \sum_j W_{ij}^{\pm}$ is the sum of positive or negative connection weights of *i*. The delta $\delta_{M_i M_j} = 1$ when *i* and *j* are in the same module and $\delta_{\mathrm{MiMj}} = 0$ otherwise (Newman, 2006). This definition is a generalization of the standard measure of modularity for matrices with nonnegative weights, which is given by the average difference between present within-module connection weights W_{ij}^{+} and chance-expected within-module connection weights e_{ij}^{+} . As mentioned above, we consider both positively and negatively weighted connections (envelope FC matrix). The positively weighted connections represent correlated activation patterns and hence reinforce the placement of positively connected pairs of nodes in the same module. The negatively weighted connections represent anticorrelated activation patterns and reinforce the placement of negatively connected pairs of nodes in distinct modules (for a complete description, see Sporns 2010).

Synchronization

We measure the global mean level of synchronization as the mean value of the Kuramoto order parameter across time. The Kuramoto order parameter is defined by the following equation:

$$R(t) = \frac{\left|\sum_{k=1}^{n} e^{(i\varphi_k(t))}\right|}{n}$$

where $\varphi_k(t)$ is the instantaneous phase of each narrowband signal at node k at a given carrier frequency by using the Hilbert derived phases of the slow component of the Band Limited Power (BLP) signals. The Kuramoto order parameter measures the global level of synchronization of the n oscillating signals. Under complete independence, the n phases are uniformly distributed and thus R is nearly zero, whereas for R=1, all phases are equal (full synchronization).

Statistical Analysis

Permutation Tests

To examine the reliability of the post-stimulus window modulation, frequency-dependent statistical significance was assessed using a non-parametric test with 1000 random permutations. The statistic test was chosen to be the median across the differences between post and pre-stimulus measures. Following Winkler et al. 2014, we simulated the null hypothesis of no stimulus modulation at any post-stimulus windows by randomly permuting pre- and post-stimulus samples at each paired trial (group exchangeability hypothesis) and computing the test statistic. These surrogate values formed a reference distribution, against which we compared the original statistic value. The proportion of permutations in which surrogate values matched or exceeded the original statistic value determined the test p-value (P) to be compared with the significance level. We obtained a p-value for each frequency band and applied multiple comparisons corrections with the False Discovery Rate (FDR) level of 0.05 using the Benjamini-Hochberg method.

Cognitive Processing Characterized by the Integration and Segregation Measures

We investigate how cognitive processing modulates the level of integration and segregation in human brain networks and how these modulations are related to the CTC theory. To do so, we exploited the high spatiotemporal resolution of intracranial electroencephalography (iEEG); a technique usually employed in pharmacologically resistant patients with epilepsy who require brain mapping before surgery (Lachaux et al. 2012; Sperling 1997; Serletis et al. 2014). We recorded iEEG data in twelve patients while they were naming pictures in their native language (Spanish) (Figure 2.1A). Naming accuracy was high (83.2 ± 11.3%) with an averaged response time of 1350 ± 306 ms (Figure 2.1B). The task was used to drive the modulation of the underlying brain networks related to the integration of task-related information. For the large majority of people, language processing is supported by a widespread large-scale network distributed across frontal, temporal, parietal and occipital lobes in the dominant hemisphere (Chai et al., 2016; Ferstl, Neumann, Bogler, & Von Cramon, 2008; Price, 2000). Channels were placed in all lobes in both hemispheres, being most of them in the left frontal, temporal and parietal lobes (see an example of implantation scheme in (Figure 2.1C). All channel recordings from grey matter and subcortical structures were considered for the analysis.

After data pre-processing, we analyzed the Band Limited Power (BLP) at a given carrier frequency ($f_{carrier}$) in order to have specific spectral information. We band-pass filtered the iEEG signals within the narrow band [$f_{carrier} - 2$, $f_{carrier} + 2$ Hz] and considered a range of $f_{carrier}$ starting from 1 to 130 Hz in steps of 4 Hz. We chose a bandwidth of 4 Hz because it provides a good trade-off between

phase estimation accuracy and number of testable comparisons. In order to compute the envelope functional connectivity (FC), we further computed the Hilbert transform (Figure 2.2).

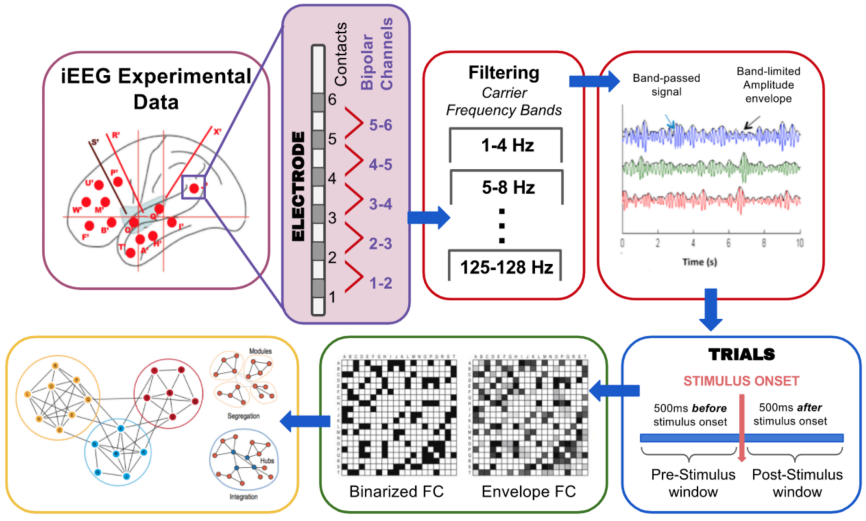

Figure 2.2 Data processing flow chart

iEEG data is recorded from 85 up to 127 unipolar channels on each patient. The bipolar montage is constituted offline by subtracting the neural activity recorded by neighboring contacts within the same electrode array. The data is first band-pass filtered at 1–150 Hz, and further band-pass filtered into narrow frequency bands $[\boldsymbol{f}_{\boldsymbol{carrier}} - \mathbf{2}, \boldsymbol{f}_{\boldsymbol{carrier}} + \mathbf{2}\ Hz]$ *(we consider here carrier frequencies* $\boldsymbol{f}_{\boldsymbol{carrier}}$ *= 1–130 Hz in steps of 4 Hz). By the Hilbert transform the corresponding amplitude envelopes are computed to further compute the envelope FC matrix. The continuous data is segmented into windows of –500 to 0 ms (pre-stimulus window) and 0–500 ms (post-stimulus window), around stimulus presentation. In order to characterize the organization of the network under both windows, we used the integration and segregation measures of global brain function.*

To study functional network topology changes during task execution, we contrasted differences in brain activity in two time-windows: 500 ms before the stimulus was presented: "pre-stimulus window", and 500 ms immediately after the stimulus was presented: "post-stimulus window" As speech production is associated with large motor activity, thus with a significant increase of integration, we focused our analysis in a time window far from the beginning of the motoric activity (response times were around 1350 ms, and we recorded the first 500 ms). In order to characterize the organization of the network in both windows, we used the integration and segregation measures of global brain function describing the level of communication across the different nodes of the brain network. We tested the statistical significance of the network measure differences between pre-stimulus and post-stimulus using a non-parametric method (Winkler et al., 2014). Specifically, we characterized the null hypothesis using constrained permutations that preserved the trial grouping of the data at both time windows.

To illustrate the results, we first focus on the ones corresponding to a single patient (Figure 2.3). The post-stimulus window as compared to the pre-stimulus one led to an increase in neural integration and to a decrease in neural segregation (Figure 2.3A-B). For both indexes, the largest modulation appeared particularly in the gamma band, around 50–90 Hz ($p < 0.05$, $N = 1000$). Note that the concepts of integration and segregation are measures that, by definition, are calculated independently from each other but, at the same time, are highly correlated; when one increases, the other consistently decreases. Thus, these results show that cognitive processing leads to an increase in neural integration and a decrease in neural segregation. We further analyze the correlates of these modulations associated with the cognitive task. First, these modulations are not related to changes in oscillations' envelope amplitudes at any frequency (Figure 2.3C). This is so both when looking at the mean amplitude of all electrodes and when evaluating the mean amplitude of each bipolar

channel separately at 60 Hz (which corresponds to the maximal modulation of the integration measure) (Figure 2.3F). Hence, changes in integration and segregation cannot be accounted by changes in oscillations' envelope amplitudes.

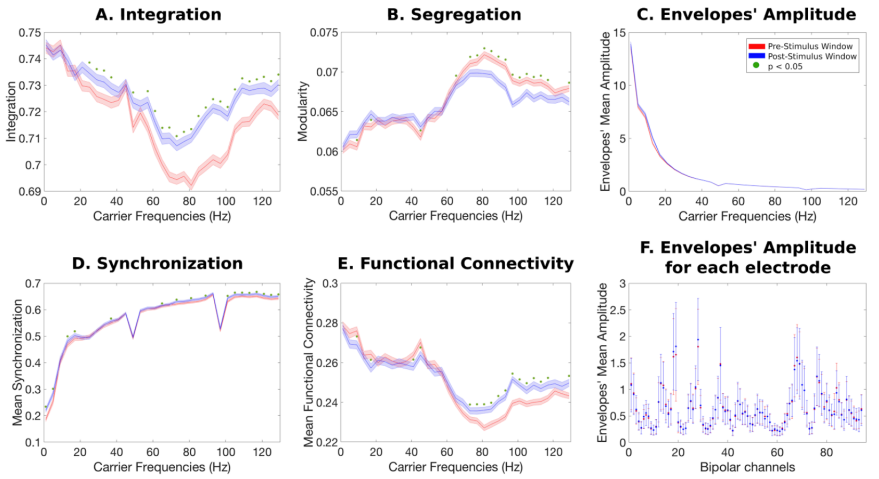

Figure 2.3 Results analysis patient K for the picture-naming task

Panel A shows a significant increase in the integration during cognitive processing. The greatest effect is observed in the gamma range (50–90 Hz). The red line corresponds to pre-stimulus window, the blue line corresponds to post-stimulus window, the shaded error regions reflect the standard deviation across trials and green dots indicate a statistical significance of $p < 0.05$ ($N = 1000$). Complementary to the integration, panel B shows a decrease of the modularity in the same frequency range. Panel C shows that there are no iEEG oscillations amplitude changes in any frequency induced by the stimulus (both curves are strongly overlapped). This result indicates that the increase of integration and decrease of modularity could not be explained by changes in the oscillations amplitude. Panel D shows an increase of mean synchronization over a broad range of frequencies that is more conspicuous in the gamma band range (50–90 Hz) for the post-stimulus window. Panel E shows that the functional connectivity behaves coherently with the other results, as it increases as a function of the stimulus presentation particularly in the gamma range. Panel F plots the amplitude of the oscillation's envelope at 60 Hz for each bipolar channel and pre- and post-stimulus window. There are no noticeable modulations across single bipolar channels between pre- and post-stimulus window. Note that the sharp peaks at 50 and 100 Hz are due to the power-line noise created by the electrical power.

Second, the modulation of integration and segregation associated with the cognitive task was related to an increase in the global synchronization of cortical activity (measured using the Kuramoto Order Parameter). This increase was present over a broad range of frequencies, being the largest at the gamma range (50–90 Hz) (Figure 2.3D).

Third, we assess whether integration and segregation were related to differences in Functional Connectivity between channels. This connectivity was calculated by considering the instant amplitude envelopes of all frequencies. Indeed, the Envelopes' Functional Connectivity is enhanced during task performance, in particular in the gamma range (50–90 Hz) (Figure 2.3E).

When comparing two different time windows in which no task was performed, no changes in integration and segregation were found. Figure 2.4A–B shows the lack of integration and segregation modulation when we contrasted the pre-stimulus windows of half the trials against the other half (same windowing as before, i.e., 500 ms before stimulus presentation). This result suggests that changes in these two measures are related to cognitive processing.

Altogether, these observations reveal that changes in integration and segregation (and their relationship) are likely related to a global increase in the connectivity, especially in the gamma band. Furthermore, changes in oscillations' envelope amplitudes cannot explain these phenomena. This pattern is consistent with the notion that communication between different brain networks is accomplished by means of the level of synchronization as posited by the Communication Through Coherence Theory (CTC) (Fries, 2005, 2015).

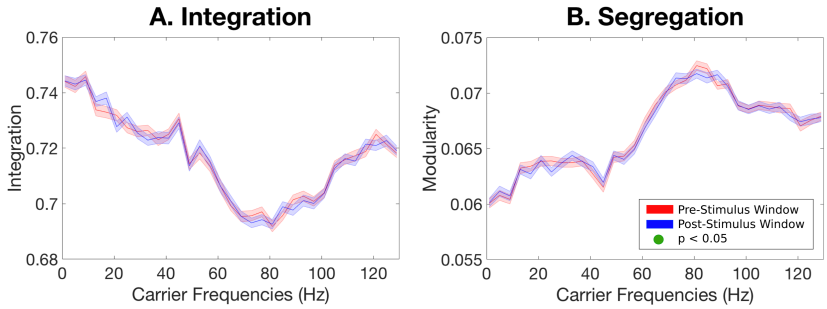

Figure 2.4 Inter pre-stimulus presentation window comparison for the picture-naming task

Panel A shows the result of the measure of Integration, and panel B shows the result of the measure of Segregation, when contrasting half of pre-stimulus trials against the other half. There is no modulation of any of the two measures before stimulus presentation. The red line corresponds to 50% of pre-stimulus windows; blue line corresponds to the other 50% of pre-stimulus window. The shaded error regions reflect the standard deviation across trials. Green dots indicate a statistical significance of P < 0.05 (N = 1000).

When looking at all patients, and despite the heterogeneity of the recording sites, the same pattern of modulation is observed for each individual as can be appreciated in Figure 2.5 and Figure 2.6, (Figure 2.7 shows the group average data for both measures). Interestingly, in most of the patients, there is a consistent decrease in the segregation in the gamma band but with a slight increase in the segregation in the sub-gamma regime. This is not observed for the integration measure. Furthermore, differences in oscillations' envelope amplitude at 60 Hz for each bipolar channel do not differ between pre- and post-stimulus windows (Figure 2.8).

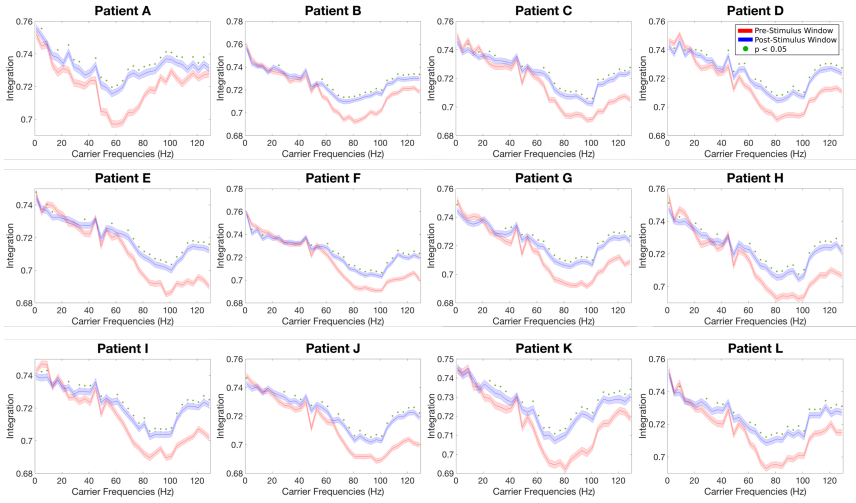

Figure 2.5 Integration measure results for each patient

Panels show the results for every single patient for the picture-naming task. As can be seen, despite the heterogeneity of the recording sites, all patients show a significant increase of the integration related to cognitive processing. For all patients, the greatest effect was found in the gamma range. The red line corresponds to pre-stimulus window, blue line corresponds to task condition, the shaded error regions reflect the standard deviation across trials and green dots indicates a statistical significance of $p < 0.05$ ($N = 1000$).

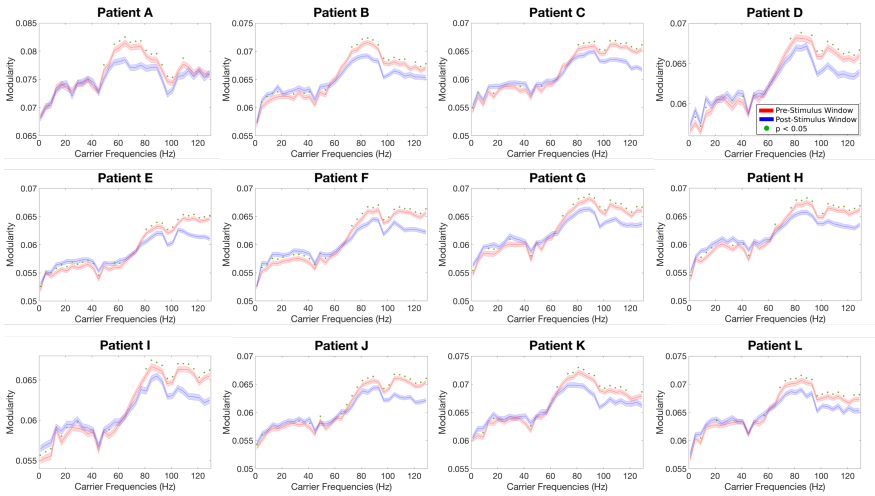

Figure 2.6 Segregation measure results for each patient

The panels show the results of segregation (measured by the modularity) during pre- and post-stimulus window for the picture-naming task. For all patients, there is a significant decrease of the segregation during cognitive processing and the greatest effect can be seen in the gamma range (50–90 Hz). The red line corresponds to pre-stimulus window, blue line corresponds to post-stimulus window, the shaded error regions reflect the standard deviation across trials and green dots indicates a statistical significance of $p < 0.05$ ($N = 1000$).

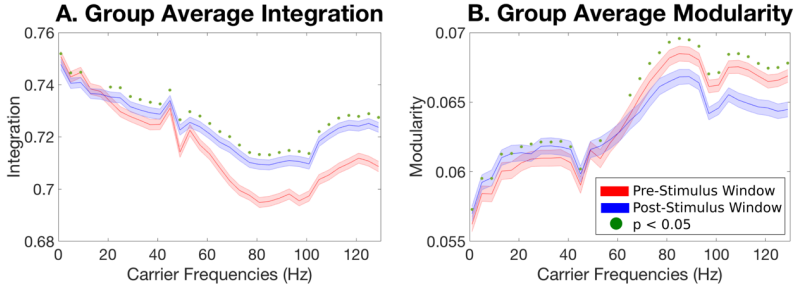

Figure 2.7 Group Analysis

Panel A shows a significant increase in integration during cognitive processing for almost all frequencies, but with the greatest effect in the gamma range (60–100 Hz)

as seen on each single subject. Complementary to the integration, panel B shows a decrease of the modularity which is more prominent in the high gamma range. The red line corresponds to pre-stimulus window, the blue line corresponds to post-stimulus window, the shaded error regions reflect the standard deviation across trials and green dots indicates a statistical significance of $p < 0.05$ ($N = 1000$).

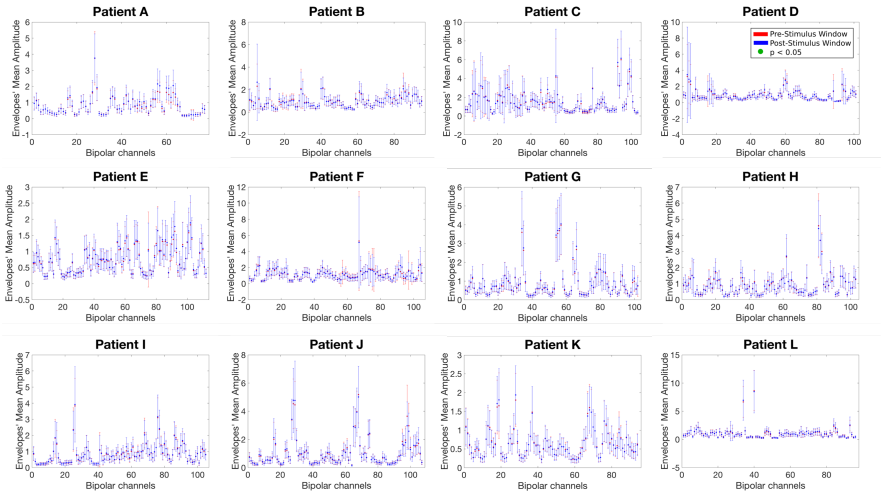

Figure 2.8 Envelopes' Amplitude at 60 Hz across electrodes for each patient

The panels show the results of the mean amplitude and std at 60 Hz for each bipolar channel and both pre- and post-stimulus window for the picture-naming task. For all patients, there is no noticeable modulation across single bipolar channels between pre- and post-stimulus windows. The red line corresponds to pre-stimulus window and the blue line corresponds to post-stimulus window. The shaded error regions reflect the standard deviation across trials. Note the strong overlap of both lines. Green dots indicate a statistical significance of $p < 0.05$ ($N = 1000$).

Importantly, the integration and segregation modulations calculated at 60 Hz were highly correlated (Figure 2.9). Conversely, the network measures were independent of patient's performance (correlation coefficient of 0.0242, N = 12 patients).

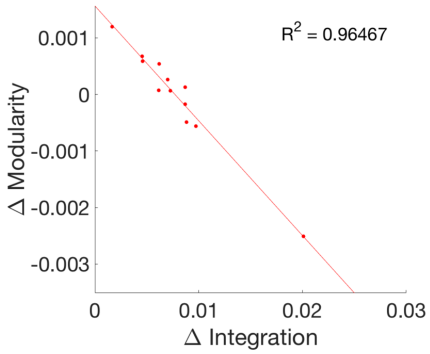

Figure 2.9 Correlation between Integration and Segregation

The figure shows the coefficient of determination between the integration and segregation measures across patients (N = 12) at 60 Hz. The R^2 represents the proportion of variance explained by a linear model. Note that both measures are highly correlated.

The main results were robust since they were also observed in the other two tasks: a lexical decision task and a size judgement task (see Materials and Methods). Accuracy in both tasks was high ($81.8 \pm 5.1\%$ and $88.7 \pm 8.3\%$ respectively) and response times for the lexical decision task was 1481 ± 398 ms and for the size judgement task 1008 ± 287 ms. A significant increase in the integration in the post-stimulus window was observed in the two tasks, as shown for one patient (see Figure 2.10). Furthermore, the most significant modulation appears in the gamma band (around 50–90 Hz) for both measures, and no changes in the oscillation's envelope mean amplitude was observed.

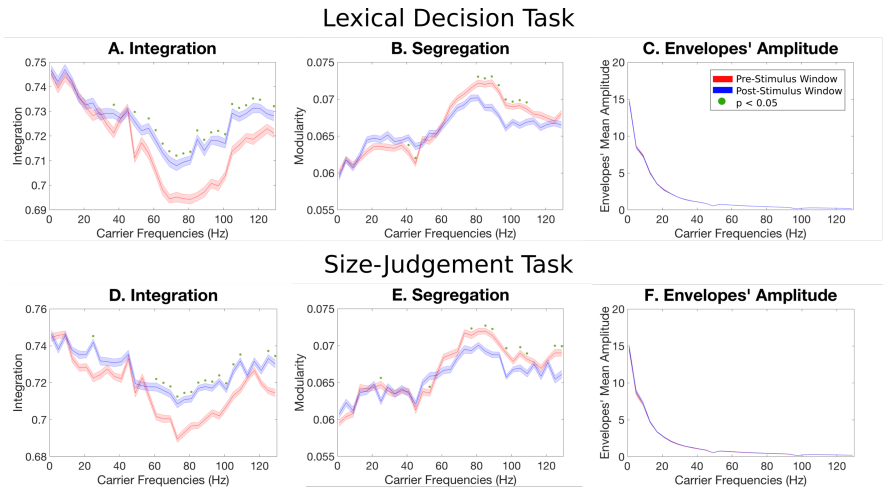

Figure 2.10 Results analysis patient K for the Lexical Decision and Size-Judgement Task

Panels A and D shows a significant increase in the integration in the post-stimulus window (red line) compared to the post-stimulus window (blue line). The greatest effect is observed in the gamma range (50–90 Hz). The shaded error regions reflect the standard deviation across trials. Green dots indicate a statistical significance of $p < 0.05$ ($N = 1000$). Complementary to the integration measure, panels B and E shows a decrease of Segregation in the same frequency range. Panels C and F shows that there are no oscillations' envelope amplitude changes in any frequency induced by the stimulus (both curves are strongly overlapped). Note that the modulatory effect is almost the same for both tasks.

The global nature of the integration is demonstrated by analyzing different subnetworks independently. In two patients, we use the precise anatomical location of each electrode channel and perform the integration analysis restricted to three specific subnetworks, namely the frontal, temporal, and parietal. As shown in Figure 2.11, even though the greatest modulations were found in both right and left temporal lobes, the parietal and frontal subnetworks were also modulated due to cognitive processing. This suggests that the broadcasting of communication across the brain has a global nature.

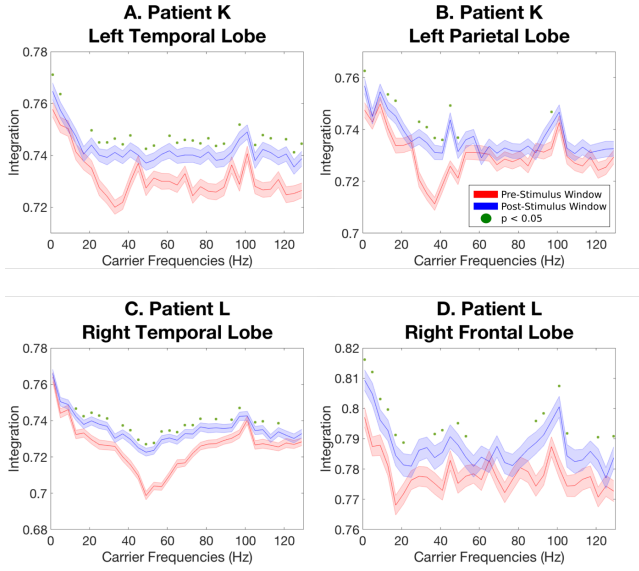

Figure 2.11 Results of the analysis of sub-networks within frontal, temporal and parietal lobes for the picture-naming task

The upper panels show a significant increase of the integration in the post-stimulus window (red line) compared to the post-stimulus window (blue line) in the left Temporal (A) and left Parietal (B) lobes for patient K. The greatest effect is observed in the gamma range (50–90 Hz). The shaded error regions reflect the standard deviation across trials. Green dots indicate a statistical significance of $p < 0.05$ ($N = 1000$). Panels (C) and (D) shows the results of the right temporal and Frontal lobes respectively, for patient L. The modulatory effect is seen in the whole range of frequencies.

Regarding technical issues, it is essential to note that the results are independent of whether we used a bipolar or monopolar montage. We compared the new integration/segregation measurements with the more classical approach considering the pairwise changes in the FC between the post- and pre-stimulus windows (see Figure 2.12 for a single patient). The results are consistent with the previous analysis and confirm the robustness of the findings. Figure 2.12 C and D

shows the FC matrices calculated at 60 Hz for the pre-stimulus window and post-stimulus window, respectively. The difference between both matrices demonstrate the distributed character of the modulation across many different nodes (Figure 2.12E). Furthermore, this result supports the notion that the cognitive-driven global changes in integration and segregation are indeed not associated with any particular anatomical position inside the networks considered. Supplement Figure S2.1 shows the results for all patients.

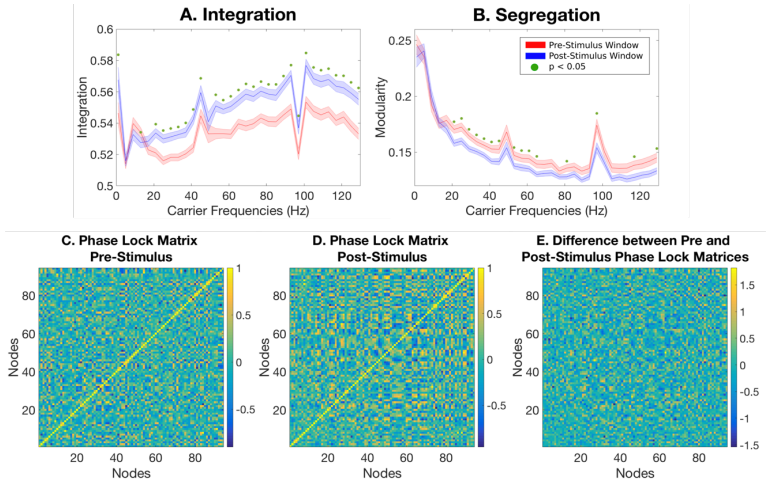

Figure 2.12 Results analysis using the FC matrix based on the monopolar montage for Patient A

Panels A and B show the integration and segregation modulation during pre- and post-stimulus presentation, respectively, for the picture-naming task. The red line corresponds to pre-stimulus window, blue line corresponds to post-stimulus window. The shaded error regions reflect the standard deviation across trials and green dots indicate a statistical significance of $p < 0.05$ ($N = 1000$). Panels C and D shows the FC matrices computed for 60 Hz for the pre- and post-stimulus windows respectively. Panel E shows the difference between pre- and post-stimulus windows. The differences between both matrices (C and D, expressed on E), evidence the distributed character of the modulation across many different nodes.

Interestingly, the integration measure we use differs and complements the more classical measure of pairwise Functional Connectivity. As shown in Figure 2.13, there is no correlation between the integration measure and the mean changes in the FC between the post- and pre-stimulus windows for different frequencies in the gamma range.

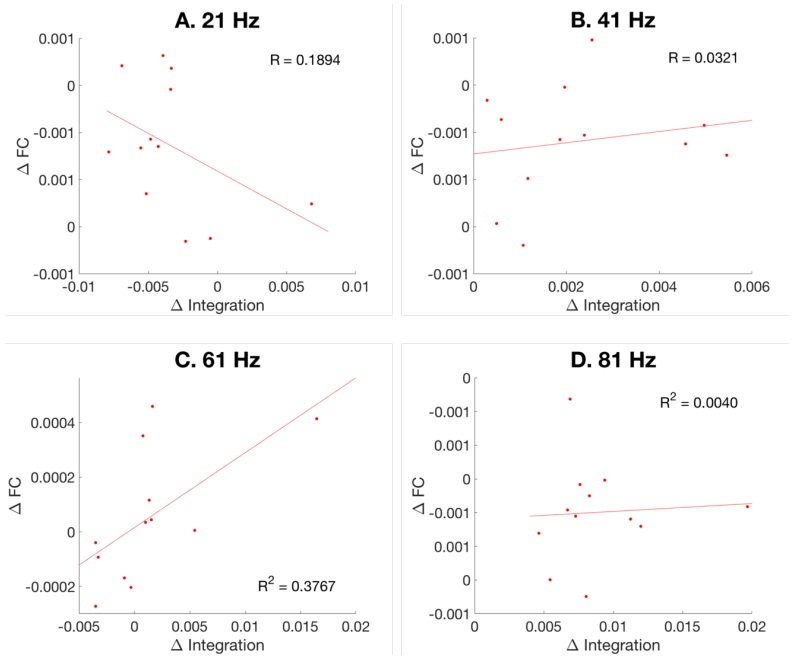

Figure 2.13 Correlation between Integration and Functional Connectivity

The figure shows the coefficient of determination between the integration and the mean variance of the functional connectivity calculated at 20, 40, 60 and 80 Hz across the studied patients (N = 12) based on the monopolar montage. The R^2 represents the proportion of variance explained by a linear model. In all cases there is no correlation between both measures.

Finally, we found that the modulation of integration is not solely driven by the stimulus's presentation, but it is persistently increasing after its onset. For this purpose, we extended the analysis of the integration measure by using the phase-lock matrix; a more explicit measure of communication according to CTC theory). The phase-lock matrix characterizes the global state of mutual synchronization between all pairs of network nodes at each single time point. Thus, with this matrix, we are able to study the temporal evolution (in milliseconds) of the integration across time (see Figure 2.14). This result was found in all three tasks.

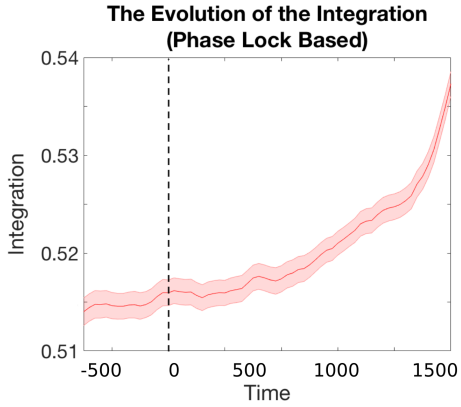

Figure 2.14 Time evolution of the Integration measure for Patient K during the picture-naming task

The figure shows the integration measure calculated for the phase-lock matrix for every single time point for the whole period of time at 80 Hz. As seen, there is a monotonic increasing behavior of the integration starting after the stimulus onset. The shaded error regions reflect the standard deviation across trials.

Discussion

As a complex system, the human brain is organized into large-scale networks. In order to support cognitive functions, these networks need to flexibly adjust their functional connectivity to integrate relevant information towards a goal-directed behavior (Bola & Sabel, 2015; Bressler & Menon, 2010; Deco et al., 2015). Traditionally, graph and theoretical information approaches have helped to characterize the global network connectivity in terms of *segregation* and *integration* (Deco et al., 2015; Fox & Friston, 2012; Sporns, 2013; Tononi et al., 1994). *Segregation* refers to the relative statistical independence of subsets of neurons or brain regions to compute information (Sporns, 2013; Tononi et al., 1994), while *integration* is a complementary concept quantifying the connectivity level across the whole-brain (Deco et al., 2015; Sporns, 2013). In particular, we used a measure of integration associated with the broadness of communication quantified by the length of the largest connected component of the functional connectivity across the whole brain (Deco et al., 2015), while for segregation we used the concept of modularity (Rubinov & Sporns, 2011).

We used intracranial EEG (iEEG) to record neural activity from 12 patients with epilepsy while they were performing three different cognitive tasks. We focus on how cognition modulates *global* functional network measurements, namely integration and segregation. We found a significant increase in integration and a decrease in segregation during cognitive processing, especially in the gamma band (50–90 Hz). This was so for all patients and all tasks. Furthermore, these modulations were not associated with changes in the underlying level of oscillations. We also found a significantly higher level of synchronization and functional connectivity during task processing, again, particularly in the gamma

band. This set of results suggest that changes in the broadness of communication across the entire extended network associated with cognitive processing could be due to a rearrangement of the coherence level between the nodes. This interpretation fits the predictions of the CTC theory extended to the whole-brain level (Deco & Kringelbach, 2016; Fries, 2005, 2015).

Our results extend the CTC hypothesis to the mesoscopic/macroscopic level by analyzing the phases and correlations of the envelopes of the Band Limited Power, as proposed by Deco and Kringelbach, 2016. This is important since the CTC hypothesis posits that information is transmitted by synchronizing distinct neuronal populations, mainly in the gamma and beta-band (30–90 Hz) (Deco & Kringelbach, 2016). Note that the original CTC theory is based on a phase synchronization mechanism defined at the neuronal level.

Our findings are in line with previous neuroimaging studies showing increases in the integration across brain networks (Kinnison et al., 2012; Kitzbichler et al., 2011; Liang et al., 2015). There is also substantial agreement with studies using FC measurements that have revealed that local computations are likely to be highly segregated in spatially distributed network communities with clustered connectivity (Bassett et al., 2011; Bola & Sabel, 2015; Ekman et al., 2012; Power et al., 2011; Wang et al., 2016). Nevertheless, it is important to note that our methodological approach is different from the classic FC approach and adds some critical information. In our results, the fact that integration and FC measures of band-limited power were not correlated suggests that the FC per se is not giving explicit information about how much the network is clustered. Indeed, one can have higher correlations but a lot of functional segregated clusters, which in our measure is associated with low integration.

When analyzing the performance, we did not find correlations between it and the modulation of the integration and segregation. Although we cannot presently elucidate the dynamical properties that lead to better performance, the present findings suggest that the behavioral errors in our experiment are not captured in the time window we were looking at or were not due to a failure at the global level of communication, but probably caused by failures at the local level of specific processing.

Interestingly, despite the global shift towards segregation in the gamma band during the task, we observed a slight increase in segregation in the sub-gamma band. The decrease of the segregation in the gamma regime is expected and consistent with the increase of integration in the same regime, which is putatively linked to increased stimuli/cognitive processing (Fries, 2015). Along the same lines, the increase of segregation in the sub-gamma bands could perhaps be associated with disengagement of large slow resting networks. Future research is needed to understand this difference in sub-gamma bands.

It is important to remark that our results support the global nature of the functional large-scale network reorganization during cognitive processing. We demonstrate here that the pattern observed, that is an increase of the integration and a decrease of the segregation, appears in all patients irrespective of the heterogeneity of the implantation scheme. Moreover, this pattern is consistent when using a monopolar or bipolar montage. Further strengthening the results, we analyzed three different cognitive tasks, and we show that the main modulatory effect on the integration and segregation, and the validity of the CTC theory is independent of the particular cognitive processing. Thus, because of our global perspective, unlike many previous studies, we did not investigate the role of single channels in the different cognitive processes. Nevertheless, we are convinced that localizing these electrodes in the human brain could lead to the discovery of

interesting differences at the local spatial level and that this could be a very interesting goal for future investigations.

Our methodology and results open new avenues for further investigations. First, we need to understand how integration and segregation measures are modulated by task performance and/or task difficulty. Second, it is important to determine which specific brain areas, or local networks, show the highest degree of task-driven effective connectivity and therefore are mostly involved in information processing. Thus, future studies could greatly benefit from diffusion tensor imaging in two ways: to visualize and describe the precise connectivity between the electrodes in the brain, as well as the basis of whole-brain models considering the connectivity and continuity of neural pathways in the patients.

Finally, we are aware of the potential methodological limitations of the iEEG technique with patients with epilepsy. First, these patients as compared to healthy controls, not only have epileptogenic neural activity but may also have differences in the structural connectivity. Second, the lack of whole-brain coverage difficult to draw claims about the global network connectivity, given that restricted spatial coverage is simultaneously sampled. Still, and despite that the cognitive-driven changes observed on integration and segregation come from a reduced set of brain regions, we hypothesize that the effect is global across the whole brain. Thus, we predict that those changes should be consistently observed in fMRI and/or EEG/MEG experiments.

Conclusions

In this chapter, we demonstrate that cognitive processing is associated with a global increase of integration and decrease in segregation, especially in the gamma band (50–90 Hz). These modulations probably reflect changes in how information is broadcasted in the brain. Going beyond our current knowledge on integration and segregation (for a review, see Sporns and Betzel, 2016), we also show that such modulations were associated with a rearrangement of the band-limited functional connectivity between the different nodes and not with changes in the level of the underlying oscillations. This whole set of results is consistent with the "Communication Through Coherence" Theory.

CHAPTER 3

The Phase of Theta Oscillations Modulates Successful Memory Formation at Encoding

"Science may set limits to knowledge, but should not set limits to imagination"

—Bertrand Russell (1872—1970)

Several studies have shown that attention and perception can depend upon the phase of ongoing neural oscillations at stimulus onset. Here, we extended this idea to the memory domain. We tested the hypothesis that ongoing fluctuations in neural activity have an impact on memory encoding using a pair-associate task to gauge episodic memory performance. In a first experiment, we capitalized on the principle of phase reset to test if subsequent memory performance fluctuates rhythmically, time-locked to a reset cue. We found indication that behavioral performance was periodically and selectively modulated at theta frequency (~4 Hz). In a second experiment, we focused on prestimulus ongoing activity using scalp EEG recorded while participants performed the pair-associate task.

We analyzed subsequent memory performance as a function of peri-stimulus theta and alpha activity around the presentation of the to-be-remembered item. We found that post-stimulus theta-power increases in left frontal scalp predicted subsequent memory performance. When narrowing down the analysis of prestimulus activity to the scalp location and frequency of this post-stimulus power effect, we found a correlation between the prestimulus theta phase and subsequent memory. Altogether, the results suggest that the prestimulus theta activity at encoding has an impact on later memory performance.

The Role of Theta Oscillations in Memory Processes

In our daily life we are bombarded with myriad stimuli and events. Some of them are later remembered, whereas others are just forgotten. Although several processes influence our ability to remember, it is generally agreed that in all cases later recognition strongly relies on successful memory formation (Brassen et al., 2006; Wimber, Heinze and Richardson-Klavehn, 2010; Jutras, Fries and Buffalo, 2009). The subsequent memory paradigm has proven a successful procedure to study the neural underpinnings of memory formation in various types of memory systems (Paller, Kutas and Mayes, 1987; Hanslmayr and Staudigl, 2014; for review see Paller and Wagner, 2002). This paradigm usually compares neural activity following the onset of stimuli as a function of whether they are later remembered or not. Differences, known as subsequent memory effects (SMEs), can help identify memory processes involved at encoding that facilitate later recall. Studies employing this approach have revealed that the brain activity during encoding is relevant for whether the stimulus will be subsequently remembered (Brewer et

al., 1998; Wagner et al., 1998; Fernández et al., 1999; Kirchhoff et al., 2000; Strange et al., 2002; Sederberg et al., 2003; for review see Paller and Wagner, 2002; Kim, 2011). Many of these studies support the notion that oscillations in neural activity at the moment of encoding, just after the stimulus is presented, are associated with effectiveness in later recall (for review see Klimesch, 1999; Hanslmayr and Staudigl, 2014). In particular, evidence for the role of neural oscillations in episodic memory formation comes from EEG/MEG studies—using the SME approach—which show that increases in theta (4—8 Hz) and gamma (>30 Hz) power, and decreases in alpha (8—13 Hz) and beta (13—30 Hz) oscillatory power, are associated with more effective recall (Backus et al., 2016; Lega, Jacobs and Kahana, 2012; Sederberg et al., 2003; Staudigl and Hanslmayr, 2013). However, while the association between oscillatory power and memory formation in humans has been investigated in numerous experiments, only a handful of studies have explored the potential role of the oscillatory phase. These studies provide evidence for a role of phase synchronization among different sensory cortices in the theta frequency during memory formation (Backus et al., 2016; Clouter, Shapiro and Hanslmayr, 2017).

The studies mentioned above have considered oscillatory activity after the stimulus to be encoded (evoked or induced). In addition, the previous results suggest that fluctuations in neural activity even *before* stimulus presentation for encoding might also play a role in determining whether or not a stimulus will be later remembered (Park and Rugg, 2010; Haque et al., 2015; Otten et al., 2006; Otten et al., 2010; Guderian et al., 2009; Fell et al. 2011; Rutishauser et al., 2010; Addante et al., 2015). Notably, the phase of the ongoing low-frequency oscillations appears to reset at the moment of the presentation of behaviorally relevant stimuli (Rizzuto et al., 2003; Haque et al., 2015). This shift in the dynamics of prestimulus ongoing oscillations might play a fundamental role in the synchronization of neuronal populations and the coordination of information transfer

necessary for efficient encoding. In fact, some studies show that phase synchronization is more precise during encoding of information that is later remembered compared to later forgotten, most likely acting as the "gluing mechanism" for binding human memories (Buzsaki and Draguhn, 2004; Backus et al., 2016; Hanslmayr, Staresina and Bowman, 2016; Clouter, Shapiro and Hanslmayr, 2017; for review see Fell and Axmacher, 2011). Altogether, these findings suggest that memory formation not only depends on stimulus-driven processes but also on endogenous brain states at the time of stimulus presentation. Here, we set out to address this question: does the phase of prestimulus ongoing oscillations have an impact on memory formation?

A similar question has been addressed by previous research in the domain of perception and attention in humans. In particular, some studies have related stimulus detection with the phase of the ongoing oscillations at stimulus onset. These studies have revealed cyclic alternations in behavioral performance mainly in the theta and alpha bands (~4–8 and 8–12 Hz, respectively) (Busch, Dubois and VanRullen, 2009; de Graaf et al., 2013; Klimesch, Sauseng and Hanslmayr, 2007; Mathewson et al., 2009; Palva and Palva, 2007; VanRullen, 2016; but see also Ruzzoli et al., 2019 for conflicting evidence). The main idea behind this phenomenon is that oscillatory neuronal activity reflects rhythmic fluctuations in the neuron's membrane potential, which are associated with changes in neuronal excitability (Buzsaki and Draguhn, 2004; Lakatos et al., 2005; Fries et al., 2007). These fluctuations can be reflected in the EEG signal when large neuronal populations are synchronized. In the case of perception, low-frequency oscillations may gate neural responses to incoming sensory information, producing peaks and troughs that correspond to favorable and unfavorable states for sensory processing. We hypothesize that if the phase of slow ongoing oscillations can modulate perceptual processing, then the phase of

prestimulus fluctuations may also modulate encoding efficiency and hence, the success in later memory performance.

We tested this hypothesis using a paired-associates memory task in two experiments performed by separate groups of healthy participants. Participants were instructed to memorize a short sequence of image pairs and then asked whether newly presented pair probes had been previously presented associated or not.

In the first experiment, we used the logic of phase reset (Rizzuto et al., 2003) on behavioral performance. We tested if subsequent performance fluctuates rhythmically time-locked to a cue (phase-reset signal) presented before the to-be-remembered pairs of pictures. According to our hypotheses, we focused the analysis on low frequencies, ranging from 2 to 20 Hz. In the second experiment, we tested the role of ongoing low-frequency neural oscillations—before the presentation of the picture pairs—in subsequent recognition performance using EEG. Specifically, we focused on the phase and amplitude of alpha and theta oscillations. To do so, we examined prestimulus changes in the EEG as participants performed the task adapted from Experiment 1 but capitalizing on spontaneous neural oscillations instead of phase reset. The hypotheses and analysis pipeline of Experiment 2 were pre-registered based on the results of Experiment 1 (see below; pre-registration available at https://osf.io/4f5qc/). The pre-registered pipeline did not yield significant results; therefore, we further explored the data following a data-driven approach.

Experiment 1

Ethics Statement and Participants

The Clinical Research Ethical Committee of the Municipal Institute of Health Care (CIEC-IMAS) Barcelona, Spain, approved the study. Following the Declaration of Helsinki, all subjects gave written consent before their participation.

Data from 30 healthy subjects (21 females, mean age 23.2 ± 4.5 years, 5 left-handed) were used in the behavioral study. Data from 8 additional subjects were excluded based on the predefined inclusion criteria (demographic characteristics of each subject are detailed in supplement Table S3.1). The inclusion criteria were set up to ensure both, a sufficient number of trials in each response category (hit/miss), and that participants responded above chance level (for more details about inclusion criteria see Experimental Design and Procedure). Participants were compensated with 10€/hour.

Experimental Design and Procedure

Participants performed a visual paired-associates memory task (Figure 3.1A) adapted from Haque and colleagues (Haque et al., 2015). In our version of the paradigm, participants were asked to memorize pairs of pictures instead of pairs of words. Participants sat ~60 cm away from a 21-inch CRT computer monitor (60 Hz refresh rate). Stimulus presentation was controlled using Matlab (Version R2016a, The MathWorks, Inc., MA, USA) and the Psychophysics Toolbox (Brainard, 1997; Kleiner et al., 2007).

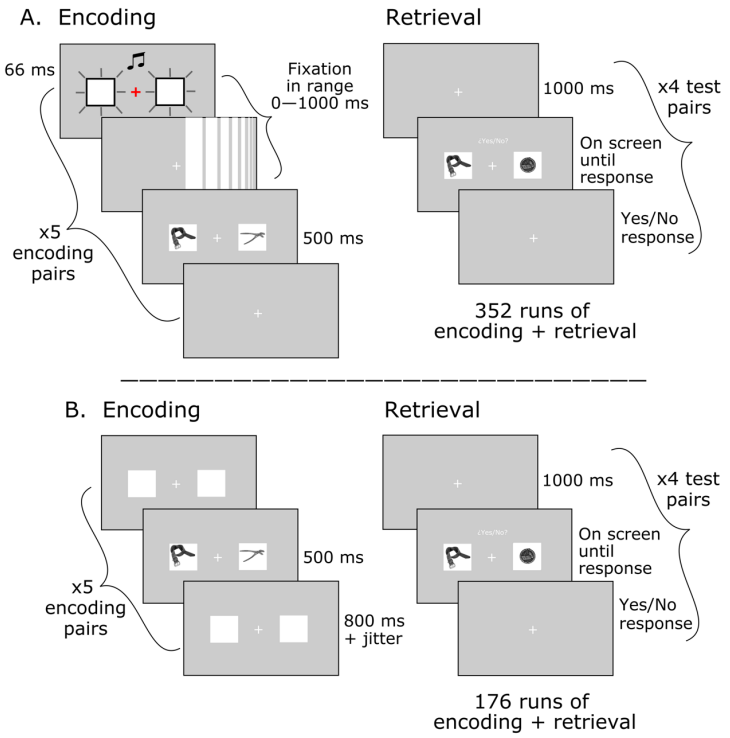

Figure 3.1 Experimental Design

A) Experiment 1. Participants performed a visual pair-associates memory task. During the encoding block, participants were asked to learn five unrelated image pairs presented side-by-side on placeholders for 500 ms. A cue—composed by a central fixation cross and placeholders—flashed once synchronously together with a sound-beep before each image pair presentation. Critically, the time-lag between the cue and the image pair to be encoded (the cue-to-target interval) was varied randomly between 0 and 1000 ms. Each encoding block was followed by a four-trials recognition block where participants judged whether a given image pair had been presented together in the previous encoding block. Each participant provided a total of 1.408 responses. B) Experiment 2. The experimental design was identical to Experiment 1 with the following exceptions: During the encoding block, image pairs were sequentially presented at a variable stimulus-onset asynchrony (SOA), with a jitter according to an exponential distribution (mean 1s) to compensate for hazard rate and prevent temporal expectation. Each image pair was followed by a blank inter stimulus interval (ISI) of 800 ms. Each participant performed half of the task, thus providing a total of 704 responses.

Due to the large number of trials, the experiment was completed over two sessions on different days within the same week (on average, three days apart). In total, it consisted of 352 runs, each composed of an encoding block of five pairs followed by a recognition block with four memory probes. Each participant provided a total of 1.408 (352x4) responses throughout the experiment.

During the encoding blocks, five image pairs in placeholders were presented in sequence with a central fixation cross in between them (placeholders and fixation were present throughout the block). Before each image pair, an audio-visual reset cue was presented. The reset cue consisted of a flash of fixation and placeholders synchronized with a sound and was intended to modulate cortical excitability by phase resetting the ongoing oscillatory activity (Lakatos et al., 2009; Fiebelkorn et al., 2011; Daitch et al., 2013). Critically, the interval between the reset cue and each target image pair to be encoded (cue-to-target interval) varied between 0 and 1000 ms in steps of 16.7 ms (62 unique times). Then, each image pair appeared for 500 ms, followed by 1500 ms interval that led to the next reset cue. We adopted this strategy to appreciate potential oscillations in behavior without using EEG to measure ongoing brain signal fluctuations. Since, based on the hypothesis, we focus on fluctuations >2 Hz, our window of interest was 0 to 500 ms. Hence, the probability of occurrence of targets within the 0-500 ms interval was doubled compared to longer time intervals (500 to 1000 ms). Long-time intervals were only included to make the stimulus onset less predictable within the times of interest, but they were not used for the analysis. We expected the audio-visual cue to reset the phase of the ongoing oscillations, so then behavioral performance at the recognition blocks should present an oscillatory pattern time-locked to the cue presentation.

Each encoding block was followed by a recognition block that consisted of a sequence of four test image pairs. On each test pair,

participants had to judge whether the two images had been presented together (paired) in the preceding encoding block. The test pairs always contained items that had previously appeared in the encoding block (whether paired or not), so that the task could not be solved by just recognizing the appearance of new items. Each image pair was preceded by a prompt—a row of question marks—that appeared on the screen for 500 ms followed by a blank interval of 1000 ms. The image pair, placeholders, and fixation cross remained on the screen until the response (yes/no) was collected through the keyboard. To minimize the number of false alarms, participants were encouraged to respond yes only when they were confident about their response and to say no if doubting. Image pairs in the recognition block could be a match (if they had appeared together in the encoding block) or a mismatch (if they appeared in different pairs during encoding). Matched pairs were slightly more likely (60% on average), compared to mismatch pairs, to ensure enough useful trials for analysis. Each recognition block could have a different number of yes/no correct responses to prevent guessing by response history. After every 10 runs (encoding plus recognition blocks), participants took a break and were updated on their overall performance to control for false alarms and keep them engaged in the task.

Prior to analysis, we established a set of individual inclusion criteria regarding performance: (1) false alarm rate below 15%, (2) hit rate above 35% to ensure that with the maximum false alarms rate accepted the participants responded above chance level, and (3) hit rate below 80% to avoid ceiling effects. These criteria were defined to ensure enough number of trials in each response category (hit, miss), allowing the possibility to capture fluctuations in behavior—in the case they existed.

Stimuli

The pictures used in the pairs were images of familiar objects in a usual perspective, from a wide range of semantic categories selected from two databases: The Bank of Standardized Stimuli (BOSS) (Brodeur et al., 2010; Brodeur et al., 2014) and the set of 2400 Unique Objects used in Brady et al. (Brady et al., 2008). Stimulus characteristics are described in detail in previous studies (Brodeur et al., 2010; Brodeur, Guerard and Bouras, 2014; Brady et al., 2008). The two sessions of the experiment used different image sets. Within a pair, images belonged to different semantic categories. Living objects were not mixed with non-living objects either on the same trial or block (80% of the pairs corresponded to non-living objects). All images were converted to black and white to avoid memory facilitation based on color associations (Lewis et al., 2013). Image size was subtending a square of approximately 5 degrees of visual angle. The auditory stimulus used as resetting signal was a beep sound (4000 Hz, ~60 dB, 66 ms) presented through headphones.

Behavioral Analyses

The goal in this experiment was to address if behavioral performance at recognition fluctuated rhythmically as a function of the reset cue (cue-to-target interval) at encoding. We followed the analytical method described in Fiebelkorn (Fiebelkorn et al., 2013) to extract rhythmic variations of behavioral performance. For each participant, we only used responses to match trials to obtain hit and miss rates. To get a temporally smoothed series relating memory behavior to encoding time, we first calculated the hit rate in a sliding 50 ms window (16.7 ms steps) for the whole window of interest (from 0 to 500 ms), and we averaged time-dependent hit rate across participants. Then, we used a Fast Fourier Transform (FFT) to extract the spectral

pattern of the detrended behavioral time series and focused our analyses in the 2—20 Hz frequency range. The minimum and maximum frequencies of interest were determined by the window of interest (500 ms) and the width of the sliding window used to calculate time resolved hit rate (50 ms). We sought for oscillatory patterns above and beyond chance within this spectral window based on the theoretical of low frequencies.

To examine the reliability of the results, we assessed statistical significance using a non-parametric procedure with 10.000 randomly generated surrogates. For each participant, we permuted hit rates across the cue-to-target interval windows, averaged across participants, and extracted the surrogate power spectrum. The *p*-value corresponds to the proportion of permutations in which the surrogate value matched or exceeded the empirical value. We obtained the *p*-values for each frequency (9 frequencies) and then applied multiple comparisons correction with False Discovery Rate (FDR) using the Benjamini-Hochberg procedure (Benjamini and Hochberg, 1995) with an alpha level of 0.05.

Behavioral Performance Modulation by the Phase at which the Stimulus Arrive

We expected the time-resolved recognition performance to show a periodic component indicative of fluctuations time-locked to the cue at the encoding. Overall, participants performed above chance level with a mean hit rate of 62.97±10.74%, and a false alarm rate of 6.09±3.82% (individual hit and miss rates plus demographic data are detailed in the supplement Table S3.1). In line with the question of this first experiment, behavioral performance at recognition

fluctuated as a function of cue-to-target interval (Figure 3.2A). We used a FFT on the behavioral time series and found that memory performance was periodically and selectively modulated with a peak frequency of ~4 Hz (Figure 3.2B). Although this result was statistically significant (p<0.0398), it did not survive correction for multiple comparisons across all frequencies included in the test (2-20 Hz).

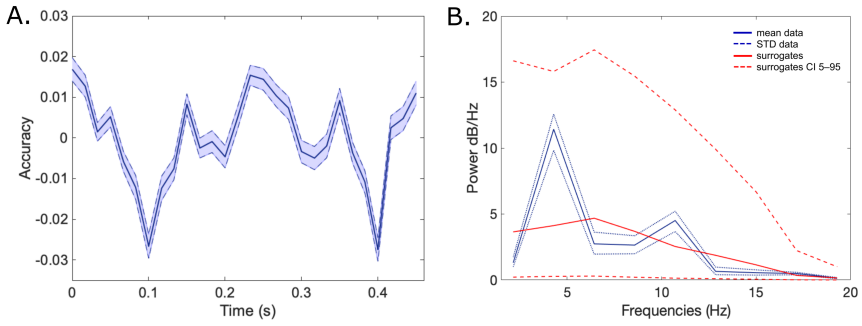

Figure 3.2 Behavioral Performance Modulation

A) Behavioral Performance. Mean hit rate and standard deviation across participants as a function of time (N=30). B) Power Spectrum. Amplitude measurement obtained using the FFT for the mean hit rate. As can be seen (blue line), there is a peak around ~4 Hz (theta band).

Because of the large spectral window analyzed (and the ensuing strong correction for multiple comparisons), our data provide only weak support for the hypothesis of a rhythmic modulation of behavioral performance at theta after phase resetting by the prestimulus cue. This putative modulation, if only tentatively, suggests that the phase in the theta band at which the stimulus arrives has an impact on later successful recognition. Despite the relatively

large spectral window analyzed and the unknown statistical power of the effect, we considered this result potentially indicative of the possible relevant frequency, and hence useful to narrow down on a more specific spectral window of interest for an EEG study, presented in Experiment 2.

Experiment 2

The aim in Experiment 2 was to investigate the role of ongoing low-frequency oscillations—before the to-be-encoded stimulus presentation—in subsequent recognition performance using EEG. Several neuroimaging studies have shown that frontotemporal regions are actively engaged during episodic encoding (Wagner, 1999; Kirchhoff et al., 2000; Hanslmayr et al., 2011; Park and Rugg, 2011; Griffiths et al., 2016). However, the results show contradictory evidence for theta frequency fluctuations of the local field potential: some provide evidence in favor of encoding-related increases (Herweg et al., 2016; Addante et al., 2011; Summerfield and Mangels, 2005; Osipova et al., 2006; Hanslmayr et al., 2011), other results report decreases (Fellner et al., 2016; 2019; Michelmann, Bowman and Hanslmayr, 2018). A well-accepted interpretation of these activations is that they reflect hippocampal theta, induced in cortical areas via hippocampal-cortical feedback connections (for a review see Herweg, Solomon and Kahana, 2020). Moreover, episodic-encoding is also associated with decreases in the alpha band in occipitoparietal regions (Klimesch and Doppelmayr, 1996; Klimesch et al., 1997; 2000), likely contributing to the encoding of visuospatial stimulus attributes and signaling directed attention (Klimesch, 1999; Klimesch et al., 2000). On these grounds, we focused our analysis on the phase and amplitude of the theta and

alpha oscillations in broad frontotemporal and occipitoparietal regions, respectively.

We hypothesized that the phase of the ongoing oscillations at which the to-be-encoded stimulus arrives modulates subsequent visual memory performance. If so, we expected to find fluctuations in behavioral performance as a function of the phase angle of the ongoing brain oscillation. The hypotheses and the initial analysis pipeline of this experiment were preregistered (https://osf.io/4f5qc/). In the results section below we indicate which part of the analyses belong to the pre-registered pipeline, and which ones are exploratory.

Participants and Ethics Statement

As in experiment 1, the local ethics committee approved the study, and all participants gave written consent before their participation.

Data from 30 subjects (15 females, mean age 22.9 ± 2.9 years, 5 left-handed) were used in the EEG study. Data from six additional subjects were excluded: 2 did not meet the behavioral inclusion criteria specified above, and 5 because of artifact contamination of the EEG (demographic characteristics of each subject are detailed in supplement Table S3.2). Participants were compensated with 10€/hour.

Experimental Design and Procedure

The experimental design and procedure were identical to Experiment 1 with the following three exceptions: First and foremost, since ongoing oscillations were registered directly with EEG, we did not use a reset cue. During the encoding blocks, image pairs were

sequentially presented at a variable inter-stimulus interval (ISI), without a prestimulus cue. Indeed, we expected the image pair presentation to work as a reset cue and link the phase of the ongoing oscillation at the image pair onset with subsequent behavioral recognition. The second difference was that the ISI was composed of a fixed 500 ms period plus a jitter according to an exponential distribution—with mean 1000 ms—to further increase temporal uncertainty (Figure 3.1B). And third, participants performed only one experimental session containing a total of 704 responses. The reduction in observations was justified by the advantage of measuring multiple frequency bands within one trial through EEG, and by the possibility to narrow down on the frequency band of interest for the analysis according to the result in Experiment 1 and hypothesis.

Stimuli

The stimuli were identical to the ones used in the first session of Experiment 1, namely, images taken from the Bank of Standardized Stimuli (BOSS) (Brodeur et al., 2010; Brodeur et al., 2014). All the stimuli were processed as described for Experiment 1

EEG Recording and Data Analyses

Electrical brain signals were recorded using an EEG system with 60 active electrodes (actiCAP, Brain Products GmbH) located according to the standard international 10–10 system and sampled at a rate of 500 Hz. Two electrodes placed at the right and left mastoids served for offline re-reference. An electrode placed at the tip of the nose

served for online reference, and the ground electrode was placed at AFz. Electrooculogram (EOG) was monitored on the horizontal and vertical directions to control for blinks and eye movements.

All data and statistical analyses were performed using custom code in Matlab (Version R2016b, The MathWorks, Inc., MA, USA), and the FieldTrip toolbox (Oostenveld et al., 2011). Raw EEG data were re-referenced to averaged mastoids, and a notch-filter at 50 Hz was applied to remove line contamination. To extract specific spectral information, we bandpass filtered the EEG data in two preselected frequency bands: theta (4–7 Hz) and alpha (8–14 Hz), using a second-order zero-phase Butterworth filter. The filtered data were then segmented from –500 ms to 100 ms with respect to the onset of each pair in the encoding blocks. Malfunctioning electrodes were removed, and their data were estimated based on neighboring electrodes using spline interpolation. Trials contaminated by blinks, muscle movements, or brief amplifier saturation were discarded from further analyses by visual inspection. As in Experiment 1, we were interested in the encoding phase of trials labeled as hit or miss according to participant´s response in the subsequent recognition block. Thus, only matching trials could be used for the analysis. To ensure a reliable estimation of oscillatory patterns, for a given participant, if the number of artifact-free trials in the less populated condition (hit or miss) was below 80, the entire participant's dataset was excluded.

Since we were interested in phase-dependent memory effects, our hypothesis capitalized on the endogenous oscillations in the EEG before the onset of image pairs at the encoding blocks. We compared the spectral power and the instantaneous EEG phases between hits and misses. Based on the results of Experiment 1 and previous literature (Addante et al., 2011; Sederberg et al., 2003; Nenert et al., 2012; Jensen et al., 2002; Schack et al., 2002; Summerfield and Mangels, 2005), we set the spectral-spatial regions of interest

(ssROIs). The frequencies and regions of interest were theta (4–7 Hz) for frontotemporal electrodes, and alpha (8–14 Hz) for occipitoparietal electrodes (see details in Figure 3.3). Data at electrodes belonging to the ssROIs at the specific frequency of interest were averaged at the individual participant level and then averaged over participants.

The Hilbert transform was used on the narrow-band filtered data to obtain, for each frequency f at time t, the associated complex analytical signal $s(t)$, defined by an instantaneous phase $\varphi(t)$, and an instantaneous amplitude $A(t)$, i.e., $s(t) = A(t)\cos(\varphi(t))$. We then calculated the intertrial coherence (ITC) separately for hits and misses for the time interval -500 to 100 ms relative to the image-pairs onset. The ITC is a direct measure of frequency-specific synchronization (Lachaux et al., 1999), and is given by,

$$ITC_{(t,f)} = \frac{1}{n}\sum_{n=1}^{k} e^{i(\varphi k_{(t,f)} 2\pi)}$$

Under complete independence across trials between EEG data and the time-locking events, ITC is nearly 0, representing absence of synchronization; whereas for ITC equals 1, all phases are concentrated, representing full synchronization.

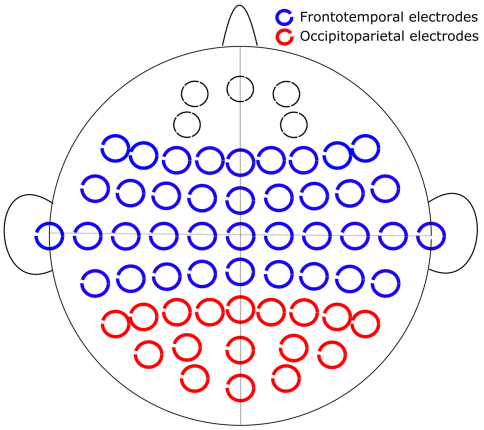

Figure 3.3 Map of scalp EEG electrode locations and their corresponding regions of interest (ROIs)

Electrodes were divided into 2 ROIs: frontotemporal—outlined in blue, and occipitoparietal—outlined in red.

Phase Opposition Analyses

To determine subsequent memory effects as a function of the phase at stimulus onset, we decided to evaluate phase differences between hits and misses using the Phase Opposition Sum (VanRullen, 2016), see pre-registration (https://osf.io/4f5qc/). The POS measurement estimates the correlation between an oscillation phase at a particular frequency, and an observed behavior. It is computed as the sum of the ITC calculated separately for two or more conditions according to the observed behavior. Moreover, it assumes that the phase in the prestimulus period is distributed randomly (i.e., follows a uniform distribution) across trials and, consequently, if the EEG phase at one point in time and frequency influences subsequent memory recognition, we expect a phase concentration opposition between hits and misses. Analytically, the POS measure is given by:

$$POS = ITC_{hits} + ITC_{misses} - 2ITC_{all}$$

Where we computed the ITC individually for hits and misses on 250 random picked trials to equate the number of trials per condition. We averaged the POS values across electrodes within each region of interest (ROI). The POS is bounded between -1 and 1. If the phase is related to the trial outcome, then the POS is positive (ITC of each trial group should exceed the overall ITC). To test for significance, we used the Monte Carlo test procedure (500 surrogates mixing hits and misses and 10,000 randomly picked group average pseudo-POS distributions for each participant). Following VanRullen (VanRullen, 2016), we equated the number of trials with the minimum trials accepted that ensured a statistical power above 0.8. To do so, we decreased the number of trials until the POS calculation reached the statistical power boundary. We used pseudo-POS distributions as the null distribution to be statistically compared the calculated POS. As a significant phase opposition should lead to large positive POS, then the *p*-value corresponds to the proportion of group average pseudo-POS larger than the actual POS. *p*-values were further corrected for multiple comparisons using the False Discovery Rate (FDR) method ($p<0.05$).

Similar to the POS method, the Pairwise Phase Consistency (PPC) metric (Vinck, van Wingerden, Womelsdorf, Fries, & Pennartz, 2010) quantifies the consistency of phase differences in a particular frequency band but with a bias-free sample estimator that for controls the imbalance in the number of trials between conditions by looking at pairs of observations instead of all observations together. The PPC is calculated as follows:

$$PPC(f) = \frac{2}{N(N-1)} \sum_{j=1}^{N-1} \sum_{k=j+1}^{N} \cos\left(\theta_j(f) - \phi_k(f)\right)$$

Where N denotes the total number of trials. PPC is a normalized measure, bounded between -1—indicating perfect phase opposition, and 1—indicating full phase consistency or perfect synchronization. In the case of phase consistency, phases point into the same direction thus, angular distances between trials are small (i.e. phase differences close to 0, hence cosine values close to 1, resulting in a large PPC value). Conversely, in case of lack of phase consistency, phases point into random directions resulting in a distribution of angular distances between 0 and 360° (i.e. cosine values between –1 and 1, and a small PPC value). Last, and relevant for our study, in case of perfect opposition, phases distances point to 180°, hence cosine values close to -1, resulting in a large negative PPC value.

The Influence of the Phase of Ongoing EEG Activity at Encoding on Subsequent Memory Performance

Participants performed the task with an overall hit rate of 64.15 ± 6.89% and a false alarm rate of 7.46 ± 3.52% (see individual results in supplement Table S2.1). The focus of this experiment was to address whether the phase of the ongoing EEG activity before the associate-pair onset at encoding (-500 to 0 ms time-window) could predict subsequent memory performance. To answer this question, according to the pre-registered analysis pipeline, we used the POS analysis (VanRullen, 2016) described above, on the preselected frequencies and regions of interest. As expected, we observed that

prestimulus phases were randomly distributed when collapsing hits and misses in the prestimulus time-window. However, the POS results showed no significant phase opposition in either Theta or Alpha frequency bands in either ROI. In principle, this result would mean that the phase of ongoing oscillations within the specified frequency ranges and ROIs was not predictive of subsequent memory performance (or that if present, the effect was undetectable with the present statistical power). However, before committing to this conclusion, we explored the data further to rule out potential alternative explanations for the null result from the preregistered analysis. The results of the exploratory analyses are reported below.

Reality Checks and Alternative Phase-Opposition Analysis

First, we questioned whether the Phase Opposition Sum (POS) index used in the main analyses was reliable. The POS analysis has a positive bias (inherited from the ITC used in the calculation) that correlates with the total number of trials and with the relative number of trials per condition (VanRullen, 2016; Moratti et al., 2007; Vinck et al., 2010). It has been shown that the statistical power of POS and other phase opposition measures decreases as the imbalance in trials between conditions increases (VanRullen, 2016). Our EEG experiment had two sources of imbalance in the number of trials for the hit vs. miss comparison: (1) because conditions were determined as a function of performance, we could not anticipate exactly how many trials per condition there would be, and (2) due to the unequal artifact rejection. For this reason, in the analyses above we equated the number of trials in each condition by random picking from the more populated condition the same number of trials as in the less

populated condition. In order to evaluate the stability of the POS estimated by this procedure, we calculated the empirical POS and generated null POS measures for one electrode and time point in the theta frequency band, for different numbers of random samples (from 25 to 1.000 samples). We observed that even when using 1.000 random samples per participant, the *p*-values obtained were not stable: at the maximum number of iterations, the p-values varied in the interval 0.06 to 0.12 (supplement Figure S3.1). This result casts doubts on the stability of the POS measure used and hence, on the null result observed.

Second, as a consequence of the above, we decided to ascertain whether phase effects could be found in our data when using an alternative, more robust measure. We assessed the impact of the phase of ongoing EEG at encoding onset on subsequent performance using the Pairwise Phase Consistency (PPC) (Vinck et al., 2010) method. Similar to the POS, the PPC metric quantifies the consistency of phase differences in a particular frequency band but with a bias-free sample estimator that controls for the imbalance in the number of trials between conditions by pairing observations. Like the POS, we did not observe any significant phase opposition in any frequency or region of interest when comparing the PPC between hit and miss trials.

Third, we investigated whether our data could replicate previous results showing that differences in oscillatory amplitude in the time window around stimulus onset are predictive of subsequent memory performance (Strunk and Duarte, 2019). In order to obtain time-resolved data, oscillatory amplitude values were computed using the Hilbert transform (as specified in the methods section) on a trial by trial basis for theta and alpha frequencies. Power was averaged across electrodes within each ROI. The difference between conditions in the period –500 to 100 ms relative to stimulus onset, was estimated as follows (power expressed in dB):

$$Power_{contrast} = 10\ log_{10}\left(\frac{Power_{hits}}{Power_{misses}}\right)$$

We assessed the significance of the power contrast between hits and misses within ROIs using a two-tail *t-test* corrected for multiple comparisons using the FDR method ($p<0.05$). In the alpha band, no significant differences in power between hits and misses were found (*t-test,* $p<0.05$, FDR corrected). However, we found a significantly higher theta power for later remembered stimuli compared to latter forgotten in the peri-stimulus time-window -500 to +100 ms (*t-test,* $p<0.05$, FDR corrected) (see Figure 3.4).

This subsequent memory effect (SME), even if including a brief prestimulus period, is most likely fully explained by evoked activity, given the temporal smoothing involved in the analysis used. SME in theta evoked activity is well in line with previous findings showing that increases in theta oscillatory power during the encoding period predict subsequent recall (Guderian et al., 2009; Sederberg et al., 2003; Osipova et al., 2006; White et al., 2013; Long et al., 2014; Solomon et al., 2019).

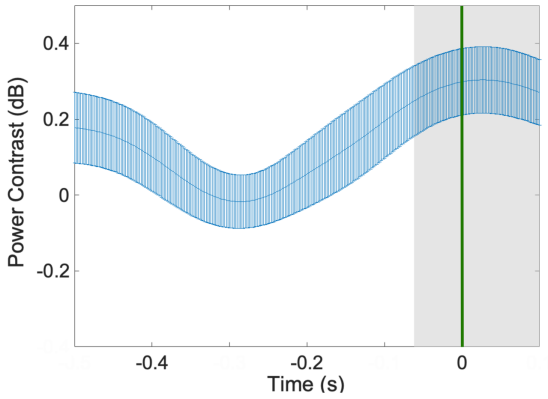

Figure 3.4 Theta power contrast between hits and misses

Theta power contrast between hits and misses (thick blue line). The Shaded grey area shows the period of significant differences (p<0.05) after FDR correction. The shaded blue area represents the standard error of the mean (SEM), and the green line shows stimulus onset.

Post-hoc Analyses with Fine-tuned Frequency and Region of Interest

Based on prior evidence for SMEs in evoked theta power (Backus et al., 2016; Lega, Jacobs and Kahana, 2012; Sederberg et al., 2003; Staudigl and Hanslmayr, 2013), and on our significant theta power contrast for hits vs. misses, we decided to adopt a data-driven approach to further seek for pre-stimulus phase effects using fine-tuned parameters. Theta power modulations following stimulus presentation and its functional impact to subsequent memory performance is an established evidence. Several studies support increases in theta amplitude during the encoding period (Osipova et al., 2006; Sederberg et al., 2003; White et al., 2013; Clouter, Shapiro, and Hanslmayr, 2017; Khader et al., 2010; Guderian et al., 2009; Long, Burke, and Kahana, 2014; Lega, Jacobs, and Kahana, 2012),

while others have found the effect in an opposite direction (Long, Burke, and Kahana, 2014; Lega, Jacobs, and Kahana, 2012; Greenberg et al., 2015; Sederberg et al., 2006). The difference in the directionality of the theta effect could respond to two different mechanisms supporting memory encoding arising from cortical and subcortical processes. In a new analysis we used the frequency and scalp region based on the theta power SME effect found above around stimulus presentation (-500 to +100ms), to fine-tune parameter selection for prestimulus phase effects on subsequent memory. This approach is justified given that the a priori ROIs were very broad and probably suboptimal. Moreover, we also know that the individual theta frequency covaries with the individual alpha frequency (Doppelmayr et al., 1998; Klimesch and Doppelmayr, 1996), and both shows large inter-individual differences (Haegens et al., 2014; Klimesch, 1999). Below, we describe the fine-tuning of the frequency of interest and scalp location adopting a data-driven approach. Later, we report the results of the ensuing pre-stimulus phase SME.

Adjustment of Frequency at the Individual Level

To select the individual frequency of interest (IFOI) we calculated the scalp average power spectrum during the encoding period (0 to 1000 ms from stimulus presentation) using a Fourier Transform (FT) (padded to 12 s to increase frequency resolution, 4 slepian tapers) in the range from 1 to 30 Hz. Then, we calculated the power spectrum for hits, misses, and for the collapsed distribution (all trials). For each participant, we used the collapsed distribution to obtain a peak in the theta frequency (4–5 Hz), namely, the IFOI. To illustrate the results, Figure 3.5 shows the scalp average power spectrum during the encoding interval for a representative participant.

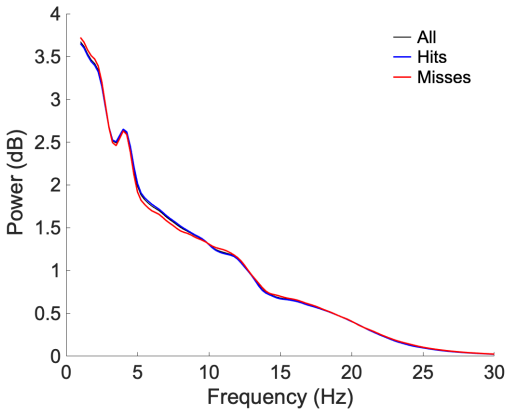

Figure 3.5 Individual Frequency of Interest (IFOI)

Individual frequency of interest (IFOI) for one representative participant. The figure represents the scalp average power spectrum during the encoding interval for the collapsed distribution of hits and misses (black), as well as separately for hits (blue) and misses (red).

Adjustment of the ROI

We band-passed the signal around the individual frequency of each participant in the narrow band IFOI ± 2 Hz using a second-order Butterworth filter, and computed the corresponding power spectrum using the Hilbert Transform. Then, the power contrast for hit vs. miss trials was obtained for each participant, electrode, and latency (0 to 500 ms in steps of 2 ms). As shown in Figure 3.6, across subjects, we identified a positive time-frequency cluster (p-value<0.0002) that initiated in the left frontal area—shortly after stimulus presentation—and extended towards central and posterior regions. Consequently, the new ROI was defined as the set of electrodes in the left frontal area which first displayed a significant power effect in the post-stimulus period (0-50 ms) and remained significant for most of the time within the window of analysis (0-500 ms): F3, F5, F7, FT7 and

FC5. Significance in power across conditions was obtained by means of a *t-test* (right-tailed) and corrected for multiple comparisons using a cluster approach (10.000 randomizations).

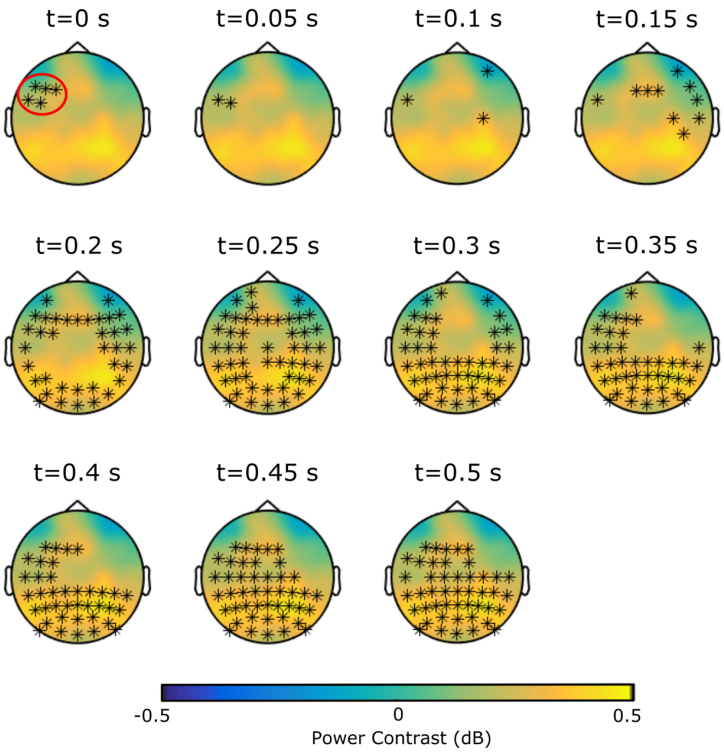

Figure 3.6 Adjusting the ROI based on the IFOI

Snapshots of the positive cluster for theta power contrast between hit and miss trials, using the individual frequency of interest (IFOI). Black stars indicate electrodes with significant activity at displayed time points. Red circle indicates the new ROI that was defined as the set of electrodes in the left frontal area which first displayed a significant power effect in the post-stimulus period.

Fine-tuned Analysis of Prestimulus Phase SMEs

We ran the Pairwise Phase Consistency (PPC) analysis in the prestimulus time-window for hits vs. misses with the new IFOI and ROI estimated as described above. For each participant, phases were extracted from the IFOI-filtered signal using the Hilbert Transform in the time-window immediately before stimulus onset (-500 to 0 ms), and the PPC was computed for each time point of the window. Statistical significance for PPC values below the null hypothesis was assessed by means of the Montecarlo randomization with distributions of 1,000 null PPC for each participant and 100,000 null means.

For multiple comparison correction, we used the Guthrie and Buchwald method (Guthrie and Buchwald, 1991) (1–dimensional clustering). Given our sample size (N=30), the alpha level (p=0.05), the estimated autocorrelation of the time series (0.997) and the length of the time series (251 points), any cluster of adjacent significant time points above (at least) 26 samples could be considered significant. Figure 3.7 shows the time resolved PPC values within the window of interest, in which two significant windows were observed between -500 to -442 ms, and -134 to -82 ms. This effect suggests phase-opposition effects in the left frontal cluster before and during stimulus presentation for hits (later remembered items) compared to misses (later forgotten).

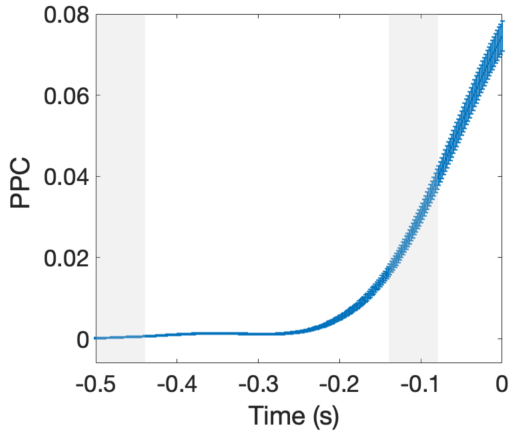

Figure 3.7: PPC Time Evolution

Average and standard error of the mean PPC time evolution. Shaded areas correspond to PPC significantly smaller than the null distribution after multiple comparison correction (Buchwald and Guthrie).

Analyses of Serial Position Effects

In lists of unrelated items (no association between adjacent items), serial position usually plays a crucial role in memory performance (Deese and Kaufman, 1957; Murdock Jr, 1962). Early items in a list have a memory advantage—*the primacy effect*—due to less competition from other items; items in the last positions also receive an advantage—*the recency effect*—because they may still be available in short-term memory during the memory test (for a review see Hurlstone et al., 2014). Middle items are normally the least remembered ones. The primacy effect in episodic memory has been correlated with increases in gamma power in posterior regions, whereas widespread low-frequency (4–14 Hz) power decreases predicted successful memory formation for later serial position items (Sederberg et al. 2006). Building on these ideas, we addressed the possible effects of serial position in our data. In our study, the

performance showed the expected U-shaped curve when plotted as a function of the item position. The effect of serial position effect on memory performance was significant as evidenced by a repeated-measures ANOVA: $F(4,145)=4.97$, $p=0.0009$. Pairwise *t-test* confirmed that the first item in the list (encoding position 1) was better remembered than all middle ones (1 vs. 2, $t(29)=2.53$, $p=0.008$; 1 vs. 3, $t(29)=6.57$, $p<0.0001$; and, 1 vs. 4 $t(29)=7.07$, $p<0.0001$). The last item in the list was significantly better remembered than the 4th item (the least recognized one, $t(29)=2.79$, $p=0.0045$) (supplement Figure S3.2). Hence, our recognition data seems to follow a U-shape.

We then turned to explore the prestimulus phase effects on the EEG, restricted to the middle items on the lists. The hypothesis behind this analysis is that any effect of prestimulus ongoing activity might be stronger for more difficult-to-remember items in the list, i.e., middle position items. In addition, high recognition rates tend to reduce the variability that is desirable for phase opposition analyses. Therefore, to address our hypothesis, we performed a new analysis using phase consistency (PPC) only on the data from the middle position items in the encoding block (positions 2, 3 & 4). In this analysis, we observed a cluster of significant negative PPC values in the time window from –500 to –412 ms before stimulus presentation, consistent with (and slightly larger than) the significant window reported above with the whole dataset (e.g., without controlling for serial position effects). The present result suggests a difference in phase concentration between hits and miss were not related to factors as the primacy or recency effect (supplement Figure S3.3).

Discussion

Several studies have demonstrated a link between the phase of ongoing neural oscillations and behavioral outcomes, especially in perception and attention tasks (Busch, Dubois and VanRullen, 2009; Mathewson et al., 2009; VanRullen et al., 2011). The interpretation of these results capitalizes on the idea that these oscillations reflect fluctuations in neural excitability and the coordinated action of neural populations across different brain regions. Here, we applied the same logic to investigate whether the phase of ongoing activity at stimulus onset has an impact on later memory performance. The question is whether fluctuations in pre-stimulus brain states, as reflected by oscillatory dynamics, will have an impact on memory formation and consequently, on subsequent recognition of the stimulus.

In the first experiment, we collected behavioral data from 30 healthy participants performing a visual paired-associates episodic memory task. Before each to-be-remembered image pair, an audio-visual reset cue was presented to induce modulation in cortical excitability by phase resetting the ongoing oscillatory activity (Lakatos et al., 2009; Fiebelkorn et al., 2011; Daitch et al., 2013). We measured later memory recognition performance as a function of the time-lag between the audio-visual reset cue and the presentation of the image pair to be encoded (randomly varied within an interval between 0 and 1000 ms, in steps of 16 ms). The data showed that subsequent memory performance for the associated pairs fluctuated periodically at ~4 Hz as a function of the time lag from the audio-visual reset cue to encoding. Although the effect did not survive multiple comparisons correction for the number of frequencies included in the analysis, it suggests that theta-band oscillatory activity pre-stimulus may modulate the encoding. Consistent with previous findings, this periodic fluctuation could be attributed to a phase resetting of the

ongoing oscillatory signal in the theta band that would be functionally relevant for encoding (Rizzuto et al., 2003; Fiebelkorn et al., 2011; Daitch et al., 2013; Fiebelkorn et al., 2018). However, the behavioral data in this experiment does not provide a direct measure of the phase of ongoing oscillatory activity; therefore, we could only assume the phase resetting as the most likely explanation of the possible modulation. Because of this, and the lack of significance after correcting for multiple comparisons, we consider that any interpretation derived from this result must be cautious.

In a second experiment, we used EEG to investigate more directly the role of ongoing low-frequency brain oscillations prior to the to-be-encoded stimulus. Specifically, we focused on the phase and amplitude of frontotemporal theta and occipitoparietal alpha oscillations as a function of trial to trial successful or unsuccessful recognition. The results indicated that theta-phase differences between hits and misses in the prestimulus time-window predicted subsequent memory performance. Note that we pre-registered an analysis pipeline focusing on the phase of frontotemporal theta and occipitoparietal alpha that returned null results. After ascertaining that the ROI and the phase opposition sum method were probably sub-optimal, we ran a post-hoc phase analysis based on PPC. This phase analysis was guided by a more precise estimation of the ROI and the individual frequency parameters estimated from the theta power effects post-stimulus (i.e., increment after successfully remembered items). Following this data-driven approach, we observed significant prestimulus phase subsequent memory effects in a cluster of left frontal electrodes, suggesting a relationship between the phase of ongoing theta oscillations before stimulus onset, and later memory performance.

The significant pre-stimulus phase effects were based on a data-driven analysis based on parameters estimated from a replication of a well-known SME in theta power. Indeed, when looking at power

effects, we observed a significant theta increase in the peri-stimulus period with similar topographic distribution as in previous studies (Osipova et al., 2006; White et al., 2013; Long et al., 2014; Khader et al., 2010; Guderian et al., 2009; Klimesch and Doppelmayr, 1996). In particular—for each participant—the theta power effect appeared frontally after stimulus presentation and spread toward centro-posterior areas at increasing latencies. We may argue that the effects of phase and power are analytically independent since they were found at different times with respect to the stimulus onset. Increases in theta power appeared around (e.g., immediately before and during) stimulus presentation, while phase effects in the theta band predictive of later recognition were observed long before the stimulus, in the –500 to –442 ms, (as well as –134 to 82 ms) time window with respect to stimulus onset.

Most of the studies looking at prestimulus oscillatory effects in subsequent memory performance have used a prestimulus orientation cue signaling the appearance of the to-be-encoded stimulus (Haque et al., 2015; Guderian et al., 2009; Otten et al., 2010). Thus, the increases in memory performance are mainly attributed to active anticipatory states. A substantial difference, at least with our second experiment, is that we focused on prestimulus ongoing oscillations; therefore, we did not use a prestimulus informative cue. In the first experiment, one could argue that the cue was not particularly time-informative (especially within the time window of relevance, 0-500 ms after the cue), although this could be more controversial. According to prior literature, in the absence of anticipatory states, i.e., under ongoing theta fluctuations, evidence from animal studies has shown an enhancement in the learning rate when the stimulus is presented during a specific hippocampal theta phase (Seager et al., 2002). The relevance of theta phase to the encoding of new information has been well-established through studies *in* vitro and in rodents and further implemented in leading theoretical models of memory (Huerta and Lisman, 1995; Hyman et al., 2003; Hasselmo,

Bodelón and Wyble, 2002; Hasselmo, 2005). Hippocampal theta is thought to be induced in cortical areas via hippocampal-cortical feedback connections, gating synaptic plasticity. In turn, the induction of long-term potentiation (LTP) is dependent on the phase of theta rhythm; whereas LTP preferentially occurs on the positive phase of the theta cycle, long-term depression occurs at opposing phases (Pavlides et al., 1988; Fell and Axmacher, 2011).

Another possible interpretation for the role of the pre-stimulus phase in the modulation of later recognition success is that it may reflect attentional mechanisms. Indeed, attention orientation is known to impact memory encoding (Chun and Turk-Browne, 2007). The idea is that the recruitment of frontal regions promotes encoding processes by top-down modulation of posterior occipitoparietal regions. In particular, frontal regions may contribute by selecting goal-relevant information and binding pieces of information (Gazzaley and Nobre, 2012; Blumenfeld and Ranganath, 2007). Thus, the fluctuations that have been observed may reflect cyclic changes in preparation for optimal stimulus processing (Sekuler and Kahana, 2007; Gazzaley and Nobre, 2012). In this line, Busch and colleagues (Busch and VanRullen, 2010) showed that detection performance was improved by attention and fluctuated over time, along with the phase of spontaneous theta oscillations, before stimulus onset. However, the evidence against attentional mechanisms arises from studies suggesting that prestimulus attentional effects are correlated with decreases in occipitoparietal alpha (Thut et al., 2006; O'Connell et al., 2009; Mazaheri et al., 2009). In our study, we did not find significant prestimulus differences in alpha power, and our experimental design does not allow us to disentangle the effects of the induced anticipatory states from the impact of attentional processes.

Recognition and free recall are two memory processes whose performance could differ on storage, recovery operations, or some

combination of both (Atkinson and Shiffrin, 1968; Kahana, 2012). Using intracranial EEG, Merkow et al. (2014) showed that selective hippocampal prestimulus theta activity was associated with better subsequent recognition, but not with subsequent recall. Their results suggest that hippocampal prestimulus theta power increases preferentially promote the encoding of item information rather than the associative information of the item with the self-generated cues necessary for retrieval. Even though our findings revealed a theta effect in frontal regions, they are consistent with the idea that prestimulus theta oscillations underlie mnemonic processes that favor later recognition. Based on their findings, we speculate that our results may not generalize to other memory paradigms, such as the free or cued recall; however, future work should be done to test this hypothesis.

One limitation of the present study is that the initial selection of the regions of interest was possibly not optimal. We divided the whole electrode set into two large clusters (anterior and posterior) that were too broad. We are aware that besides characterizing the functional significance of the observed effects in phase and amplitude, it is relevant to identify the brain areas that play a role in the observed effects. Although this is challenging to do with EEG, through additional analyses, we redefined the ROI as the set of electrodes displaying post-stimulus increases in theta power (putatively) after stimulus onset in our data, which replicate a relatively well-known pattern (Osipova et al., 2006; Sederberg et al., 2003; White et al., 2013; Clouter, Shapiro and Hanslmayr, 2017; Khader et al., 2010; Guderian et al., 2009).

Consistent with VanRullen, 2016, we verified that the phase opposition measure (POS) is particularly sensitive to the relative number of trials in each group. In our study, the proportion of correct trials was high (well above chance level), leading to an imbalance of trials in the miss and hit categories. By using simulations, we

observed that even with 1000 random samples per participant, the *p*-values obtained were not stable. Conversely, the pairwise phase consistency (PPC) (Vinck et al., 2010) appeared to be a better method to estimate EEG phase-related correlations in behavior when the experimental design comprises non-equiprobable outcomes.

Conclusions

In summary, the principal finding to emerge from this study is that the spatiotemporal pattern preceding the stimulus onset can predict behavioral performance in a memory task. This provides further evidence that the state of neural activity preceding stimulus presentation has an impact on the subsequent processing, extending prior results in perceptual and attentional tasks. In the particular case of the memory task used here, the relevant spatiotemporal pattern is characterized by theta-band fluctuations and phase differences between hits and misses reflected in the left frontal scalp. These novel insights highlight the role of theta phase in cortical oscillations at encoding and support episodic memory models linking behavioral data to phasic properties of theta rhythm (Hasselmo, Bodelón and Wyble, 2002; Hasselmo, 2005).

CHAPTER 4

Whole-brain Multimodal Neuroimaging Model Integrating Neurotransmitter Data

"The most beautiful thing we can experience is the mysterious. It is the source of all true art and science"

—Albert Einstein (1879–1955)

Understanding the underlying mechanisms of the human brain in health and disease requires models with necessary and sufficient details to explain how function emerges from the underlying anatomy and is shaped by neuromodulation. In this chapter, we provide such a detailed causal explanation using a whole-brain model integrating multimodal imaging in healthy human participants undergoing manipulation of the serotonin system. Specifically, we present a model that combines anatomical data from diffusion magnetic resonance imaging (dMRI) and functional magnetic resonance imaging (fMRI) with neurotransmitter data obtained with positron emission tomography (PET) of the detailed serotonin 2A receptor (5-

HT2AR) density map[4]. The model allowed us to fit the resting state (with and without concurrent music listening) and mechanistically explain the functional effects of 5-HT2AR stimulation with lysergic acid diethylamide (LSD) on healthy participants. The whole-brain model used a dynamical mean-field quantitative description of populations of excitatory and inhibitory neurons as well as the associated synaptic dynamics, where the neuronal gain function of the model is modulated by the 5-HT2AR density. The model identified the causative mechanisms for the non-linear interactions between the neuronal and neurotransmitter system, which are uniquely linked to (1) the underlying anatomical connectivity, (2) the modulation by the specific brain-wide distribution of neurotransmitter receptor density, and (3) the non-linear interactions between the two. Taking neuromodulatory activity into account when modeling global brain dynamics will lead to novel insights into human brain function in health and disease and opens exciting possibilities for drug discovery and design in neuropsychiatric disorders.

[4] The results presented in this chapter are published in: Deco, G., Cruzat, J., Cabral, J., Knudsen, G. M., Carhart-Harris, R. L., Whybrow, P. C., Logothetis, N.K. & Kringelbach, M. L. (2018). Whole-brain multimodal neuroimaging model using serotonin receptor maps explains non-linear functional effects of LSD. *Current Biology,* 28(19), 3065-3074.

A mechanistic explanation of neuromodulatory effects

Human brain activity results from the self-organization of large neural networks, emerging from complex recursive non-linear interactions between interconnected neural populations (Breakspear, 2017; Deco et al., 2009; 2015). Understanding brain function and dysfunction clearly requires measurements of such activity in various spatiotemporal scales, some of which may be done by combining neurophysiological and neuroimaging methods, including electrical measurements, fMRI, dMRI (diffusion MRI), and PET (positron emission tomography) (Deco and Kringelbach, 2014; Cabral et al., 2017). Moreover, modeling of such large-scale brain dynamics is absolutely essential for gaining insights into the generative mechanisms of ongoing neuronal dynamics (Honey et al., 2007; Ghosh et al., 2008).

Not surprisingly, following the development and optimization of various methodologies over the last 2 decades, significant progress has been made in measuring the spontaneous spatiotemporal unfolding of brain activity, revealing a repertoire of what is currently called resting-state networks (Biswal et al., 1995; Raichle et al., 2001). In parallel, the spatial patterns of correlated activity in such networks have been increasingly studied with a variety of computational methods, including whole-brain models relying on the mean activity and variance of excitatory and inhibitory neuronal populations (Breakspear, 2017; Deco et al., 2015; Honey et al., 2007; Deco et al., 2017a; Cabral et al., 2014a; Ghosh et al., 2008; Kringelbach et al., 2015).

However, the explanatory and potentially predictive power of neuronal population models, such as those of neural mass and mean-field, strongly depend on the integration of information that may

selectively and differentially affect the activity of populations at different spatial scales (Cabral et al., 2017). More specifically, whole-brain models commonly rely on structural and functional connectivity of a number of anatomically defined brain regions, the activity of each of which is described by the estimated mean activity of local neuronal populations. Yet, it is now well established that such activity is strongly modulated by the synergistic interactions of the diffuse ascending systems, spreading in a global or local fashion by so-called neuromodulators, including acetylcholine, various monoamines, and tryptamines (Bargmann, 2012; Smythies, 2005; Marder, 2012). The effects of these neuromodulators go well beyond the activity profiles of typical excitation-inhibition microcircuits and could only be computationally assessed by having detailed maps of regional density of their receptors.

To address this important problem, we combine standard anatomical and functional maps of the human brain with a detailed map of 5-HT_{2A} receptor (5-HT_{2A}R) density of the neuromodulator serotonin, obtained from a new high-resolution human brain *in vivo* atlas (Beliveau et al., 2017), recently composed on the basis of images from 210 healthy individuals (see details of radiotracers in (Beliveau et al., 2017)). We added the receptor maps to the standard whole-brain model by investigating how gain values can be adapted by the local regional values of the PET-based empirical values of 5-HT_{2A}R density. To this end, we defined a global gain scaling parameter, S_E, which was added to the original fixed gain parameters (which were the same for all regions) and thus scaling the regional 5-HT_{2A}R values influencing the recursive circuits of excitatory and inhibitory neurons. We first fitted the model to the placebo condition but *not* the LSD condition, i.e., assuming zero values of S_E that correspond to the original gain values. The main question then becomes whether any S_E values would fit the LSD condition (using the sensitivity of the functional connectivity dynamics) while still using the original

whole-brain placebo model but now including the new element of receptor binding through the global gain scaling parameter, which modulates each region with the different empirical measures of 5-HT_{2A}R binding. If this were found to be true, neurotransmitter modulation of whole-brain activity dynamics would be—for the first time—quantitatively ascribed to one type of receptor binding (here 5-HT_{2A}) that would be modulating brain-wide neural responses.

Experimental Data and Subjects Details

In the following, for each of the three empirical data set, we provide the participants details and the methods for obtaining 1) *structural connectivity*: probabilistic tractography derived from the dMRI, 2) *functional connectivity*: functional dynamics estimated from the fMRI in the placebo and LSD condition, and 3) *neurotransmitter density*: estimation of the density of the 5HT-2A receptors that has been obtained using PET.

Anatomical Connectivity Dataset (dMRI)

We used diffusion MRI (dMRI) data collected in 16 healthy right-handed participants at Aarhus University, Denmark (5 women, mean age: 24.8 ± 2.5). The study was approved by the internal research board at CFIN, Aarhus University, Denmark. Ethics approval was granted by the Research Ethics Committee of the Central Denmark Region (De Videnskabsetiske Komitéer for Region Midtjylland). Written informed consent was obtained from all participants prior to participation.

The imaging data were recorded in a single session on a 3 T Siemens Skyra scanner at CFIN, Aarhus University, Denmark. The following parameters were used for the structural MRI T1 scan: voxel size of 1 mm^3; reconstructed matrix size 256 3 256; echo time (TE) of 3.8 ms and repetition time (TR) of 2300 ms. dMRI data were collected using TR = 9000 ms, TE = 84 ms, flip angle = 90°, reconstructed matrix size of 106 3 106, voxel size of 1.98 3 1.98 mm with slice thickness of 2 mm and a bandwidth of 1745 Hz/Px. Furthermore, the data were recorded with 62 optimal nonlinear diffusion gradient directions at b = 1500 s/mm^2. One non-diffusion weighted image (b = 0) per 10 diffusion-weighted images was acquired, approximately. One of dMRI images was collected applying anterior to posterior phase encoding direction and the other acquired in the opposite direction.

Functional Dataset (fMRI)

All 15 participants (four women; mean age, 30.5 ± 8.0) were recruited via word of mouth and provided written informed consent to participate after study briefing and screening for physical and mental health. The study was approved by the National Research Ethics Service committee London-West London and was conducted in accordance with the revised declaration of Helsinki (2000), the International Committee on Harmonization of Good Clinical Practice guidelines, and National Health Service Research Governance Framework. Imperial College London sponsored the research, which was conducted under a Home Office license for research with schedule 1 drugs. The screening for physical health included electrocardiogram (ECG), routine blood tests, and urine test for recent drug use and pregnancy. A psychiatric interview was conducted, and participants provided full disclosure of their drug use history. Key exclusion criteria included: < 21 years of age, personal history of diagnosed psychiatric illness, immediate family history of

a psychotic disorder, an absence of previous experience with a classic psychedelic drug (e.g., LSD, mescaline, psilocybin/magic mushrooms or DMT/Ayahuasca), any psychedelic drug use within 6 weeks of the first scanning day, pregnancy, problematic alcohol use (i.e., > 40 units consumed per week), or a medically significant condition rendering the volunteer unsuitable for the study.

Screening took place at Imperial's clinical research facility (ICRF) at the Hammersmith hospital campus. Participants who were found eligible for the study attended two study days that were separated by at least 14 days. On one day, the participants received placebo, and on the other day they received LSD. The order of the conditions was balanced across participants and participants were blind to this order, but the researchers were not.

On scanning days, volunteers arrived at the study center at 8:00am. They were briefed in detail about the study day schedule, gave a urine test for recent drug use and pregnancy, and carried out a breathalyzer test for recent alcohol use. A cannula was inserted into a vein in the antecubital fossa by a medical doctor and secured. The participants were encouraged to close their eyes and relax in a reclined position when the drug was administered. All participants received 75 mg of LSD, administered intravenously via a 10ml solution infused over a two minutes' period, followed by an infusion of saline. The administration was followed by an acclimatization period of approximately 60 min, in which (for at least some of the time) participants were encouraged to relax and lie with their eyes closed inside a mock MRI scanner. This functioned to psychologically prepare the participants for being in the subsequent (potentially anxiogenic) MRI scanning environment.

Participants reported noticing subjective drug effects between 5 to 15 min post-dosing, and these approached peak intensity between 60 to 90 min post-dosing. The duration of a subsequent plateau of drug

effects varied among individuals but was generally maintained for approximately four hours post-dosing. MRI scanning started approximately 70 min post-dosing, and lasted for approximately 60 min. This included a structural scan and BOLD fMRI. Once the subjective effects of LSD had sufficiently subsided, the study psychiatrist assessed the participant's suitability for discharge.

The BOLD scanning consisted of three eyes-closed resting state scans, each lasting seven minutes. After each seven-minute scan, VAS ratings were performed in the scanner via a response-box. The first and third scans were eyes-closed rest, but the second scan also incorporated listening to two excerpts of music from two songs by ambient artist Robert Rich (Kaelen et al., 2017). The stimuli were both 7.3 min long and were balanced in their acoustic properties, and rich in timbre, but not in rhythm. Pre-study assessments in a separate group confirmed balance for their emotional potency. In order to reduce interference of fMRI scanning noise with the music experience, volume-maximization and broadband compression was carried out using Ableton Live 9 software. Each participant listened to both stimuli, in a balanced order across conditions. Prior to each scan, participants were instructed via onscreen instructions to close their eyes and relax. Here we used the music + LSD condition since this has been demonstrated to yield a larger effect on brain activity (Carhart-Harris et al., 2016c) but we also found the effects for LSD without music. For more details about the functional data, the reader is invited to see Carhart-Harris et al., 2016c.

Two BOLD-weighted fMRI data were acquired using a gradient echo planer imaging sequence, TR/TE = 2000/35 ms, field-of-view = 220 mm, 64 x 64 acquisition matrix, parallel acceleration factor = 2, 90º flip angle. Thirty-five oblique axial slices were acquired in an interleaved fashion, each 3.4 mm thick with zero slice gap (3.4 mm isotropic voxels). The precise length of each of the two BOLD scans was 7:20 min.

Neurotransmitter Dataset (PET)

The participants were healthy male and female controls from the Cimbi database (Knudsen et al., 2016); all data from this database are freely accessible. The data analysis was restricted to include individuals aged between 18 and 45 years. Participants were recruited by advertisement for different research protocols approved by the Ethics Committee of Copenhagen and Frederiksberg, Denmark. A total of 232 positron emission tomography (PET) scans and corresponding structural MRI scans were acquired for 210 individual participants; 189 participants had only one scan, 20 participants had two scans, and a single had three scans.

PET data were acquired in list mode on a Siemens HRRT scanner operating in 3D acquisition mode with an approximate in-plane resolution of 2 mm (1.4 mm in the center of the field of view and 2.4 mm in cortex (Olesen et al., 2009)). The PET scanning used the recently developed [11C] Cimbi-36 as a selective serotonin 2A (5-HT_{2A}) receptor agonist radioligand (Ettrup et al., 2014; 2016). The radioligands for the other serotonin receptors are described in the paper by Beliveau and colleagues (Beliveau et al., 2017). PET frames were reconstructed using a 3D–OSEM–PSF algorithm (Comtat et al., 2008; Sureau et al., 2008). Scan time and frame length were designed according to the radiotracer characteristics. Dynamic PET frames were realigned using AIR 5.2.5 (Woods et al., 1992). T1- and T2-weighted structural MRI were acquired on four different Siemens scanners with standard parameters. All structural MRIs (T1 and T2) were unwarped offline using FreeSurfer's gradient-_nonlin_unwarp version 0.8 or online on the scanner (Jovicich et al., 2006). For further details on structural MRI acquisition parameters, see (Knudsen et al., 2016).

Further processing was performed with FreeSurfer 5.3 (Fischl, 2012) (http://surfer.nmr.mgh.harvard.edu) using a surface and a volume

stream. The individual cortical surfaces were reconstructed using the structural MRI corrected for gradient nonlinearities. The pial surfaces were further refined using T2-weighted structural images and corrected manually where necessary. PET–MR co-registration was estimated using boundary-based registration (Greve and Fischl, 2009) between the time- weighted sum of the PET time–activity curves (TACs) and the structural MRI. Additionally, the transformation from individual MR space to normal MNI152 space was estimated with combined volume–surface (CVS) registration (Postelnicu et al., 2009).

Quantification and Statistical Analysis

First, we provide a general overview of the analysis pipeline used to integrate structural and functional connectivity (diffusion magnetic resonance imaging, dMRI, and functional magnetic resonance, fMRI) with neurotransmission (positron emission tomography, PET) in a model of the placebo and LSD response in healthy participants (see Figure 4.1).

This overview is subsequently followed by the specific methods, namely:

1. Structural connectivity: probabilistic tractography derived from the dMRI
2. Functional connectivity: functional dynamics estimated from the fMRI in the placebo and LSD condition
3. Parcellation: all structural, functional and neuromodulation data are integrated into the Automated Anatomical Labeling (AAL) parcellation.

4. Whole-brain computational model: a dynamic mean-field model was used to integrate the available data to fit the placebo condition.
5. Neuromodulation in whole-brain model: integration of the neurotransmission data by changing the gain of neurons in the placebo-fitted whole-brain model in order to fit the LSD condition.

Structural Connectivity

Tractography

For the present study, we used the structural connectivity between the 90 AAL regions obtained in a previous study (Deco et al., 2017a) averaged across 16 healthy young adults (5 females, mean ± SD age: 24.75 ± 2.54). The linear registration tool from the FSL toolbox (*http://www.fmrib.ox.ac.uk/fsl*, FMRIB, Oxford) (Jenkinson et al., 2002) was used to co-register the EPI image to the T1-weighted structural image. The T1-weighted image was co-registered to the T1 template of ICBM152 in MNI space (Collins et al., 1994). The resulting transformations were concatenated and inversed and further applied to warp the AAL template (Tzourio-Mazoyer et al., 2002) from MNI space to the EPI native space, where interpolation using nearest-neighbor method ensured that the discrete labeling values were preserved. Thus, the brain parcellations were conducted in each individual's native space. We generated the structural connectivity (SC) maps for each participant using the dMRI data acquired. We processed the two datasets acquired (each with different phase encoding to optimize signal in difficult regions). The construction of these structural connectivity maps or structural brain networks consisted of a three-step process. First, the regions of the whole-brain network were defined using the AAL template as used in the

functional MRI data. Second, the connections between nodes in the whole-brain network (i.e., edges) were estimated using probabilistic tractography. Third, data was averaged across participants.

We note that the recent results from Gordon and colleagues would seem to suggest that the AAL parcellation is less than optimal, in that the AAL was the least homogeneous parcellation scheme tested (Gordon et al., 2016). Nevertheless, it is not clear if the methodology used in that paper is particularly meaningful. Indeed, in the recent paper by Eickhoff and colleagues, they review the literature on the topographic organization of the brain and conclude that it is presently not clear what is the right spatial parcellation (Eickhoff et al., 2018). Both papers are mostly concerned with the spatial organization of the brain, while in this ms, we focus on the spatiotemporal global dynamics. For this goal, AAL would appear to be a good choice for the following reasons: 1) AAL yields excellent significant results in the whole-brain literature in general (Cabral et al., 2017; Cabral et al., 2014a; Deco et al., 2017b). 2) The relative low number of parcels in the AAL is highly suitable for our very extensive computational demands.

We used the FSL diffusion toolbox (Fdt) in FSL to carry out the various processing stages of the diffusion MRI data. We used the default parameters of this imaging pre-processing pipeline on all participants. Following this preprocessing, we estimated the local probability distribution of fiber direction at each voxel (Behrens et al., 2007). We used the probtrackx tool in Fdt to provide automatic estimation of crossing fibers within each voxel. This has been shown to significantly improve the tracking sensitivity of non-dominant fiber populations in the human brain (Behrens et al., 2007). The connectivity probability from a seed voxel *i* to another voxel *j* was defined by the proportion of fibers passing through voxel *i* that reach voxel *j* using a sampling of 5000 streamlines per voxel (Behrens et al., 2007). This was extended from the voxel level to the region level,

i.e., in an AAL parcel consisting of n voxels, 5000x n fibers were sampled. The connectivity probability P_{ij} from region i to region j is calculated as the number of sampled fibers in region i that connect the two regions divided by 5000 x n, where n is the number of voxels in region i. We threshold the SC matrix at 0.1%, i.e., five streamlines.

For each brain region, the connectivity probability to each of the other 89 regions within the AAL was calculated. Due to the dependence of tractography on the seeding location, the probability from i to j is not necessarily equivalent to that from j to i. However, these two probabilities are highly correlated across the brain for all participants (the least Pearson $r = 0.70$, $p < 10^{50}$). As directionality of connections cannot be determined based on diffusion MRI, the unidirectional connectivity probability P_{ij} between regions i and j was defined by averaging these two connectivity probabilities. This unidirectional connectivity was considered as a measure of the structural connectivity between the two areas, with $C_{ij} = C_{ij}$. We implemented the calculation of regional connectivity probability using in-house Perl scripts. For both phase encoding directions, 90x90 symmetric weighted networks were constructed based on the AAL90 parcellation and normalized by the number of voxels in each AAL region; thus, representing the structural connectivity network organization of the brain.

We applied the AAL90 template using the FLIRT tool from the FSL toolbox (*http://www.fmrib.ox.ac.uk/fsl*, FMRIB, Oxford) to co-register the b0 image in diffusion MRI space to the T1-weighted structural image and then to the T1 template of ICBM152 in MNI space (Collins et al., 1994). The two transformation matrices from these co-registration steps were concatenated and inversed to subsequently be applied to warp the AAL templates (Tzourio-Mazoyer et al., 2002) from MNI space to the diffusion MRI native space.

Functional Connectivity

Preprocessing

We first preprocessed the fMRI data using MELODIC 3.14 (Beckmann and Smith, 2004), part of FSL (FMRIB's Software Library, *http://www.fmrib.ox.ac.uk/fsl*) with standard parameters and not discarding any ICA components. Head motion during the experiments was corrected using the FSL tools mcflirt as part of the standard MELODIC pipeline and was within normal acceptable range for neuroimaging experiments. Specifically, the cloud plot in Figure S7 in the original LSD data paper (Carhart-Harris et al., 2016c) shows that motion is similar in the placebo and LSD conditions in terms of its effects on biasing potential related motion artifacts. For each participant and for each brain state (i.e., placebo and LSD), we used FSL tools to extract and average the BOLD signals from all voxels within each ROI defined in the AAL atlas (considering only the 90 cortical and subcortical non-cerebellar brain regions) (Tzourio-Mazoyer et al., 2002). We computed both the static functional connectivity (FC) and the functional connectivity dynamics (FCD). In brief, the FCD is a matrix that expresses the spatiotemporal statistics of a snapshot of FC across different sliding windows. The matrix is thus not locked in time to a particular instance and the spatiotemporal evolution (between different sessions, subjects or simulations) is thus not aligned. As a consequence, comparing the differences between empirical and whole-brain model level of fitting, we need to compare the distributions of the elements of those matrices. For this the standard method is to use the Kolmogorov-Smirnov (KS) distance (see details in Deco et al., 2017b) where a smaller value means better fit. For the grand average FC, the standard approach is to use correlation between the FC matrices, because the matrices are aligned and what matters are the correlations between different pairs, i.e., a higher

correlation value would mean a better fit. More specifically, we computed FC and FCD in the following ways:

1) Static Functional Connectivity

The static FC is defined as the *NxN* matrix of BOLD signal correlations between brain areas computed over the whole recording time. The empirical and simulated FC matrices were compared by computing the Pearson correlation between their upper triangular elements (due to matrix symmetry).

2) Functional Connectivity Dynamics

To consider the temporal dynamics of resting-state FC, we computed the FC over a sliding window of 30 TR with increments of 2 TR, resulting in a time-evolving FC matrix (see Figure 4.2). Subsequently, we compute a time-versus-time matrix of Functional Connectivity Dynamics (FCD), where each entry, $FCD_{(t_x t_y)}$, corresponds to the correlation between the FC centered at times $t_x tx$ and the FC centered at t_y. Typically, the FCD matrices computed in the resting-state reveal a characteristic checkered pattern indicative of spontaneous switching between different FC patterns. Importantly, the distribution of FCD values contains valuable information regarding the time-dependencies of resting-state activity and we use it to as way to characterize the dynamical properties of resting-state activity in the different conditions and simulations. To do so, we generate the distributions of the upper triangular elements of the FCD matrices over all participants in a given condition (LSD or placebo), as well as of the FCD matrices obtained from simulations. The different distributions are then compared using the Kolmogorov-Smirnov (KS) distance, allowing for a meaningful evaluation of the model performance in predicting the changes observed in resting-state FC in dynamical terms.

Parcellation

Based on our previous whole-brain studies we used the AAL atlas but considering only the 90 cortical and subcortical non-cerebellar brain regions (Tzourio-Mazoyer et al., 2002). All structural, functional and neuromodulation data was integrated using this atlas. We used FSL tools on the freely available $5HT_{2A}$ receptor density map in MNI space to extract the average receptor density for each individual AAL region.

Implementation of the Serotonergic Modulation into a Whole-brain Dynamic Mean Field Model

We used the dynamic whole-brain model, proposed by Deco et al., (2014), to simulate spontaneous mean-field activity. The simulated dynamics were then transformed into BOLD signal using the generalized Balloon–Windkessel model of Stephan et al., (2007). Both models were previously described in detail in the Introduction section. To obtain a quantitative measure of 5-HT_{2A} receptor density in each AAL region n, $d5HT2A_n$, we used the high-resolution atlas of human brain serotonin system measured with PET by Beliveau et al., (2017). Density values were divided by the maximum, such that $max(d5HT2A) = 1$. We used $d5HT2A_n$ to modulate the firing rates $r_i^{(E,I)}$ of the excitatory and inhibitory pools of each brain region, following a number of experimental studies in cats and rats showing that serotonin injection modulates the firing rate of neurons with 5-HT receptors (Grasso et al., 2016; Licata et al., 1993; 1995; Licata et al., 1993; Chance et al., 2002). Moreover, while some neurons respond with an increased firing rate, others consistently decrease the firing rate after serotonin injection, indicating that 5-HT_{2A} receptors

have both excitatory and inhibitory effects (Grasso et al., 2016; Licata et al., 1993). Precisely, we consider that $d5HT2A_n$ modulates the gain of the neuronal response function $H^{(E)}$ in each brain area according to the modified Equation 3 (see the Introduction section), using the standard computational definition of gain modulation given by Chance et al., (2002):

$$r_n^{(E)} = H^{(E)}\left(I_n^{(E)}\right) = \frac{g' g_E\left(I_n^{(E)} - I_{thr}^{(E)}\right)}{1 - exp\left(-d_E g' g_E\left(I_n^{(E)} - I_{thr}^{(E)}\right)\right)}, \qquad (12)$$

$$g' = 1 + s_E d5HT2A_n \qquad (13)$$

Here, the scaling factor s_E is the only free parameter equally scaling in all brain areas the slope of H in the E pool according to the normalized density of serotonin receptors in each area, $d5HT2A_n$. To simulate the resting-state activity under placebo condition, we use $s_E = 0$.

Explaining the Influence of Neuromodulation

The main aim is to provide a detailed mechanistic explanation of how neuromodulation is coupled with the neuronal system and serves to shape how function emerges from the underlying anatomy. Here, we describe the results of using a whole-brain model, integrating a whole-brain density map of the 5-HT_{2A}R (Beliveau et al., 2017) with

traditional structural and functional connectivity representations obtained by means of dMRI and fMRI, respectively. The combination of the multimodal data in the whole-brain model is described in schematized form in Figure 4.1. Notably, the model only uses two parameters: a neuronal parameter scaling the global coupling of neuronal populations and a neuromodulator parameter scaling the effects of neurotransmitter on the neuronal gain function weighted by the empirical regional receptor density. For each of the multimodal neuroimaging modalities, we used the automated anatomical labeling (AAL) parcellation with 90 cortical and subcortical regions (Tzourio-Mazoyer et al., 2002), which has been extensively and successfully used over the last decade for resting-state neuroimaging studies and whole-brain modeling.

We investigated the influence of neuromodulation on the neuronal system using the well-known effects of LSD on the serotonin system by using data obtained in healthy participants receiving small doses of LSD or placebo, with or without music, which can acutely induce synesthesia, altered perceptions, bliss, depersonalization, and mystical experiences (Carhart-Harris et al., 2016c). Importantly, LSD with music has been found to enhance the emotional response and produced greater feelings of wonder and transcendence compared with listening to music after placebo (Kaelen et al., 2015). We therefore used the music conditions with placebo and LSD in order to increase the impact on the serotonin system (see Figure 4.1, and we also confirmed the results for the non-music condition in supplement Figure S4.1).

Specifically, the model was first fitted to the placebo condition, and subsequently, the regional 5-HT_{2A}R densities from the *in vivo* atlas were used to explain the functional resting-state activity in the LSD condition. The role of the empirical 5-HT_{2A}R was ultimately assessed by comparing the LSD maps with neuromodulatory maps of randomly shuffled 5-HT_{2A}R densities. As shown below, we found

that a robust explanation of global activity changes induced by the LSD administration is only possible when the neuromodulation profiles estimated by the density of the 5-HT_{2A}Rs from the *in vivo* serotonin atlas is taken into account.

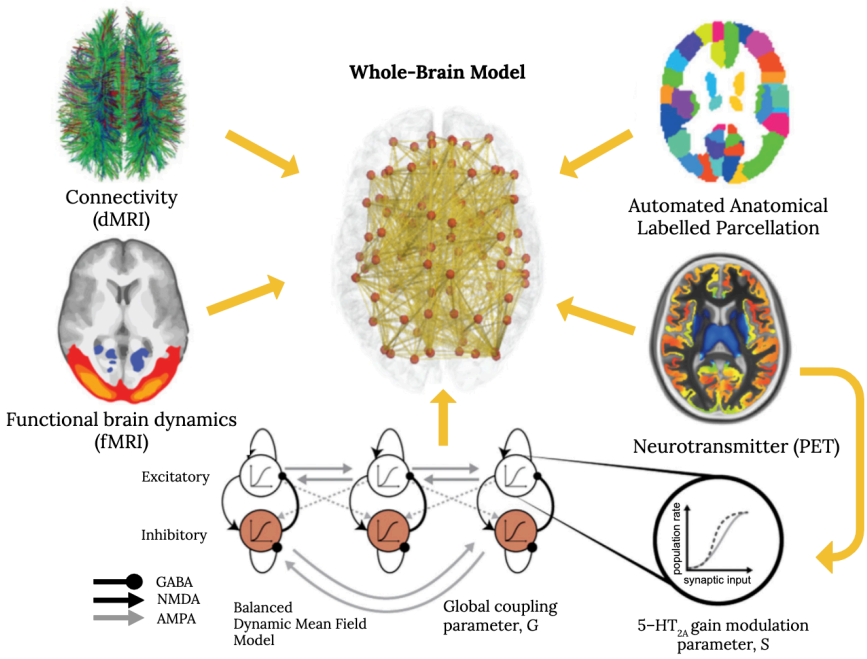

Figure 4.1 Overview of Integrating Multimodal Data Including Neuromodulation into a Whole-brain Neuronal Model

We show the basic ingredients for the integration of multimodal neuroimaging data from structural (dMRI, top left), functional (fMRI, bottom left), and neurotransmission (PET, top right) using the same parcellation for each neuroimaging modality (bottom right) for generating a whole-brain computational model (middle). Each node of the model is using a realistic underlying biophysical neuronal model including AMPA, GABA, and NMDA synapses as well as neurotransmitter gain modulation (bottom row) of these.

Briefly summarizing the methods, the whole-brain model was composed of 90 anatomically delineated brain regions linked by the structural connectivity (SC) matrix of fiber densities obtained by tractography (Hagmann et al., 2008; Cabral et al., 2014a). The activity of each region was represented by a dynamic neuronal mean-field model derived from the collective behavior of empirically validated integrate-and-fire (80% excitatory and 20% inhibitory) neurons (Deco et al., 2014; Brunel and Wang, 2001). The population responses for pools of excitatory neurons were given by independent sigmoid functions, regulated by a gain parameter s_E, common in all brain regions and initially set to zero (Deco et al., 2014). In the model, the inter-regional coupling (given by the SC) was scaled by a single global parameter, G, corresponding to the conductivity of each fiber (same for all fibers). Modulation of the brain's dynamic working point, i.e., changes in the magnitude of coupling of the network (from weak to strong), could be implemented by changing the G parameter.

Our optimization of the whole-brain model on the basis of the aforementioned diverse structural, functional, and regulatory data started with the fitting of the whole-brain mean-field model to the placebo condition, using the same fixed gain-value parameters for all regions and adapting only the G coupling parameter. This optimal global coupling parameter value was subsequently used for explaining the LSD condition by selectively changing the neuronal gain of each region according to the empirical measured 5-HT_{2A}R density. To take into account the spatiotemporal fluctuations in functional brain dynamics over time, the model was fitted to the spatiotemporal dynamics of the data (i.e., to the functional connectivity dynamics [FCD]) (Hansen et al., 2015; Allen et al., 2014; Deco and Kringelbach, 2016) rather than to the static grand-average functional connectivity (Deco and Kringelbach, 2016) (see Figure 4.2, describing the process of estimating and fitting the FCD in the whole-brain model). As previously shown, the FCD is a powerful sensitive measure of the spatiotemporal changes in

functional connectivity, which maximally constrains the working space parameters of whole-brain models (Hansen et al., 2015; Deco et al., 2017b). For this reason, the sensitivity of the FCD offers an excellent metric for determining subtle differences.

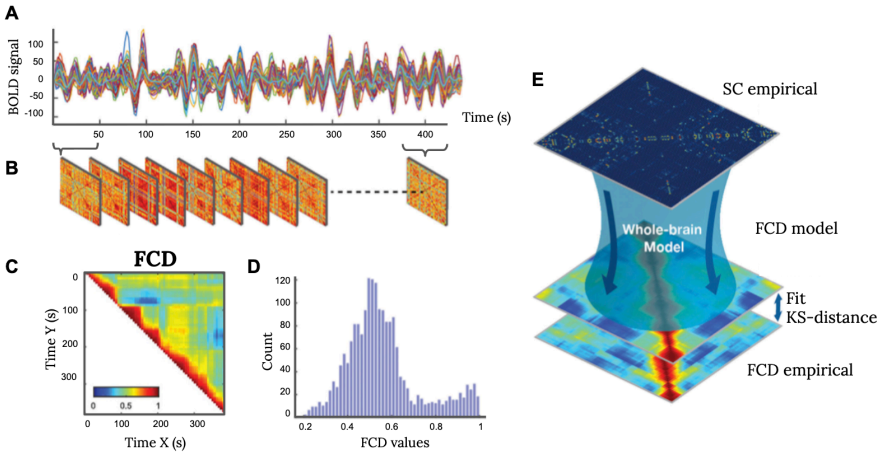

Figure 4.2 Overview of Process for Estimating and Fitting the FCD in the Whole-brain Model

A) First, we extract the timeseries from the fMRI data from each brain region in the parcellation (shown here for a single participant). B) The average functional connectivity is computed over a sliding window of 30 repetition time (TR) with increments of 2 TR, resulting in time-evolving FC matrices. C) Subsequently, we compute a time-versus-time matrix of FCD, where each entry, $FCD_{(t_x t_y)}$, corresponds to the correlation between the FC centered at times t_x and the FC centered at t_x. D) We generate the distributions of the upper triangular elements of the FCD matrices over all participants in a given condition (LSD or placebo) and here shows the histogram for the single participant. E) The distribution of FCD for the placebo condition is used to fit the whole-brain computational model, which is compared using the Kolmogorov-Smirnov distance, allowing for an effective evaluation of the model performance in explaining the changes observed in resting-state FC in dynamical terms.

Importantly, the gain values were adapted by taking into account the local regional values of 5-HT_{2A}R density. Specifically, we defined a global gain-scaling parameter, s_E, which was added to the original fixed gain parameters (same for all regions) and thus could serve for scaling of the regional 5-HT_{2A} values, potentially signaling the influence of the receptors on the recursive circuits of excitatory and inhibitory neurons. Zero values of s_E yield the original gain values, fitting the model to the placebo condition but *not* the LSD condition. An important subsequent question is whether any *sE* values would fit the LSD condition (using the sensitivity of the FCD measure) while still using the optimal coupling G parameter of the placebo condition. If this were true, LSD-induced whole-brain activity dynamics would be quantitatively ascribed to one type (i.e., 5-HT_{2A}) of serotonergic modulation of brain-wide neural responses.

Results of Fitting Whole-brain Neuromodulation Model to Empirical Data

To find the causal mechanisms linking neuromodulation and neuronal activity, we first estimated the optimal coupling parameter *G* such that the whole-brain model (with original gain values, i.e., $s_E = 0$ for all regions) optimally fits the placebo condition. Figure 4.3A shows the dependency for *G* of the fitting in terms of (1) the grand-average static functional connectivity (FC) and (2) the FCD. For the FC fitting, higher values indicate a better fit since it reflects a simple correlation between model and empirical data. We include this measure as the grand-average FC spatial correlation has traditionally been used to constrain whole brain, yet it is not particularly sensitive to the spatiotemporal information (Hansen et al., 2015; Deco and

Kringelbach, 2016) and thus not relevant for constraining the model here. Instead, we show that a better measure for model fitting is the FCD, which take into account the spatiotemporal information and where lower values indicate a better fit of the Kolmogorov-Smirnov distance between the FCD of the model and empirical data. As is shown in Figure 4.3A and B, the results using this measure (level of fitting) are excellent. For the subsequent analyses, we use this placebo condition for which we selected the optimum point of G, when the model was fitted to the FCD ($G = 2.1$ at minimum of green line in Figure 4.3A).

The neuromodulatory effects in the LSD condition were then modeled by estimating the neuronal gain function, namely by scaling the parameter s_E and the corresponding regional empirical 5-HT_{2A}R data. Figure 4.3B shows how this approach significantly changed the fit, revealing an optimal s_E value of approximately 0.2. In contrast, trying to improve the fit with the placebo condition at the optimal coupling point G as a function of changing the PET-based excitatory gain modulation did not show any improvement. There was no optimal gain modulation. Instead the placebo fit to FCD (green line in Figure 4.3B) decreased monotonically, as can be seen by the green line in Figure 4.3B. The finding clearly demonstrates that the brain-activity profiles, induced by the 5-HT_{2A}R agonist LSD (as fitted to the FCD) depend on the precise 5-HT_{2A}R density distribution map. While we show that this response is non- linear, this finding is consistent with the existing physiological literature revealing a main action of psychedelics such as LSD on the 5-HT_{2A}R (Nichols, 2016).

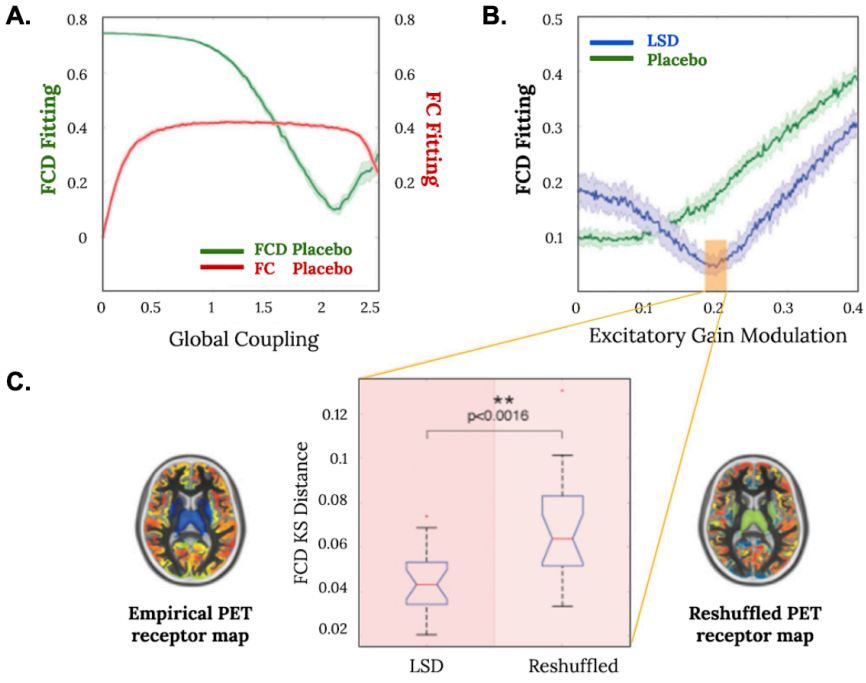

Figure 4.3 Results of Whole-brain Model of Placebo and Explaining Effects of LSD with 5HT2A Modulation of Gain Function

A) Whole brain fitting of the placebo condition shows the fit of grand average functional connectivity (FC, in red) and functional connectivity dynamics (FCD, in green) as a function of the global coupling parameter, G (with the error bars indicating the standard error across simulations). For the FC fit, higher values indicate a better fit since it reflects a simple correlation between the model and empirical data. However, for the FCD fit, lower values indicate a better fit since we use the Kolmogorov-Smirnov distance between the FCD of the model and empirical data (see Methods for full details). Similar to our previous published research, this shows that the FCD fitting is much more informative that the static grand-average FC, which is to be expected given that FCD provides the functional dynamics. The obtained optimum of G for fitting the model to the FCD (at minimum of green line, G = 2.1) is then used for the subsequent neuro- modulatory analyses. B) For the LSD condition, when using this optimal coupling point of the placebo condition and systematically scaling the excitatory gain function in each region with the empirical 5-HT_{2A}R data, we find that there is an optimum at around (0.2,0.045) (minimum of blue line). In contrast, varying the scaling of the neuronal

gain for the placebo condition does not yield an optimum (see monotonically rising green line), and thus the fit is not improved by changing the scaling of the neuronal gain by 5-HT_{2A}R density. This clearly demonstrates that the LSD brain activity is dependent on the precise 5-HT_{2A} density distribution maps. C) Further, reshuffling the 5-HT_{2A}R densities randomly across the regions at the optimum point in B), shown within orange box, makes the fit significantly worse ($p < 0.0016$). This again demonstrates that the precise distribution of 5-HT_{2A} is very important for how LSD affects the brain state.

Furthermore, to demonstrate that the LSD function is dependent on the precise distribution of the 5-HT_{2A}R, at the optimal gain value s_E, we randomly shuffled the empirical 5-HT_{2A}R densities; i.e., the original 90 values for the receptor maps were randomly re-assigned to different regions, and the model was run 200 times with each different randomly re-assigned receptor map. Figure 4.3C shows the results of randomly shuffling the empirical 5-HT_{2A}R densities across the regions at the optimum point s_E (obtained and shown in Figure 4.3B). This randomly reshuffled manipulation yields a significantly worse fit compared to the actual empirical receptor densities (as shown by the Wilcoxon statistics in the boxplot).

In order to further test the robustness of our whole-brain modeling approach, we used a number of different strategies to test the specificity of receptor-binding maps. In Figure 4.4 we show a boxplot of the results of using a uniform receptor-binding distribution (to the far right). This is significantly worse than all other receptor-binding distributions. We also show the results of using the other serotonin receptors, namely 5-HT_{1A}, 5-HT_{1B}, 5-HT_4, and the serotonin transporter, 5-HTT. These maps all perform significantly worse than that for the 5-HT_{2A}R, which confirms the main role this receptor plays in the effects of LSD (Nichols, 2016). It has been suggested that the 5-HT_{1A} receptor also contributes to the effects of LSD (Nichols, 2016; Halberstadt, 2015), and indeed, this is confirmed by the

improved performance of the 5-HT_{1A} receptor-binding map compared to the 5-HT_{1B}, 5-HT_4, and 5-HTT maps (Nichols, 2016).

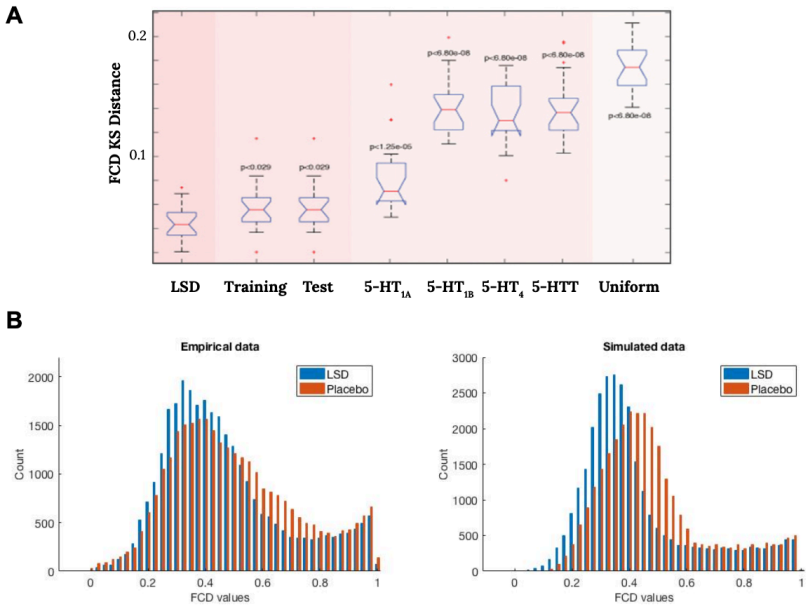

Figure 4.4 Results of the Whole-brain Model of Placebo and Explaining the Effects of LSD with other Serotonin Receptors

A) To further test the robustness of our whole-brain modeling approach, we tested the specificity of other receptor-binding maps. Here, we show a boxplot of the results of the generalization capability of our model by training and testing the 5-HT_{2A}R maps on 50% subset of participants (columns 2 and 3). The results are remarkably similar to using the full set of participants, attesting to the robustness of our results. We also show the results of using other serotonin receptor-binding maps, namely 5-HT_{1A}, 5-HT_{1B}, 5-HT_4, and 5-HTT (columns 4–7), which all perform significantly worse than 5-HT_{2A}, confirming the main role this receptor to the effects of LSD (Nichols 2016). Interestingly, however, 5-HT_{1A} receptor-binding map performs slightly better than the 5-HT1B, 5-HT_4, and 5-HTT receptor maps, which confirms its role in LSD (Nichols 2016). In the last row, we show the results of using a uniform receptor-binding distribution (column 8), which is significantly

worse than all other receptor-binding distributions. B) Finally, the FCD histograms of LSD and placebo for both the empirical data and the optimized model clearly show the excellent fit. We also confirmed the results for the non-music conditions, as shown in supplement Figure S4.1.

We also wanted to test the generalization capability of our model by training and testing the 5-HT_{2A}R maps on a random 50% subset of participants. While our sample was comparably small for a generalization study, we nevertheless were able to show that the training performance was very similar to the original results, while the testing performance was equally good (see Figure 4.4).

Further demonstrating the excellent fit, we plot the FCD histograms of LSD and placebo for both the empirical data and the optimized model in Figure 4.4B, where the histograms of the LSD and placebo conditions are different for both empirical and model. This suggests that the 5-HT_{2A}R density is fundamental for describing the neuromodulatory effects of psychedelics.

Discussion

The findings presented here show for the first time the potential of whole-brain modeling to capture the modulation of brain-wide regional activities, typically induced by the ascending neuromodulatory systems that regulate the balance, excitability, and specificity of cortical microcircuits and subcortical neuronal assemblies. We built a novel whole-brain model integrating neuronal and neuromodulation multimodal data from dMRI and fMRI with

neurotransmitter data obtained with PET, revealing a detailed whole-brain map of 5-HT_{2A}R densities. This provided new causative insights into the non-linear interactions between anatomy, neuronal activity, and more importantly, *specific* neurotransmitter receptor density.

Our framework enabled us to model the resting state (with and without music listening) and, more importantly, mechanistically explain the functional effects of 5-HT_{2A}R stimulation with well-known 5-HT_{2A}R agonist compound LSD in healthy participants. We were able to do so by creating a whole-brain model using the underlying anatomical connectivity linking local nodes, which were modeled using a dynamical mean-field quantitative description of populations of excitatory and inhibitory neurons as well the associated synaptic dynamics, where the neuronal gain function of the model was modulated by the 5-HT_{2A}R density. As such, we were able to model the non-linear interactions between the underlying anatomical connectivity and the modulation by the *specific* brain-wide distribution of neurotransmitter receptor density.

Importantly, the results were informed by the properties of the serotonin (5-hydroxytryptamine) system, which is a remarkable evolutionary conserved neuromodulator/neurotransmitter that not only regulates psychophysiological functions like sleep, food intake, body temperature, depression/anxiety, alcohol/drug-reinforcement, emotional behavior, environmental sensitivity, and adaptive responsivity but also modulates cognitive capacities such as learning and memory by interacting with other neuromodulatory and neurotransmitter systems (King et al., 2008; Štrac et al., 2016; Atasoy et al., 2018; Carhart-Harris and Nutt, 2017). 5-HT is synthesized within the brainstem's raphe nuclei (dorsal and median), which have distributed projections to subcortical, limbic, and neocortical regions (Azmitia and Gannon, 1986; Wilson and Molliver, 1991; Jacobs and Azmitia, 1992). On the basis of structural,

functional, and transductional features, 5-HT receptors have been grouped into seven receptor groups, including a total of 14 subtypes, and one transporter (5-HTT), which typically transfers a neuromodulator, e.g., serotonin, from the synaptic cleft to the presynaptic neuron (Serretti et al., 2006; Amara and Kuhar, 1993). The most abundant and extensively researched subtypes of serotonin receptors are the 5-HT_{1A} and 5-HT_{2A} receptors (Carhart-Harris and Nutt, 2017); the latter has been shown to mediate adaptive plasticity (i.e., behavioral capacity for change) that is critical for dealing with pathologies, such as stress, adversity, and depression (Carhart-Harris and Nutt, 2017). The hallucinogenic effects of psychedelics such as LSD are mediated through their stimulation of 5-HT_{2A}R (Carhart-Harris and Nutt, 2017; Preller et al., 2017) (but also to a lesser degree some of the other receptors), and this mode of action may explain the potentially beneficial effects on some of the aforementioned pathologies (Carhart-Harris et al., 2016a; Nichols, 2018).

The present results extend the recent findings of Shine and colleagues (Shine et al., 2018) to the human whole-brain level and especially emphasize the role of PET-based binding receptors for global brain dynamics. Until now, it was generally believed that whole-brain dynamics are shaped mainly by the underlying anatomy and the local dynamics. But this is not enough to fully describe the dynamics, as shown by the elegant results of Shine and colleagues emphasizing the role of gain modulation. The present results supplement this work while emphasizing that the incorporation of neuromodulatory properties can significantly add to an account of global functional dynamics. Even more importantly, future research should seek to describe the full entanglement of the two very different neural and neurotransmitter dynamical systems with very different timescales.

Here, neuromodulation was artificially induced by using a serotonin agonist, namely the psychedelic LSD. Yet, the method can be further optimized—potentially by including the receptor distribution of

additional neuromodulators—and used for discerning self-generated changes in brain states. Clearly, a new approach that can reliably describe the evolution of brain states would be of great value both for the diagnosis of diseases and drug optimization.

Numerous investigations in human and animals using a great repertoire of non-invasive and invasive techniques has convincingly demonstrated that the functional whole-brain activity depends both on effective connectivity and so-called brain states, reflecting system properties such as anatomical organization, dynamic thalamocortical loops, and the function of ascending arousal systems. Evidently, such evolving activity patterns are affected by diseases and might be eventually used to predict approaching "criticalities", as the latter transitions are often preceded by the robust gradual reorganization of complex systems in general (Atasoy et al., 2017).

Further integration of information and modeling is undoubtedly important given the inadequacy of animal models and studies at the microscopic level to fully describe human neuropsychiatric disorders, which have contributed the paucity of effective clinical neuropharmacological interventions such as antidepressants having limited success compared to placebo (Kirsch et al., 2008; Fountoulakis and Möller, 2011), clearly indicating that new research strategies are needed (Holtzheimer and Mayberg, 2011; Kapur et al., 2012). In fact, the development and discovery of new effective pharmacological treatments for neuropsychiatric disorders are making incremental progress only, and it has been argued that treatments available today are no more effective than those available over 50 years ago, despite intensive neurobiological investigation (Holtzheimer and Mayberg, 2011; Conn et al., 2008; Starcevic and Brakoulias, 2008).

What is needed is a mechanistic understanding of the imbalances found in neuropsychiatric disorders, specifically at both local and

global whole-brain levels (Deco and Kringelbach, 2014). This could help open up rational ways for effective brain interventions to rebalance the brain networks and help the identification of biomarkers stratifying a broad illness phenotype into a finite number of treatment-relevant subgroups (Trusheim et al., 2007; Cuthbert and Insel, 2013; Stephan et al., 2016; 2016b).

Neuropsychiatric disorders are bound together by changes on many networks of the brain and in particular in the reward network of the brain (Berridge and Kringelbach, 2015), with anhedonia, i.e., lack of pleasure, being the cardinal symptom (Thomsen et al., 2015). Systematic studies of changes in local and global neuromodulatory activity, development, optimization and classification of models, and observations of drug effects on them may greatly increase our understanding of pathological states and their potential treatment.

Based on the current findings, we offer here an example of a pipeline (Figure 4.5) that could potentially be used to combine structural, functional, and neurotransmitter neuroimaging data for modeling a disease state (leftmost). Once the model is established, the regional drug-receptor modulation can be optimized by finding the optimal weighting of the receptor density such that the optimized model generates the functional dynamics of the healthy state. The current evidence suggests that it would be important to combine such direct brain manipulations with environmental manipulations, e.g., drug-assisted psychotherapy, which could be a particularly fruitful approach (Carhart-Harris et al., 2018b).

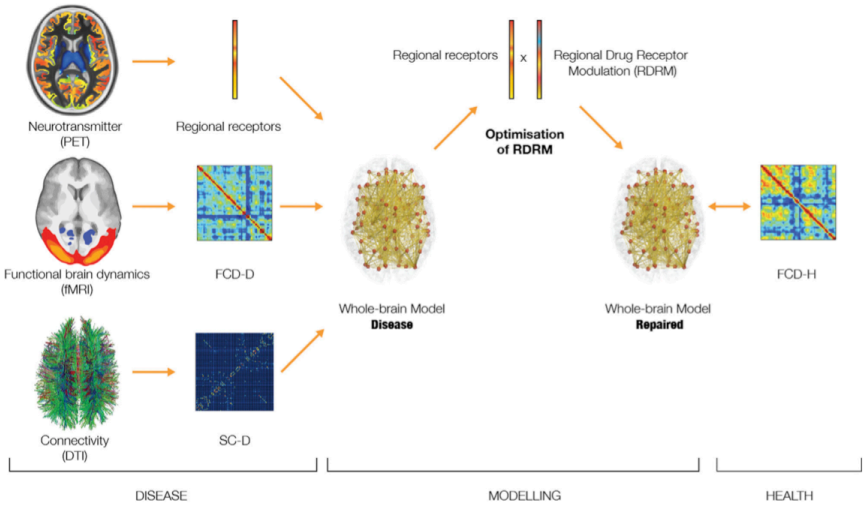

Figure 4.5 Potential of Using Whole-brain Modeling for Optimal Drug Modulation Discovery.

The principles of combining whole-brain computational modeling with neurotransmitter density maps to fit functional brain dynamics open up for novel rational drug discovery design. The figure provides a pipeline for how to combine structural, functional, and neurotransmitter neuroimaging data to model the disease state (leftmost). Once the model is established, the regional drug receptor modulation (RDRM) can be optimized by finding the optimal weighting of the receptor density such that the optimized model generates the functional dynamics of the healthy state.

Conclusions

We have demonstrated how the anatomical brain-wide distribution of neuromodulatory activity can be integrated in a whole-brain computational model to provide new causative insights into the non-linear interactions between anatomy, neuronal activity, and more importantly, *specific* neurotransmitter receptor density. These novel insights are only possible when using a whole-brain model given the fact that it is not possible to scramble the neurotransmitter receptor density *in vivo*. With time, this new approach could eventually lead to fundamental insights into human brain function in health and disease and be used for drug discovery and design in neuropsychiatric disorders.

CHAPTER 5

General Discussion

"If the past is over, and the future has not yet come, all that exists is now; so how long does now last?"

—St. Augustine (354—430 AD)

The ultimate goal of Cognitive Computational Neuroscience is to explain the full biological mechanisms underlying human cognition and complex behavior. To achieve this goal, it is essential to understand the emerging phenomena *computationally*. Computation refers to the fundamental principles and methods, from physics to psychology, that are used in the brain to represent and process information. The research work presented in this dissertation—although far from providing the principles that govern the link between brain activity and behavior—extends the state of scientific knowledge in that direction. We aimed to investigate crucial unsolved questions in neuroscience, namely, how does cognitive function emerge from large-scale brain networks? And, how

information is flexibly integrated and processed through large-scale brain networks? Valuable insights into how these might be solved are presented here.

In the first chapter, we provided a brief overview of key concepts in the context of this work. First, we highlighted the two principles by which the brain is governed: segregation and integration. The former refers to the ability of single brain regions to perform specialized local computations. In contrast, the latter refers to the process by which the brain combines information widely distributed necessary to perform complex cognitive functions. Importantly, these principles do not contradict each other; both specialization and cooperation are necessary for brain function, cognition and behavior. Then, we review two mechanisms responsible for coordinating the interaction among regions of the brain that allows large-scale integration: phase-synchronization and the influence of the ascending neuromodulatory system. Phase-synchronization refers to the appearance of synchronization of oscillatory phases between different brain regions. It has long been recognized as a mechanism supporting communication, as proposed by the "Communication Through Coherence" (CTC) theory (Fries, 2005; 2015; Deco and Kringelbach, 2016). The ascending neuromodulatory system provides a strong influence in global network dynamics by selectively changing the balance of the excitation and inhibition of individual brain regions (Cohen, Braver and Brown, 2002; Aston-Jones and Cohen, 2005; Shine et al., 2018). Finally, we addressed the advantages of using whole-brain computational models for elucidating the mechanisms underlying global dynamic changes. In this regard, we introduced the dynamic mean-field model which is a biophysically realistic model that simulates the spontaneous neural activity using the mean-field approximation of firing rates of an excitatory and inhibitory pool of neurons.

It is generally agreed that cognitive function emerges from the dynamics of extended cortical and subcortical networks, but how do brain networks dynamically reorganize to allow broad communication between many different brain regions in order to integrate information? In the second chapter, we explored how cognition modulates global functional network measurements. To do so, we used high-resolution direct neural recordings of 12 human patients with epilepsy while performing three cognitive tasks. We assessed how the functional connectivity between different brain areas changes to facilitate communication across them. At the topological level, this facilitation was characterized by measures of integration and segregation. Consistent across tasks and patients, we found a significant increase in integration and a decrease in segregation during cognitive processing, especially in the gamma band (50–90 Hz) (Cruzat et al., 2018). Importantly, these modulations were not associated with changes in the underlying level of oscillations (amplitude), but with increases in the level of synchronization and functional connectivity in the same frequency range as proposed by the "Communication Through Coherence" theory.

The results further render a framework for investigating cognitive neuroscience in the context of dynamical systems, associating the course of cognition to the progressive reconfiguration of functional networks in the human brain. Besides, they spotlight the utility of intracranial EEG for large-scale approaches in identifying fundamental relations between local and global dynamics.

Even low-level neurobiological mechanisms can have a striking impact on behavior. Several studies in perception and attention have shown cyclic alternations in behavioral performance mainly in the theta and alpha bands (4–8 and 8–12 Hz, respectively) (Busch, Dubois and VanRullen, 2009; Klimesch, Sauseng and Hanslmayr, 2007; Mathewson et al., 2009; Palva and Palva, 2007; VanRullen,

2016; de Graaf et al., 2013). Extending on this idea, in the third chapter we tested the hypothesis that ongoing fluctuations in neural activity have an impact on memory encoding using a paired-associates memory task in two experiments performed by healthy participants. In a first experiment, we used the logic of phase reset (Rizzuto et al., 2003) to test if subsequent memory performance fluctuates rhythmically time-locked to a resetting cue (phase-reset signal). We found that behavioral performance exhibited a periodic and selective modulation at theta frequency (~4 Hz). With this in mind, in a second experiment, we tested the role of ongoing low-frequency neural oscillations before the presentation of the to-be-encoded picture pairs in subsequent recognition performance using scalp EEG. We analyzed subsequent memory performance as a function of the phase and amplitude of alpha and theta oscillations. Consistent with previous literature, we found that post-stimulus theta power increases in the left frontal scalp predicted subsequent memory performance. When narrowing down the analysis of prestimulus activity to the scalp location and frequency of the post-stimulus power effect, we found a correlation between the prestimulus theta phase and subsequent memory. Altogether, the results suggest that the spatiotemporal pattern preceding the stimulus onset can predict behavioral performance in a memory task. In the particular case of the task used here, the relevant spatiotemporal pattern was characterized by theta-band fluctuations and phase differences between hits and misses reflected in the left frontal scalp.

Finally, we moved forward the characterization of global dynamics to search for the impact of the neuromodulatory system in mediating the reconfiguration of brain networks. In the fourth chapter, we presented a novel whole-brain model that successfully addresses one of the major challenges in neuroscience, which is to explain the paradoxical flexibility of human brain function despite having a fixed anatomical connectome. The model allowed us to explore possible mechanisms explaining the global dynamic network changes

observed when stimulating the serotonin 2A receptors (5-HT_{2A}R) with lysergic acid diethylamide (LSD) on healthy participants. The biophysical whole-brain multimodal neuroimaging model integrated anatomical data from dMRI and resting-state functional data from fMRI, with neurotransmitter data obtained with PET, revealing the detailed 5-HT_{2A}R density map. The spontaneous activity of each brain region was modeled using a dynamical mean-field quantitative description of populations of excitatory and inhibitory neurons as well as the associated synaptic dynamics, where the 5-HT_{2A}R density modulated the neuronal gain function of the model. The model successfully identified the causative mechanisms for the non-linear interactions between the neuronal and neurotransmitter systems, which were uniquely explained by the underlying anatomical connectivity, the specific brain-wide distribution of the neurotransmitter receptor density, and the non-linear interaction between the two.

The model provides a novel computational drug-design framework that could have substantial implications in the study of neuropsychiatric disorders including, major depression, obsessive-compulsive disorder, schizophrenia, and anxiety. In particular, this framework offers the unique opportunity to test biochemical system perturbations—by changing regional neurotransmitter values, or electrical perturbations—such as deep brain stimulation (DBS) or transcranial magnetic stimulation (TMS), that can help reconfigure the functional properties of brain networks in disease. Extending on these ideas, our drug-design framework could be further complemented with the innovative *in* silico perturbative approach recently developed by Deco and colleagues (Deco et al., 2019). For these purposes, it would be crucial to acquire multimodal neuroimaging data from the same group of subjects and even try the model at the single-subject level. Note that in our study the data was provided by different sources due to the lack of a complete

repository. Hopefully, this methodological weakness will likely be overcome in the future through improvements in data acquisition.

Furthermore, it would be of great interest to test other types of neurotransmitters using the model. Dopamine (DA), for instance, is a major neurotransmitter involved in behavioral control, motivation and stimulus-reward learning process, and adjusts synaptic dynamics in multiple time scales through different pathways (Schultz, 1997; Asl, Vahabie and Valizadeh, 2019). Given its strong influence in nearly every aspect of cognition and behavior, impaired dopamine signals underlie the pathophysiology of cognitive and neuropsychiatric disorders such as Parkinson's disease, drug addiction, schizophrenia, attention-deficit/hyperactivity disorder, and obsessive-compulsive disorder. Therefore, dopamine receptors are a primary target for many current treatment strategies. In some cases, 5-HT and DA interact interdependently to sustain the psychobiological regulation of cognitive function (Boureau and Dayan, 2011), making it difficult to understand how a breakdown in one system leads to a particular trait or disease[5]. In this notion, experimental evidence, as well as computational and theoretical models of neuromodulation, have identified a close association between 5-HT/DA imbalance and cytoarchitectonic changes underlying learning and memory impairment (González-Burgos and Feria-Velasco, 2008), schizophrenia (Remington, 2008), Parkinson's

[5] For detailed reviews of 5-HT receptor distribution and functional interactions with the dopaminergic system see (Alex & Pehek, 2007; Barnes & Sharp, 1999).

disease (Balasubramani et al., 2015; Bédard et al., 2011), depression (Fibiger, 1995; Zangen et al., 2001; Landén and Thase, 2006) and anxiety (Krichmar, 2013). Although the 5-HT/DA interaction in the brain has been extensively investigated, almost all studies have focused on the microscale level, ignoring its impact on large-scale dynamics. Future research would greatly benefit from computational, theoretical, and disease models to understand dopaminergic and serotonergic interaction at the whole-brain level. For example, one could explore the effects of forcing direct inhibition of the dopaminergic system by the serotonergic system, while applying local manipulations that would be impossible to do in vivo in humans.

Current methods for creating functional connectivity maps with fMRI are restricted in the temporal domain due to the sluggishness of the blood oxygen level-dependent signal (BOLD). This restriction, in turn, limits the ability to identify dynamic changes in the millisecond time scale, which is precisely the relevant timescale for understanding spatiotemporal dynamics throughout the whole brain. In fact, in recent work, we used independent measures of entropy and hierarchy to find the relevant timescale for obtaining the spatiotemporal structures underlying whole-brain dynamics to reflect the temporal evolution of spatial brain networks. We showed that both methods found a similar optimum at a timescale of around 200 ms in resting state and in task data (Deco, Cruzat and Kringelbach, 2019). Regarding neuromodulators' action, it is known that they manipulate neural processing over a coarse timescale ranging from short-term adjustments in neurons and synapse function to persistent long-term regulation (Dayan, 2012; Brzosko, Mierau and Paulsen, 2019). Therefore, it will be essential for future studies to consider the use of data acquired using a neuroimaging technique with the ability to identify dynamic changes of the entire brain on the millisecond time scale, such as EEG or MEG.

One of the main limitations of the model is that we have considered only one neuronal system influenced by static neurotransmitter concentrations modulating the neuronal gain while ignoring the dynamics of the neuromodulatory ascending system. To overcome this issue, we further improved the model by bi-directionally coupling the two dynamic systems. Specifically, we mutually coupled the whole-brain neuronal and neurotransmitter systems by including an explicit description of the neurotransmitter dynamical system and the mutual coupling with the neuronal system. This was done by modeling the dynamics of the neurotransmitter system through simulating the release-and-reuptake dynamics, where the density of the serotonin receptor of each brain area is measured with PET. The neurotransmitter dynamics are, in turn, coupled with the neuronal activity through the firing rate activity of the Raphe brain region, the source of the serotonin neurotransmitter. As proof of principle, we considered the effects of psilocybin on the serotonin system and therefore used the anatomical connectivity between the raphe nucleus and the rest of the brain. Overall, the results show that the interaction between these two dynamical systems is fundamental for explaining the empirical data (Figure 5. **1**). In other words, the dynamic mutual interaction between neuronal and neuromodulator systems at the whole-brain level is crucial to fully explain the functional modulation of brain activity by psilocybin, a powerful psychedelic drug acting on the serotonin system.

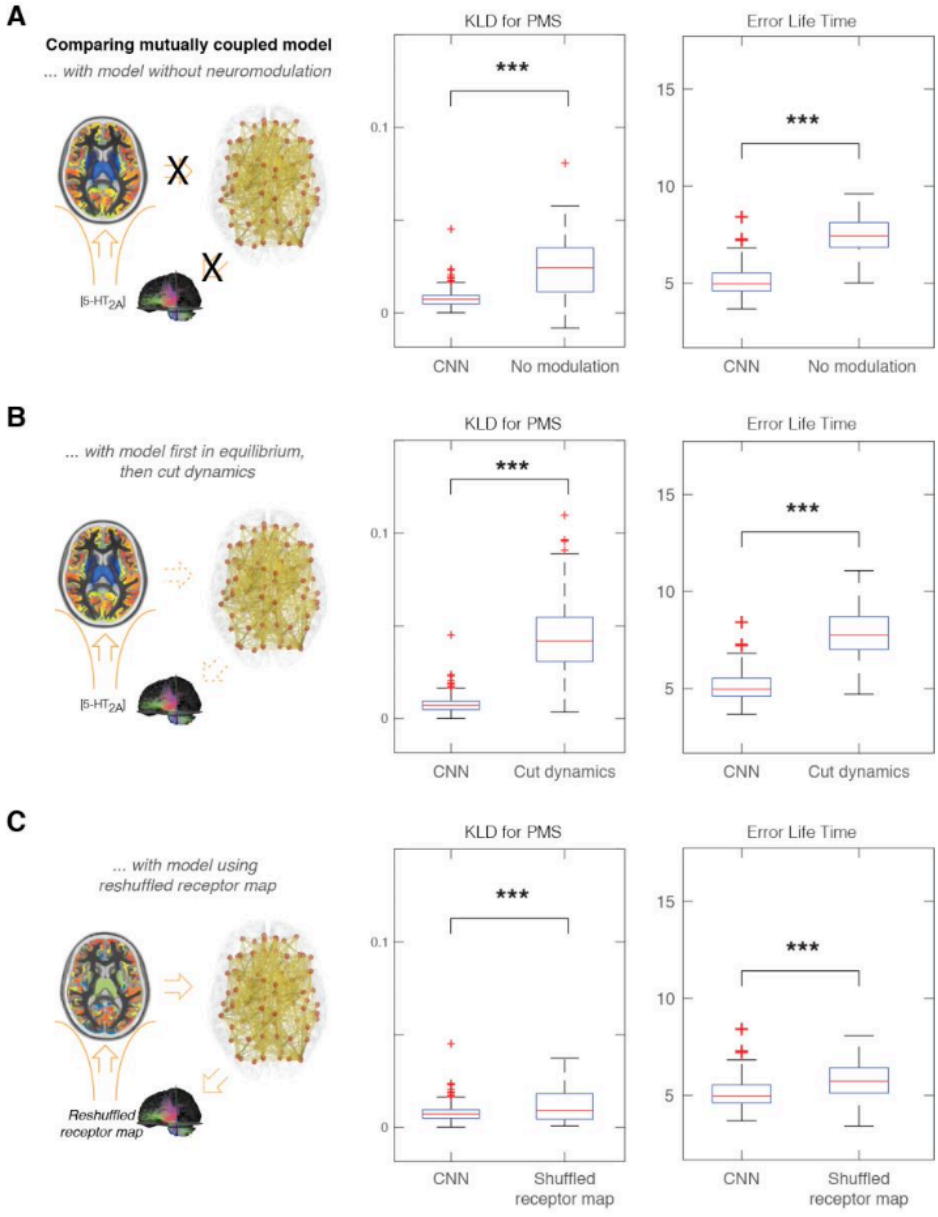

Figure 5. 1 Optimal dynamical coupled neuronal-neurotransmission (CNN) whole-brain model is significantly better then alternative models

The results provide insights into the underlying dynamics of neuromodulation involved in psilocybin. They were obtained by comparing the Kullback-Leibler distance (KLD) for the PMS and the error life times between the empirical data and the whole-brain model undergoing various manipulations. A) In terms of dynamics, we first uncoupled the neuromodulators from the neuronal systems. For the optimal fit of the mutually coupled whole-brain model, we found a very significant difference between the optimal fit and the uncoupled system (i.e. without neuromodulation) ($p<10^{-6}$). B) We then ran further simulations to investigate the role of specific parts of the dynamic coupling. We tested this by allowing the full mutually coupled whole-brain model to achieve a steady-state, upon which we kept just the average of the neurotransmitter variables while froze the feedback dynamics from neuromodulators to the neuronal system by removing the coupling through the raphe nucleus. We also found a significant difference when removing the feedback dynamics p<10-6). C) In further sets of experiments designed to investigate the importance of the receptor distribution, we changed the distribution of regional receptor densities by randomly shuffling the 5-HT_{2A}. We found a significant difference between using the empirical 5-HT_{2A} receptor densities across the regions at the optimal fit compared with randomly shuffling the receptor densities ($p<10^{-4}$). This demonstrates the causal importance of the 5-HT_{2A} receptor densities.

Closing Remarks

We have seen that our understanding of brain function not only depends on our knowledge of the different brain structures but mostly on their continuous interactions. Extending on the idea that cognition relies on the flexible integration of information widely distributed across many different brain regions, we showed that cognitive processing is associated with an increase in integration and a decrease in segregation, mainly in the gamma range (50–90 Hz) (Cruzat et al., 2018). These modulations were also associated with an increase in the band-limited functional connectivity between the nodes and not

with changes in the level of the underlying oscillations. We placed particular emphasis on the fact that our results provide support for the communication through coherence theory at the whole-brain level. Furthermore, we argue that phase synchronization is one of the primary mechanisms supporting large-scale integration and that this particular feature also has implications at the behavioral level. We provided experimental evidence demonstrating that the spatiotemporal pattern preceding the stimulus onset could predict behavioral performance in a pair-associates memory task. In particular, the pattern was characterized by phase differences between hits and misses reflected in the left frontal scalp. Then, we turned to functional brain imaging studies with psychedelics to explore the influence of neuromodulators in reorganizing global network dynamics. Using a whole-brain multimodal neuroimaging model, we explained the functional effects of 5-HT_{2A}R stimulation with LSD (Deco et al., 2018). We argued that the mechanisms for the non-linear interactions are intimately related to the specific brain-wide distribution of the receptor density. Along these lines, it is worthwhile to stress that whole-brain models are essential to link the different levels of observation and that they have the potential to allow us to make more precise hypotheses regarding the mechanism of brain function in health, disease, between species and across the lifespan.

APPENDIX

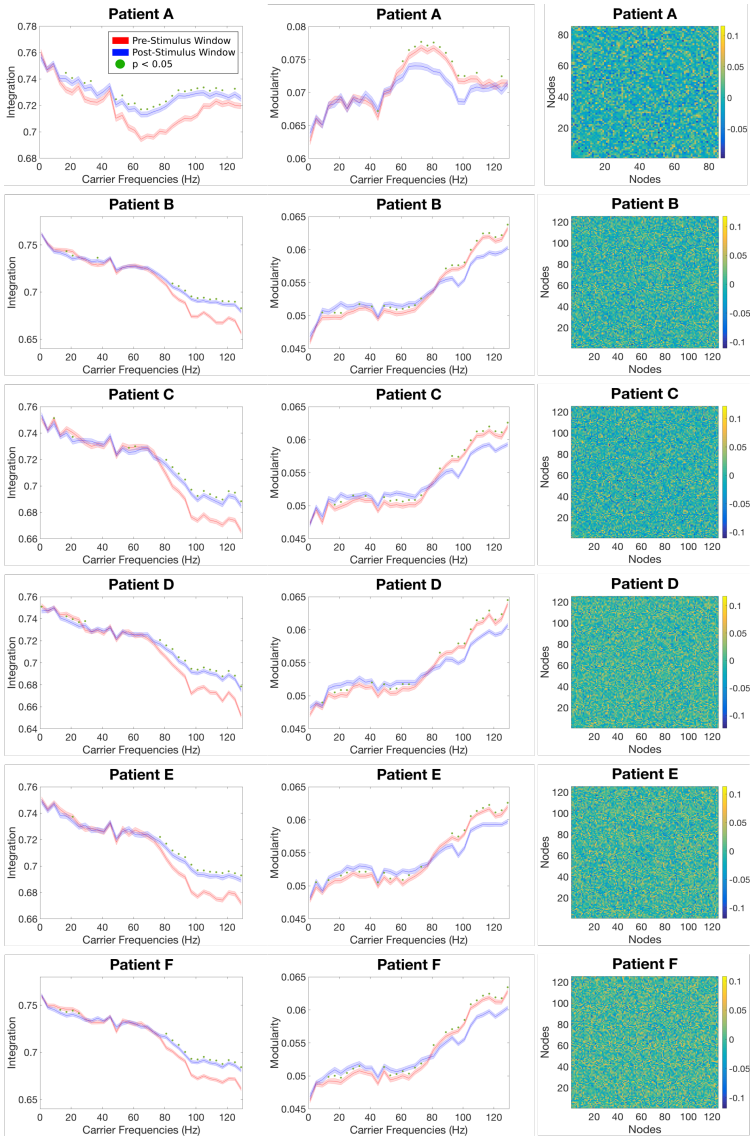
Patient A
Pre-Stimulus Window
Post-Stimulus Window
p < 0.05
Integration
Modularity
Nodes
Carrier Frequencies (Hz)
Patient B
Patient C
Patient D
Patient E
Patient F

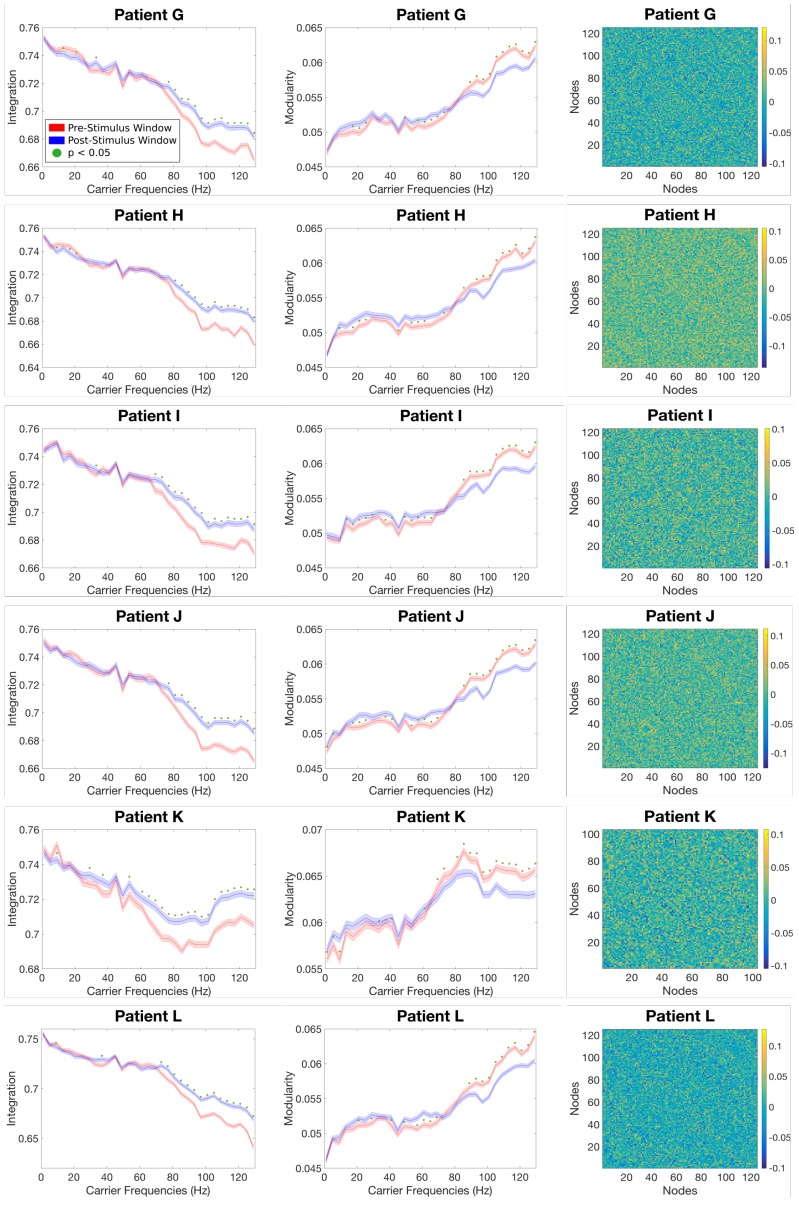

Figure S2.1: Integration measure using the FC matrices based on the monopolar montage for each participant

The panels in the left column show the integration modulation during pre- and post-stimulus presentation, respectively, for the picture-naming task. The modulation is seen in the whole range of frequencies. Panels in the middle column show the modulation of the segregation (measured by the modularity) during pre- and post-stimulus presentation, respectively, for the same task. Even though the difference of both windows is significant, note that the modulation is much smaller than the obtained when using the bipolar montage. The red line corresponds to pre-stimulus window, blue line corresponds to post-stimulus window. The shaded error regions reflect the standard deviation across trials and green dots indicates a statistical significance of $p<0.05$ ($N=1000$). The panels in the right column show the difference between pre- and post-stimulus windows FC matrices, based on the monopolar montage and computed for 60 Hz. The panels evidence the distributed character of the modulation across many different nodes.

Table 1
Demographic and clinical characteristics of each patient.

Patient	Gender	Age (years)	Epileptogenic zone laterality	Seizure onset zone	Implanted Regions	N° of electrodes implanted	N° unipolar channels	N° of bipolar channels for analysis
A	Male	38	Left	Mesial temporal and amygdala	L (F-T-I-P)	8	85	76
B	Male	21	Left	Anterior temporal	L (F-T-I-P-O) & R (F-T)	15	125	95
C	Male	44	Right	Anterior temporal	L (T) & R (F-T-P)	12	125	104
D	Male	44	Right	Temporo-parietal	L (T) & R (F-T-I-P)	16	127	101
E	Female	43	Left	Anterior medial temporal	L (F-T-I-P-O)	11	127	112
F	Male	25	Right	Temporo-parieto occipital	R (F-T-I-P-O)	14	127	105
G	Male	23	Left	Temporal	L (F-T-I-P)	13	125	102
H	Female	43	Left	Posterior Temporal	L (F-T-I-P)	14	125	103
I	Male	44	Left	Mesial Temporal	L (F-T-I-P)	12	123	105
J	Female	46	Left	Anterior medial temporal	L (F-T-I-P-O)	11	124	107
K	Male	43	Left	Mesial Temporal	L (F-T-P)	9	103	94
L	Male	23	Right	Anterior temporal	R (F-T-P)	15	125	96

R: Right; L: Left; F: Frontal; T: Temporal; P: Parietal; O: Occipital; I: Insula.

Table S2.1: Demographic and clinical characteristics of each patient

Participant	Gender	Age	Handedness	Hit Rate (%)	False Alarm Rate (%)
1	F	22	R	43,75	11,11
2	F	21	R	89,11	6,47
3	M	21	L	74,22	4,91
4	F	22	R	60,27	1,46
5	F	20	L	84,13	6,82
6	F	21	R	49,94	16,99
7	F	24	R	63,05	1,23
8	F	20	R	38,49	11,07
9	F	25	R	95,36	5,65
10	M	21	R	64,29	2,90
11	F	42	R	71,85	3,35
12	F	21	R	73,64	1,55
13	F	23	R	66,78	4,59
14	M	22	R	58,49	6,62
15	F	20	R	81,94	4,41
16	F	19	R	68,48	11,34
17	F	20	R	49,76	8,39
18	F	20	R	68,67	1,06
19	F	21	R	76,67	8,91
20	M	21	R	85,23	9,15
21	M	24	R	55,05	7,34
22	F	20	R	67,14	3,32
23	M	27	R	45,00	12,74
24	M	23	R	66,18	2,27
25	F	21	R	76,62	3,03
26	M	26	L	47,23	9,30
27	M	20	L	79,90	3,52
28	F	21	R	52,58	7,91
29	F	32	R	67,21	4,15
30	F	31	R	58,60	7,10
31	F	22	R	66,54	4,47
32	F	24	R	87,79	8,33
33	M	23	R	65,57	12,15
34	F	22	R	91,07	3,23
35	F	21	R	68,76	11,30
36	F	24	R	76,33	1,83
37	F	32	R	54,18	10,94
38	M	26	L	64,07	3,04

Table S3.1: Demographic characteristics and performance for each participant in Experiment 1

Excluded participants are marked in red.

Participant	Gender	Age	Handedness	Hit Rate (%)	False Alarm Rate (%)
1	F	22	R	58,31	9,03
2	M	26	R	58,91	10,25
3	M	21	R	75,53	10,39
4	F	21	R	56,80	13,33
5	M	29	R	45,63	27,76
6	F	23	R	87,67	4,38
7	F	22	R	46,12	6,51
8	F	23	R	78,25	2,49
9	M	23	R	70,52	5,00
10	F	23	L	61,37	8,51
11	M	24	R	52,73	11,66
12	M	24	R	63,72	0,00
13	M	26	R	66,98	6,57
14	F	29	R	56,40	7,80
15	F	26	R	71,46	10,80
16	F	20	R	68,27	3,82
17	M	22	R	64,59	9,09
18	M	19	R	77,62	6,34
19	M	27	R	76,33	6,23
20	F	19	R	77,14	4,93
21	F	23	R	69,17	4,45
22	M	20	R	60,29	4,90
23	F	23	R	76,56	1,40
24	M	18	R	70,26	10,10
25	M	19	L	70,12	6,81
26	M	25	R	66,51	3,11
27	M	20	R	60,14	11,23
28	F	22	L	63,36	7,12
29	F	21	R	69,09	1,08
30	F	23	L	60,43	10,10
31	F	20	R	72,60	7,22
32	F	23	R	67,29	5,38
33	M	22	R	74,54	4,04
34	M	20	L	60,19	4,73
35	M	25	R	57,41	10,39
36	M	26	R	67,76	12,68
37	F	31	R	61,56	10,36

Table S3.2: Demographic characteristics and performance for each participant in experiment 2

Excluded participants are marked in red.

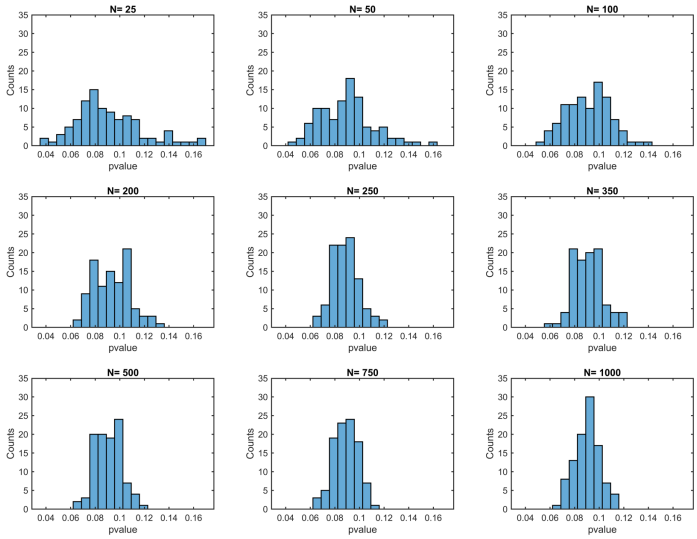

Figure S3.1: Assessing the stability of the POS measure

Histograms of p-values obtained for POS analysis with different number of random pickings. Each histogram contains 100 values.

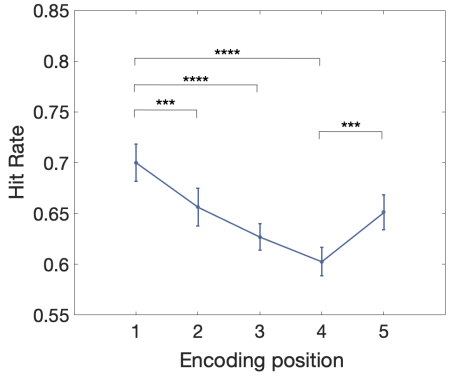

Figure S3.2: Serial position effect

Average hit rate for items as a function of their serial position in the list at encoding.

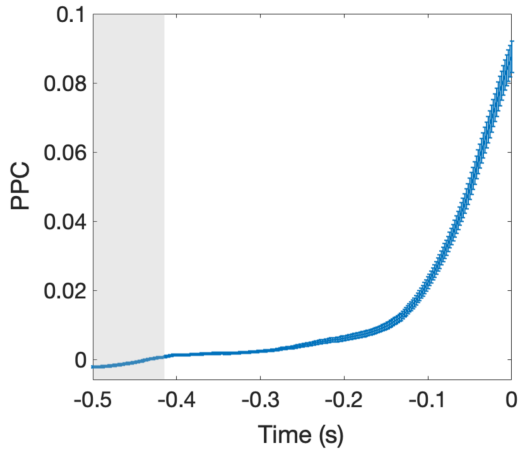

Figure S3.3: Average PPC time evolution for trials in middle encoding positions

Trials in the encoding middle positions (2, 3 & 4). Shaded area corresponds to PPC significantly smaller than null distribution after multiple comparison correction (Buchwald and Guthrie).

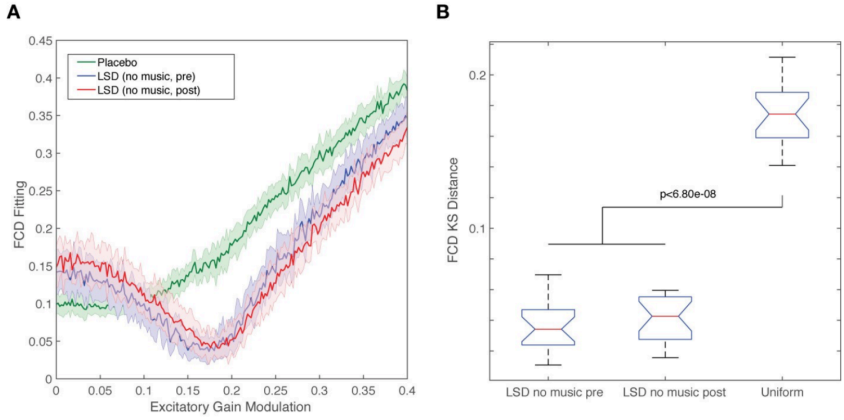

Figure S4.1: Results of whole-brain model of non-music LSD condition, related to Figure 4.1.

In order to confirm the results from the music LSD condition, we modelled the two non-music LSD conditions. (A) For the LSD conditions (no music pre and post), when using the optimal coupling point of the placebo condition and systematically scaling the excitatory gain function in each region with the empirical 5-HT_{2A} receptor data, we find that there is an optimum at around (0.17,0.036) (minimum of blue line, pre music) and at around (0.18,0.041) (minimum of red line, post music). In contrast, varying the scaling of the neuronal gain for the placebo condition does not yield an optimum (see monotonically rising green line) and thus the fit is not improved by changing the scaling of the neuronal gain by 5-HT_{2A} receptor density (with the error bars for three lines indicating the standard error across simulations). This clearly demonstrates that the LSD brain activity is dependent on the precise 5-HT_{2A} density distribution maps irrespective of music-listening. (B) Further, in the boxplot, we compare results of using the 5-HT_{2A} receptor densities across the regions at the optimum points, which are both significantly different ($p<6.80e-08$) from a uniform receptor density receptor map. This clearly demonstrates that the precise distribution of 5-HT_{2A} is very important for how LSD affects the brain state with or without music-listening.

LIST OF ABBREVIATIONS

5-HT$_{2A}$	5-hydroxytryptamine
AAL	Automated Anatomical Labelling
BLP	Bandpass Limited Power
BOLD	Blood-Oxygen-Level Dependent
CTC	Communication Through Coherence
DMF	Dynamic Mean-Field
DMN	Default-Mode Network
dMRI	Diffusion Magnetic Resonance Imaging
DTI	Diffusion Tensor Imaging
EEG	Electroencephalography/ Electroencephalogram
FC	Functional Connectivity
FCD	Functional Connectivity Dynamics
FDR	False Discovery Rate
FIC	Feedback Inhibition Control
fMRI	Functional Magnetic Resonance Imaging
GABA	gamma-Aminobutyric Acid
HCP	Human Connectome Project
HMM	Hidden Markov Model
ICA	Independent Component Analysis
IIT	Integrated Information Theory
iEEG	Intracranial Electroencephalography

KS	Kolmogorov-Smirnov
LFP	Local Field Potential
LSD	Lysergic acid diethylamide
MEG	Magnetic Resonance Imaging
MNI	Montreal Neurological Institute
NMDA	N-methyl-D-aspartate Acid
PET	Positron emission tomography
PhD	Doctor of Philosophy
ROI	Region of Interest
rsMRI	Resting State Magnetic Resonance Imaging
RSN	Resting State Network
SC	Structural Connectivity
std	Standard Deviation
TPM	Transition Probability Matrix
TTC	Temporo-spatial Theory of Consciousness

BIBLIOGRAPHY

Abbott, L. F., & Chance, F. S. (2005). Drivers and modulators from push-pull and balanced synaptic input. *Progress in Brain Research*. https://doi.org/10.1016/S0079-6123(05)49011-1

Achard, S., Salvador, R., Whitcher, B., Suckling, J., & Bullmore, E. D. (2006). A resilient, low-frequency, small-world human brain functional network with highly connected association cortical hubs. *Journal of Neuroscience*, *26*(1), 63–72. https://doi.org/10.1523/JNEUROSCI.3874-05.2006

Addante, R. J., de Chastelaine, M., & Rugg, M. D. (2015). Pre-stimulus neural activity predicts successful encoding of inter-item associations. *NeuroImage*, *105*, 21–31.

Addante, R. J., Watrous, A. J., Yonelinas, A. P., Ekstrom, A. D., & Ranganath, C. (2011). Prestimulus theta activity predicts correct source memory retrieval. *Proc Natl Acad Sci U S A*, *108*(26), 10702–10707. https://doi.org/10.1073/pnas.1014528108

Alex, K. D., & Pehek, E. A. (2007). Pharmacologic mechanisms of serotonergic regulation of dopamine neurotransmission. *Pharmacology and Therapeutics*. https://doi.org/10.1016/j.pharmthera.2006.08.004

Allen, E. A., Damaraju, E., Plis, S. M., Erhardt, E. B., Eichele, T., & Calhoun, V. D. (2014). Tracking whole-brain connectivity dynamics in the resting state. *Cerebral Cortex*, *24*(3), 663–676. https://doi.org/10.1093/cercor/bhs352

Amara, S. G., & Kuhar, M. J. (1993). Neurotransmitter transporters: recent progress. *Annual Review of Neuroscience*, *16*(1), 73–93.

Asl, M. M., Vahabie, A.-H., & Valizadeh, A. (2019). Dopaminergic Modulation of Synaptic Plasticity, Its Role in Neuropsychiatric Disorders, and Its Computational Modeling. *Basic and Clinical Neuroscience*, *10*(1), 1.

Aston-Jones, G., & Cohen, J. D. (2005). AN INTEGRATIVE THEORY OF LOCUS COERULEUS-NOREPINEPHRINE FUNCTION: Adaptive Gain and Optimal Performance. *Annual Review of Neuroscience*. https://doi.org/10.1146/annurev.neuro.28.061604.135709

Atasoy, S., Deco, G., Kringelbach, M. L., & Pearson, J. (2018). Harmonic Brain Modes: A Unifying Framework for Linking Space and Time in Brain Dynamics. *Neuroscientist*. https://doi.org/10.1177/1073858417728032

Atasoy, S., Roseman, L., Kaelen, M., Kringelbach, M. L., Deco, G., & Carhart-Harris, R. L. (2017). Connectome-harmonic decomposition of human brain activity reveals dynamical repertoire re-organization under LSD. *Scientific Reports*. https://doi.org/10.1038/s41598-017-17546-0

Atkinson, R. C., & Shiffrin, R. M. (1968). Human Memory: A Proposed System and its Control Processes. *Psychology of Learning and Motivation - Advances in Research and Theory*. https://doi.org/10.1016/S0079-7421(08)60422-3

Axmacher, N., Schmitz, D. P., Wagner, T., Elger, C. E., & Fell, J. (2008). Interactions between medial temporal lobe, prefrontal cortex, and inferior temporal regions during visual working memory: a combined intracranial EEG and functional magnetic resonance imaging study. *Journal of Neuroscience*, *28*(29), 7304–7312.

Azmitia, E. C., & Gannon, P. J. (1986). The primate serotonergic system: a review of human and animal studies and a report on Macaca fascicularis. *Advances in Neurology*.

Baars, B. J. (2002). The conscious access hypothesis: Origins and recent evidence. *Trends in Cognitive Sciences*.

https://doi.org/10.1016/S1364-6613(00)01819-2

Baars, B. J. (2005). Global workspace theory of consciousness: Toward a cognitive neuroscience of human experience. *Progress in Brain Research*. https://doi.org/10.1016/S0079-6123(05)50004-9

Backus, A. R., Schoffelen, J.-M., Szebényi, S., Hanslmayr, S., & Doeller, C. F. (2016). Hippocampal-prefrontal theta oscillations support memory integration. *Current Biology*, *26*(4), 450–457.

Balasubramani, P. P., Chakravarthy, V. S., Ravindran, B., & Moustafa, A. A. (2015). A network model of basal ganglia for understanding the roles of dopamine and serotonin in reward-punishment-risk based decision making. *Frontiers in Computational Neuroscience*. https://doi.org/10.3389/fncom.2015.00076

Ball, T., Demandt, E., Mutschler, I., Neitzel, E., Mehring, C., Vogt, K., … Schulze-Bonhage, A. (2008). Movement related activity in the high gamma range of the human EEG. *Neuroimage*, *41*(2), 302–310.

Bargmann, C. I. (2012). Beyond the connectome: how neuromodulators shape neural circuits. *Bioessays*, *34*(6), 458–465.

Barnes, N. M., & Sharp, T. (1999). A review of central 5-HT receptors and their function. *Neuropharmacology*. https://doi.org/10.1016/S0028-3908(99)00010-6

Bassett, D. S., Wymbs, N. F., Porter, M. A., Mucha, P. J., Carlson, J. M., & Grafton, S. T. (2011). Dynamic reconfiguration of human brain networks during learning. *Proceedings of the National Academy of Sciences*, *108*(18), 7641–7646.

Becher, A., Höhne, M., Axmacher, N., Chaieb, L., Elger, C. E., & Fell, J. (2015). Intracranial electroencephalography power and phase synchronization changes during monaural and binaural beat stimulation. *European Journal of Neuroscience*, *41*(2),

254–263.

Beckmann, C. F., & Smith, S. M. (2004). Probabilistic independent component analysis for functional magnetic resonance imaging. *IEEE Transactions on Medical Imaging*, *23*(2), 137–152. https://doi.org/10.1109/TMI.2003.822821

Bédard, C., Wallman, M. J., Pourcher, E., Gould, P. V., Parent, A., & Parent, M. (2011). Serotonin and dopamine striatal innervation in Parkinson's disease and Huntington's chorea. *Parkinsonism and Related Disorders*. https://doi.org/10.1016/j.parkreldis.2011.05.012

Behrens, T. E. J. J., Berg, H. J., Jbabdi, S., Rushworth, M. F. S. S., & Woolrich, M. W. (2007). Probabilistic diffusion tractography with multiple fibre orientations: What can we gain? *Neuroimage*, *34*(1), 144–155. https://doi.org/10.1016/j.neuroimage.2006.09.018

Beliveau, V., Ganz, M., Feng, L., Ozenne, B., Højgaard, L., Fisher, P. M. M., … Knudsen, G. M. M. (2017). A High-Resolution In Vivo Atlas of the Human Brain's Serotonin System. *Journal of Neuroscience*, *37*(1), 120–128. https://doi.org/10.1523/JNEUROSCI.2830-16.2016

Benjamini, Y., & Hochberg, Y. (1995). Controlling the false discovery rate: a practical and powerful approach to multiple testing. *Journal of the Royal Statistical Society: Series B (Methodological)*, *57*(1), 289–300.

Berridge, K. C., & Kringelbach, M. L. (2015). Pleasure Systems in the Brain. *Neuron*. https://doi.org/10.1016/j.neuron.2015.02.018

Bertrand, J.-A., Tremblay, J., Lassonde, M., Vannasing, P., Nguyen, D. K., Robert, M., … Lepore, F. (2014). Recognizing an object from the sum of its parts: An intracranial study on alpha rhythms. *Journal of Cognitive Neuroscience*, *26*(8), 1797–1805.

Bettinardi, R. G., Deco, G., Karlaftis, V. M., Van Hartevelt, T. J.,

Fernandes, H. M., Kourtzi, Z., … Zamora-López, G. (2017). How structure sculpts function: Unveiling the contribution of anatomical connectivity to the brain's spontaneous correlation structure. *Chaos*. https://doi.org/10.1063/1.4980099

Biswal, B., Zerrin Yetkin, F., Haughton, V. M., & Hyde, J. S. (1995). Functional connectivity in the motor cortex of resting human brain using echo-planar MRI. *Magnetic Resonance in Medicine*, *34*(4), 537–541. https://doi.org/10.1002/mrm.1910340409

Blumenfeld, R. S., & Ranganath, C. (2007). Prefrontal cortex and long-term memory encoding: An integrative review of findings from neuropsychology and neuroimaging. *Neuroscientist*. https://doi.org/10.1177/1073858407299290

Bogenschutz, M. P., Forcehimes, A. A., Pommy, J. A., Wilcox, C. E., Barbosa, P., & Strassman, R. J. (2015). Psilocybin-assisted treatment for alcohol dependence: A proof-of-concept study. *Journal of Psychopharmacology*. https://doi.org/10.1177/0269881114565144

Bola, M., & Sabel, B. A. (2015). Dynamic reorganization of brain functional networks during cognition. *Neuroimage*, *114*, 398–413.

Boucher, O., D'Hondt, F., Tremblay, J., Lepore, F., Lassonde, M., Vannasing, P., … Nguyen, D. K. (2015). Spatiotemporal dynamics of affective picture processing revealed by intracranial high-gamma modulations. *Human Brain Mapping*, *36*(1), 16–28.

Boureau, Y. L., & Dayan, P. (2011). Opponency revisited: Competition and cooperation between dopamine and serotonin. *Neuropsychopharmacology*. https://doi.org/10.1038/npp.2010.151

Brady, T. F., Konkle, T., Alvarez, G. A., & Oliva, A. (2008). Visual long-term memory has a massive storage capacity for object details. *Proc Natl Acad Sci U S A*, *105*(38), 14325–14329. https://doi.org/10.1073/pnas.0803390105

Brainard, D. H. (1997). The Psychophysics Toolbox. *Spat Vis*, *10*(4), 433–436. Retrieved from https://www.ncbi.nlm.nih.gov/pubmed/9176952

Brassen, S., Weber-Fahr, W., Sommer, T., Lehmbeck, J. T., & Braus, D. F. (2006). Hippocampal–prefrontal encoding activation predicts whether words can be successfully recalled or only recognized. *Behavioural Brain Research*, *171*(2), 271–278.

Breakspear, M. (2017). Dynamic models of large-scale brain activity. *Nature Neuroscience*. https://doi.org/10.1038/nn.4497

Breakspear, M., & Jirsa, V. K. (2007). Neuronal dynamics and brain connectivity. In *Handbook of brain connectivity* (pp. 3–64). Springer.

Bressler, S. L., & Kelso, J. A. S. (2001). Cortical coordination dynamics and cognition. *Trends in Cognitive Sciences*. https://doi.org/10.1016/S1364-6613(00)01564-3

Bressler, Steven L. (1995). Large-scale cortical networks and cognition. *Brain Research Reviews*. https://doi.org/10.1016/0165-0173(94)00016-I

Bressler, Steven L., & Tognoli, E. (2006). Operational principles of neurocognitive networks. *International Journal of Psychophysiology*. https://doi.org/10.1016/j.ijpsycho.2005.12.008

Bressler, Steven L, & Menon, V. (2010). Large-scale brain networks in cognition: emerging methods and principles. *Trends in Cognitive Sciences*, *14*(6), 277–290.

Brewer, J. B., Zhao, Z., Desmond, J. E., Glover, G. H., & Gabrieli, J. D. E. (1998). Making memories: brain activity that predicts how well visual experience will be remembered. *Science*, *281*(5380), 1185–1187.

Brodeur, M. B., Dionne-Dostie, E., Montreuil, T., & Lepage, M. (2010). The Bank of Standardized Stimuli (BOSS), a new set of

480 normative photos of objects to be used as visual stimuli in cognitive research. *PLoS One*, *5*(5), e10773. https://doi.org/10.1371/journal.pone.0010773

Brodeur, M. B., Guerard, K., & Bouras, M. (2014). Bank of Standardized Stimuli (BOSS) phase II: 930 new normative photos. *PLoS One*, *9*(9), e106953. https://doi.org/10.1371/journal.pone.0106953

Brookes, M. J., Hale, J. R., Zumer, J. M., Stevenson, C. M., Francis, S. T., Barnes, G. R., … Nagarajan, S. S. (2011). Measuring functional connectivity using MEG: methodology and comparison with fcMRI. *Neuroimage*, *56*(3), 1082–1104.

Brookes, M. J., Woolrich, M., Luckhoo, H., Price, D., Hale, J. R., Stephenson, M. C., … Morris, P. G. (2011). Investigating the electrophysiological basis of resting state networks using magnetoencephalography. *Proceedings of the National Academy of Sciences*, *108*(40), 16783–16788.

Brunel, N., & Wang, X.-J. J. (2001). Effects of neuromodulation in a cortical network model of object working memory dominated by recurrent inhibition. *Journal of Computational Neuroscience*, *11*(1), 63–85. https://doi.org/10.1023/A:1011204814320

Brunel, N., & Wang, X. J. (2003). What determines the frequency of fast network oscillations with irregular neural discharges? I. Synaptic dynamics and excitation-inhibition balance. *Journal of Neurophysiology*. https://doi.org/10.1152/jn.01095.2002

Brzosko, Z., Mierau, S. B., & Paulsen, O. (2019). Neuromodulation of Spike-Timing-Dependent Plasticity: Past, Present, and Future. *Neuron*. https://doi.org/10.1016/j.neuron.2019.05.041

Buckner, R. L., Sepulcre, J., Talukdar, T., Krienen, F. M., Liu, H., Hedden, T., … Johnson, K. A. (2009). Cortical hubs revealed by intrinsic functional connectivity: mapping, assessment of stability, and relation to Alzheimer's disease. *Journal of Neuroscience*, *29*(6), 1860–1873.

https://doi.org/10.1523/JNEUROSCI.5062-08.2009

Bullmore, E., & Sporns, O. (2009). Complex brain networks: Graph theoretical analysis of structural and functional systems. *Nature Reviews Neuroscience*. https://doi.org/10.1038/nrn2575

Bullmore, E., & Sporns, O. (2012). The economy of brain network organization. *Nature Reviews Neuroscience*. https://doi.org/10.1038/nrn3214

Burke, J. F., Zaghloul, K. A., Jacobs, J., Williams, R. B., Sperling, M. R., Sharan, A. D., & Kahana, M. J. (2013). Synchronous and asynchronous theta and gamma activity during episodic memory formation. *Journal of Neuroscience*, *33*(1), 292–304.

Burns, B. D., & Webb, A. C. (1976). The spontaneous activity of neurones in the cat's cerebral cortex. *Proceedings of the Royal Society of London. Series B, Biological Sciences*, 211–223.

Busch, N A, Dubois, J., & VanRullen, R. (2009). The phase of ongoing EEG oscillations predicts visual perception. *J Neurosci*, *29*(24), 7869–7876. https://doi.org/10.1523/JNEUROSCI.0113-09.2009

Busch, Niko A., & VanRullen, R. (2010). Spontaneous EEG oscillations reveal periodic sampling of visual attention. *Proc Natl Acad Sci U S A*, *107*(37), 16048–16053. https://doi.org/10.1073/pnas.1004801107

Buzsáki, G. (2009). Rhythms of the Brain. In *Rhythms of the Brain*. https://doi.org/10.1093/acprof:oso/9780195301069.001.0001

Buzsaki, G., & Draguhn, A. (2004). Neuronal oscillations in cortical networks. *Science*, *304*(5679), 1926–1929. https://doi.org/10.1126/science.1099745

Cabral, J, Kringelbach, M. L., & Deco, G. (2014). Exploring the network dynamics underlying brain activity during rest. *Prog Neurobiol*, *114*, 102–131. https://doi.org/10.1016/j.pneurobio.2013.12.005

Cabral, Joana, Hugues, E., Sporns, O., & Deco, G. (2011). Role of local network oscillations in resting-state functional connectivity. *NeuroImage*. https://doi.org/10.1016/j.neuroimage.2011.04.010

Cabral, Joana, Kringelbach, M. L., & Deco, G. (2017). Functional connectivity dynamically evolves on multiple time-scales over a static structural connectome: Models and mechanisms. *NeuroImage*. https://doi.org/10.1016/j.neuroimage.2017.03.045

Cabral, Joana, Luckhoo, H., Woolrich, M., Joensson, M., Mohseni, H., Baker, A., … Deco, G. (2014). Exploring mechanisms of spontaneous functional connectivity in MEG: how delayed network interactions lead to structured amplitude envelopes of band-pass filtered oscillations. *Neuroimage*, *90*, 423–435.

Carhart-Harris, R. L., Bolstridge, M., Day, C. M. J., Rucker, J., Watts, R., Erritzoe, D. E., … Nutt, D. J. (2018). Psilocybin with psychological support for treatment-resistant depression: six-month follow-up. *Psychopharmacology*. https://doi.org/10.1007/s00213-017-4771-x

Carhart-Harris, R. L., Kaelen, M., Bolstridge, M., Williams, T. M., Williams, L. T., Underwood, R., … Nutt, D. J. (2016). The paradoxical psychological effects of lysergic acid diethylamide (LSD). *Psychological Medicine*. https://doi.org/10.1017/S0033291715002901

Carhart-Harris, R. L., & Nutt, D. J. (2017). Serotonin and brain function: A tale of two receptors. *Journal of Psychopharmacology*. https://doi.org/10.1177/0269881117725915

Carhart-Harris, Robin L., Bolstridge, M., Rucker, J., Day, C. M. J., Erritzoe, D., Kaelen, M., … Nutt, D. J. (2016). Psilocybin with psychological support for treatment-resistant depression: an open-label feasibility study. *The Lancet Psychiatry*. https://doi.org/10.1016/S2215-0366(16)30065-7

Carhart-Harris, Robin L., Muthukumaraswamy, S., Roseman, L.,

Kaelen, M., Droog, W., Murphy, K., … Nutt, D. J. (2016). Neural correlates of the LSD experience revealed by multimodal neuroimaging. *Proceedings of the National Academy of Sciences of the United States of America*. https://doi.org/10.1073/pnas.1518377113

Carhart-Harris, Robin L., Roseman, L., Haijen, E., Erritzoe, D., Watts, R., Branchi, I., & Kaelen, M. (2018). Psychedelics and the essential importance of context. *Journal of Psychopharmacology*. https://doi.org/10.1177/0269881118754710

Chai, L. R., Mattar, M. G., Blank, I. A., Fedorenko, E., & Bassett, D. S. (2016). Functional network dynamics of the language system. *Cerebral Cortex*, *26*(11), 4148–4159.

Chan, A. M., Baker, J. M., Eskandar, E., Schomer, D., Ulbert, I., Marinkovic, K., … Halgren, E. (2011). First-pass selectivity for semantic categories in human anteroventral temporal lobe. *Journal of Neuroscience*, *31*(49), 18119–18129.

Chance, F. S., Abbott, L. F., & Reyes, A. D. (2002). Gain modulation from background synaptic input. *Neuron*. https://doi.org/10.1016/S0896-6273(02)00820-6

Chang, C., & Glover, G. H. (2010). Time-frequency dynamics of resting-state brain connectivity measured with fMRI. *NeuroImage*. https://doi.org/10.1016/j.neuroimage.2009.12.011

Chun, M. M., & Turk-Browne, N. B. (2007). Interactions between attention and memory. *Current Opinion in Neurobiology*. https://doi.org/10.1016/j.conb.2007.03.005

Clouter, A., Shapiro, K. L., & Hanslmayr, S. (2017). Theta Phase Synchronization Is the Glue that Binds Human Associative Memory. *Curr Biol*, *27*(20), 3143-3148 e6. https://doi.org/10.1016/j.cub.2017.09.001

Cocchi, L., Gollo, L. L., Zalesky, A., & Breakspear, M. (2017). Criticality in the brain: A synthesis of neurobiology, models and

cognition. *Progress in Neurobiology*. https://doi.org/10.1016/j.pneurobio.2017.07.002

Cohen, J. D., Braver, T. S., & Brown, J. W. (2002). Computational perspectives on dopamine function in prefrontal cortex. *Current Opinion in Neurobiology*. https://doi.org/10.1016/S0959-4388(02)00314-8

Cohen, J. R., & D'Esposito, M. (2016). The segregation and integration of distinct brain networks and their relationship to cognition. *Journal of Neuroscience*. https://doi.org/10.1523/JNEUROSCI.2965-15.2016

Cole, M. W., Bassett, D. S., Power, J. D., Braver, T. S., & Petersen, S. E. (2014). Intrinsic and task-evoked network architectures of the human brain. *Neuron*. https://doi.org/10.1016/j.neuron.2014.05.014

Cole, M. W., Reynolds, J. R., Power, J. D., Repovs, G., Anticevic, A., & Braver, T. S. (2013). Multi-task connectivity reveals flexible hubs for adaptive task control. *Nature Neuroscience*. https://doi.org/10.1038/nn.3470

Collins, D. L., Neelin, P., Peters, T. M., & Evans, A. C. (1994). Automatic 3D intersubject registration of MR volumetric data in standardized Talairach space. *Journal of Computer Assisted Tomography*, *18*(2), 192–205. https://doi.org/10.1097/00004728-199403000-00005

Comtat, C., Sureau, F. C., Sibomana, M., Hong, I. K., Sjöholm, N., Trélbossen, R., … Trebossen, R. (2008). Image based resolution modeling for the HRRT OSEM reconstructions software. *Nuclear Science Symposium Conference Record, 2008. NSS'08. IEEE*, 4120–4123. https://doi.org/10.1109/NSSMIC.2008.4774188

Conn, P. J., Tamminga, C., Schoepp, D. D., & Lindsley, C. (2008). Schizophrenia: Moving beyond monoamine antagonists. *Molecular Interventions*. https://doi.org/10.1124/mi.8.2.7

Cruzat, J., Deco, G., Tauste-Campo, A., Principe, A., Costa, A., Kringelbach, M. L., & Rocamora, R. (2018). The dynamics of human cognition: Increasing global integration coupled with decreasing segregation found using iEEG. *NeuroImage*. https://doi.org/10.1016/j.neuroimage.2018.01.064

Cuthbert, B. N., & Insel, T. R. (2013). Toward the future of psychiatric diagnosis: The seven pillars of RDoC. *BMC Medicine*. https://doi.org/10.1186/1741-7015-11-126

Daitch, A. L., Sharma, M., Roland, J. L., Astafiev, S. V, Bundy, D. T., Gaona, C. M., … Corbetta, M. (2013). Frequency-specific mechanism links human brain networks for spatial attention. *Proceedings of the National Academy of Sciences*, *110*(48), 19585–19590.

Davison, E. N., Schlesinger, K. J., Bassett, D. S., Lynall, M. E., Miller, M. B., Grafton, S. T., & Carlson, J. M. (2015). Brain Network Adaptability across Task States. *PLoS Computational Biology*. https://doi.org/10.1371/journal.pcbi.1004029

Dayan, P. (2012). Twenty-Five Lessons from Computational Neuromodulation. *Neuron*. https://doi.org/10.1016/j.neuron.2012.09.027

de Graaf, T. A., Gross, J., Paterson, G., Rusch, T., Sack, A. T., & Thut, G. (2013). Alpha-band rhythms in visual task performance: phase-locking by rhythmic sensory stimulation. *PLoS One*, *8*(3), e60035. https://doi.org/10.1371/journal.pone.0060035

Deco, G., Cabral, J., Woolrich, M. W., Stevner, A. B. A. A., Van Hartevelt, T. J., & Kringelbach, M. L. (2017). Single or multiple frequency generators in on-going brain activity: A mechanistic whole-brain model of empirical MEG data. *Neuroimage*, *152*, 538–550. https://doi.org/10.1016/j.neuroimage.2017.03.023

Deco, G., & Corbetta, M. (2011). The dynamical balance of the brain at rest. *Neuroscientist*. https://doi.org/10.1177/1073858409354384

Deco, G., Cruzat, J., Cabral, J., Knudsen, G. M., Carhart-Harris, R. L., Whybrow, P. C., … Kringelbach, M. L. (2018). Whole-brain multimodal neuroimaging model using serotonin receptor maps explains non-linear functional effects of LSD. *Current Biology*, *28*(19), 3065-3074. e6.

Deco, G., Cruzat, J., Cabral, J., Tagliazucchi, E., Laufs, H., Logothetis, N. K., & Kringelbach, M. L. (2019). Awakening: Predicting external stimulation to force transitions between different brain states. *Proceedings of the National Academy of Sciences of the United States of America*. https://doi.org/10.1073/pnas.1905534116

Deco, G., Cruzat, J., & Kringelbach, M. L. (2019). Brain songs framework used for discovering the relevant timescale of the human brain. *Nature Communications*. https://doi.org/10.1038/s41467-018-08186-7

Deco, G., Jirs, V., McIntosh, A. R., Sporns, O., & Kötter, R. (2009). Key role of coupling, delay, and noise in resting brain fluctuations. *Proceedings of the National Academy of Sciences of the United States of America*. https://doi.org/10.1073/pnas.0901831106

Deco, G., & Jirsa, V. K. (2012). Ongoing cortical activity at rest: criticality, multistability, and ghost attractors. *Journal of Neuroscience*, *32*(10), 3366–3375. https://doi.org/10.1523/JNEUROSCI.2523-11.2012

Deco, G., Jirsa, V. K., & McIntosh, A. R. (2011). Emerging concepts for the dynamical organization of resting-state activity in the brain. *Nature Reviews Neuroscience*. https://doi.org/10.1038/nrn2961

Deco, G., Jirsa, V. K., & McIntosh, A. R. (2013). Resting brains never rest: Computational insights into potential cognitive architectures. *Trends in Neurosciences*. https://doi.org/10.1016/j.tins.2013.03.001

Deco, G., Jirsa, V. K., Robinson, P. A., Breakspear, M., & Friston,

K. (2008). The dynamic brain: From spiking neurons to neural masses and cortical fields. *PLoS Computational Biology*. https://doi.org/10.1371/journal.pcbi.1000092

Deco, G., & Kringelbach, M. L. (2014). Great expectations: using whole-brain computational connectomics for understanding neuropsychiatric disorders. *Neuron*, *84*(5), 892–905.

Deco, G., & Kringelbach, M. L. (2016). Metastability and coherence: extending the communication through coherence hypothesis using a whole-brain computational perspective. *Trends in Neurosciences*, *39*(3), 125–135.

Deco, G., & Kringelbach, M. L. (2017). Hierarchy of information processing in the brain: a novel 'intrinsic ignition'framework. *Neuron*, *94*(5), 961–968.

Deco, G., Kringelbach, M. L., Jirsa, V. K., & Ritter, P. (2017). The dynamics of resting fluctuations in the brain: metastability and its dynamical cortical core. *Scientific Reports*, *7*(1), 3095.

Deco, G., Ponce-Alvarez, A., Hagmann, P., Romani, G. L., Mantini, D., & Corbetta, M. (2014). How local excitation–inhibition ratio impacts the whole brain dynamics. *Journal of Neuroscience*, *34*(23), 7886–7898.

Deco, G., Ponce-Alvarez, A., Mantini, D., Romani, G. L., Hagmann, P., & Corbetta, M. (2013). Resting-state functional connectivity emerges from structurally and dynamically shaped slow linear fluctuations. *Journal of Neuroscience*. https://doi.org/10.1523/JNEUROSCI.1091-13.2013

Deco, G., Tononi, G., Boly, M., & Kringelbach, M. L. (2015). Rethinking segregation and integration: contributions of whole-brain modelling. *Nature Reviews Neuroscience*, *16*(7), 430–439.

Deese, J., & Kaufman, R. A. (1957). Serial effects in recall of unorganized and sequentially organized verbal material. *Journal of Experimental Psychology*, *54*(3), 180.

Dehaene, S., & Changeux, J.-P. P. (2011). Experimental and theoretical approaches to conscious processing. *Neuron*, *70*(2), 200–227. https://doi.org/10.1016/j.neuron.2011.03.018

Dehaene, S., Kerszberg, M., & Changeux, J.-P. P. (1998). A neuronal model of a global workspace in effortful cognitive tasks. *Proceedings of the National Academy of Sciences*, *95*(24), 14529–14534. https://doi.org/10.1073/pnas.95.24.14529

Di, X., Gohel, S., Kim, E. H., & Biswal, B. B. (2013). Task vs. rest-different network configurations between the coactivation and the resting-state brain networks. *Frontiers in Human Neuroscience*. https://doi.org/10.3389/fnhum.2013.00493

Doppelmayr, M., Klimesch, W., Pachinger, T., & Ripper, B. (1998). Individual differences in brain dynamics: important implications for the calculation of event-related band power. *Biological Cybernetics*, *79*(1), 49–57.

Eickhoff, S. B., Constable, R. T., & Yeo, B. T. T. (2018). Topographic organization of the cerebral cortex and brain cartography. *NeuroImage*. https://doi.org/10.1016/j.neuroimage.2017.02.018

Eickhoff, S. B., Schleicher, A., Scheperjans, F., Palomero-Gallagher, N., & Zilles, K. (2007). Analysis of neurotransmitter receptor distribution patterns in the cerebral cortex. *NeuroImage*. https://doi.org/10.1016/j.neuroimage.2006.11.016

Eickhoff, S. B., Yeo, B. T. T., & Genon, S. (2018). Imaging-based parcellations of the human brain. *Nature Reviews Neuroscience*. https://doi.org/10.1038/s41583-018-0071-7

Ekman, M., Derrfuss, J., Tittgemeyer, M., & Fiebach, C. J. (2012). Predicting errors from reconfiguration patterns in human brain networks. *Proceedings of the National Academy of Sciences*, *109*(41), 16714–16719.

Engel, A. K., Moll, C. K. E., Fried, I., & Ojemann, G. A. (2005). Invasive recordings from the human brain: clinical insights and

beyond. *Nature Reviews Neuroscience*, *6*(1), 35.

Ettrup, A., Da Cunha-Bang, S., Mcmahon, B., Lehel, S., Dyssegaard, A., Skibsted, A. W., … Knudsen, G. M. (2014). Serotonin 2A receptor agonist binding in the human brain with [11 C]Cimbi-36. *Journal of Cerebral Blood Flow and Metabolism*. https://doi.org/10.1038/jcbfm.2014.68

Ettrup, A., Svarer, C., McMahon, B., da Cunha-Bang, S., Lehel, S., Møller, K., … Knudsen, G. M. (2016). Serotonin 2A receptor agonist binding in the human brain with [11C]Cimbi-36: Test-retest reproducibility and head-to-head comparison with the antagonist [18F]altanserin. *NeuroImage*. https://doi.org/10.1016/j.neuroimage.2016.02.001

Fallani, F. D. V., Astolfi, L., Cincotti, F., Mattia, D., Tocci, A., Salinari, S., … Babiloni, F. (2008). Brain network analysis from high-resolution EEG recordings by the application of theoretical graph indexes. *IEEE Transactions on Neural Systems and Rehabilitation Engineering*, *16*(5), 442–452.

Fell, J, Ludowig, E., Staresina, B. P., Wagner, T., Kranz, T., Elger, C. E., & Axmacher, N. (2011). Medial temporal theta/alpha power enhancement precedes successful memory encoding: evidence based on intracranial EEG. *J Neurosci*, *31*(14), 5392–5397. https://doi.org/10.1523/JNEUROSCI.3668-10.2011

Fell, Juergen, & Axmacher, N. (2011). The role of phase synchronization in memory processes. *Nature Reviews Neuroscience*, *12*(2), 105.

Fell, Juergen, Klaver, P., Elfadil, H., Schaller, C., Elger, C. E., & Fernández, G. (2003). Rhinal-hippocampal theta coherence during declarative memory formation: Interaction with gamma synchronization? *European Journal of Neuroscience*. https://doi.org/10.1046/j.1460-9568.2003.02522.x

Fell, Juergen, Ludowig, E., Rosburg, T., Axmacher, N., & Elger, C. E. (2008). Phase-locking within human mediotemporal lobe predicts memory formation. *NeuroImage*.

https://doi.org/10.1016/j.neuroimage.2008.07.021

Fell, Jürgen, Klaver, P., Lehnertz, K., Grunwald, T., Schaller, C., Elger, C. E., & Fernández, G. (2001). Human memory formation is accompanied by rhinal–hippocampal coupling and decoupling. *Nature Neuroscience*, *4*(12), 1259.

Fellner, M. C., Gollwitzer, S., Rampp, S., Kreiselmeyr, G., Bush, D., Diehl, B., … Hanslmayr, S. (2019). Spectral fingerprints or spectral tilt? Evidence for distinct oscillatory signatures of memory formation. *PLoS Biology*. https://doi.org/10.1371/journal.pbio.3000403

Fellner, M. C., Volberg, G., Wimber, M., Goldhacker, M., Greenlee, M. W., & Hanslmayr, S. (2016). Spatial mnemonic encoding: Theta power decreases and medial temporal lobe BOLD increases co-occur during the usage of the method of loci. *ENeuro*. https://doi.org/10.1523/ENEURO.0184-16.2016

Fernández, G., Effern, A., Grunwald, T., Pezer, N., Lehnertz, K., Dümpelmann, M., … Elger, C. E. (1999). Real-time tracking of memory formation in the human rhinal cortex and hippocampus. *Science*, *285*(5433), 1582–1585.

Ferstl, E. C., Neumann, J., Bogler, C., & Von Cramon, D. Y. (2008). The extended language network: a meta-analysis of neuroimaging studies on text comprehension. *Human Brain Mapping*, *29*(5), 581–593.

Fibiger, H. C. (1995). Neurobiology of depression: Focus of dopamine. *Depression and Mania: From Neurobiology to Treatment*.

Fiebelkorn, I. C., Foxe, J. J., Butler, J. S., Mercier, M. R., Snyder, A. C., & Molholm, S. (2011). Ready, set, reset: stimulus-locked periodicity in behavioral performance demonstrates the consequences of cross-sensory phase reset. *J Neurosci*, *31*(27), 9971–9981. https://doi.org/10.1523/JNEUROSCI.1338-11.2011

Fiebelkorn, I. C., Pinsk, M. A., & Kastner, S. (2018). A Dynamic Interplay within the Frontoparietal Network Underlies Rhythmic Spatial Attention. *Neuron*, *99*(4), 842-853 e8. https://doi.org/10.1016/j.neuron.2018.07.038

Fiebelkorn, I. C., Saalmann, Y. B., & Kastner, S. (2013). Rhythmic sampling within and between objects despite sustained attention at a cued location. *Curr Biol*, *23*(24), 2553–2558. https://doi.org/10.1016/j.cub.2013.10.063

Fischl, B. (2012). FreeSurfer. *Neuroimage*, *62*(2), 774–781. https://doi.org/10.1016/j.neuroimage.2012.01.021

Fountoulakis, K. N., & Möller, H. J. (2011). Efficacy of antidepressants: A re-analysis and re-interpretation of the Kirsch data. *International Journal of Neuropsychopharmacology*. https://doi.org/10.1017/S1461145710000957

Fox, M. D., Snyder, A. Z., Vincent, J. L., Corbetta, M., Van Essen, D. C., & Raichle, M. E. (2005). The human brain is intrinsically organized into dynamic, anticorrelated functional networks. *Proceedings of the National Academy of Sciences of the United States of America*. https://doi.org/10.1073/pnas.0504136102

Fox, P. T., & Friston, K. J. (2012). Distributed processing; distributed functions? *Neuroimage*, *61*(2), 407–426.

Fries, P, Nikolic, D., & Singer, W. (2007). The gamma cycle. *Trends Neurosci*, *30*(7), 309–316. https://doi.org/10.1016/j.tins.2007.05.005

Fries, Pascal. (2005). A mechanism for cognitive dynamics: neuronal communication through neuronal coherence. *Trends in Cognitive Sciences*, *9*(10), 474–480.

Fries, Pascal. (2009). Neuronal gamma-band synchronization as a fundamental process in cortical computation. *Annual Review of Neuroscience*, *32*, 209–224.

Fries, Pascal. (2015). Rhythms for cognition: communication through coherence. *Neuron*, *88*(1), 220–235.

Friston, K. J. (1994). Functional and effective connectivity in neuroimaging: A synthesis. *Human Brain Mapping*. https://doi.org/10.1002/hbm.460020107

Friston, K. J. (2011). Functional and Effective Connectivity: A Review. *Brain Connectivity*. https://doi.org/10.1089/brain.2011.0008

Friston, K. J., Harrison, L., & Penny, W. (2003). Dynamic causal modelling. *Neuroimage*, *19*(4), 1273–1302.

Gaillard, R., Dehaene, S., Adam, C., Clémenceau, S., Hasboun, D., Baulac, M., … Naccache, L. (2009). Converging intracranial markers of conscious access. *PLoS Biology*, *7*(3), e1000061.

Gasser, P., Holstein, D., Michel, Y., Doblin, R., Yazar-Klosinski, B., Passie, T., & Brenneisen, R. (2014). Safety and efficacy of lysergic acid diethylamide-assisted psychotherapy for anxiety associated with life-threatening diseases. *Journal of Nervous and Mental Disease*. https://doi.org/10.1097/NMD.0000000000000113

Gazzaley, A., & Nobre, A. C. (2012). Top-down modulation: bridging selective attention and working memory. *Trends in Cognitive Sciences*, *16*(2), 129–135.

Ghosh, A., Rho, Y., McIntosh, A. R., Kötter, R., & Jirsa, V. K. (2008). Cortical network dynamics with time delays reveals functional connectivity in the resting brain. *Cognitive Neurodynamics*. https://doi.org/10.1007/s11571-008-9044-2

Ghosh, Anandamohan, Rho, Y., McIntosh, A. R., Kötter, R., & Jirsa, V. K. (2008). Noise during rest enables the exploration of the brain's dynamic repertoire. *Cognitive Neurodynamics*. https://doi.org/10.1371/journal.pcbi.1000196

Glerean, E., Salmi, J., Lahnakoski, J. M., Jääskeläinen, I. P., & Sams,

M. (2012). Functional magnetic resonance imaging phase synchronization as a measure of dynamic functional connectivity. *Brain Connectivity*, *2*(2), 91–101. https://doi.org/10.1089/brain.2011.0068

Glomb, K., Ponce-Alvarez, A., Gilson, M., Ritter, P., & Deco, G. (2017). Resting state networks in empirical and simulated dynamic functional connectivity. *NeuroImage*. https://doi.org/10.1016/j.neuroimage.2017.07.065

Godwin, D., Barry, R. L., & Marois, R. (2015). Breakdown of the brain's functional network modularity with awareness. *Proceedings of the National Academy of Sciences*, *112*(12), 3799–3804.

Golos, M., Jirsa, V., & Daucé, E. (2015). Multistability in Large Scale Models of Brain Activity. *PLoS Computational Biology*. https://doi.org/10.1371/journal.pcbi.1004644

González-Burgos, I., & Feria-Velasco, A. (2008). Serotonin/dopamine interaction in memory formation. *Progress in Brain Research*. https://doi.org/10.1016/S0079-6123(08)00928-X

Gordon, E. M., Laumann, T. O., Adeyemo, B., Huckins, J. F., Kelley, W. M., & Petersen, S. E. (2016). Generation and Evaluation of a Cortical Area Parcellation from Resting-State Correlations. *Cerebral Cortex*. https://doi.org/10.1093/cercor/bhu239

Grasso, C., Volsi, G. L., & Barresi, M. (2016). Serotonin modifies the spontaneous spiking activity of gracile nucleus neurons in rats: Role of 5-HT1Aand 5-HT2receptors. *Archives Italiennes de Biologie*. https://doi.org/10.12871/00039829201621

Greenberg, J. A., Burke, J. F., Haque, R., Kahana, M. J., & Zaghloul, K. A. (2015). Decreases in theta and increases in high frequency activity underlie associative memory encoding. *Neuroimage*, *114*, 257–263.

Gregoriou, G. G., Gotts, S. J., Zhou, H., & Desimone, R. (2009).

High-frequency, long-range coupling between prefrontal and visual cortex during attention. *Science*, *324*(5931), 1207–1210.

Greve, D. N., & Fischl, B. (2009). Accurate and robust brain image alignment using boundary-based registration. *Neuroimage*, *48*(1), 63–72. https://doi.org/10.1016/j.neuroimage.2009.06.060

Griffiths, B., Mazaheri, A., Debener, S., & Hanslmayr, S. (2016). Brain oscillations track the formation of episodic memories in the real world. *NeuroImage*. https://doi.org/10.1016/j.neuroimage.2016.09.021

Griffiths, R. R., Johnson, M. W., Carducci, M. A., Umbricht, A., Richards, W. A., Richards, B. D., … Klinedinst, M. A. (2016). Psilocybin produces substantial and sustained decreases in depression and anxiety in patients with life-threatening cancer: A randomized double-blind trial. *Journal of Psychopharmacology*. https://doi.org/10.1177/0269881116675513

Grob, C. S., Danforth, A. L., Chopra, G. S., Hagerty, M., McKay, C. R., Halberstad, A. L., & Greer, G. R. (2011). Pilot study of psilocybin treatment for anxiety in patients with advanced-stage cancer. *Archives of General Psychiatry*. https://doi.org/10.1001/archgenpsychiatry.2010.116

Guderian, S., Schott, B. H., Richardson-Klavehn, A., & Duzel, E. (2009). Medial temporal theta state before an event predicts episodic encoding success in humans. *Proc Natl Acad Sci U S A*, *106*(13), 5365–5370. https://doi.org/10.1073/pnas.0900289106

Guthrie, D., & Buchwald, J. S. (1991). Significance testing of difference potentials. *Psychophysiology*, *28*(2), 240–244.

Haegens, S., Cousijn, H., Wallis, G., Harrison, P. J., & Nobre, A. C. (2014). Inter-and intra-individual variability in alpha peak frequency. *Neuroimage*, *92*, 46–55.

Hagmann, P, Cammoun, L., Gigandet, X., Meuli, R., Honey, C. J., Wedeen, V. J., & Sporns, O. (2008). Mapping the structural core of human cerebral cortex. *PLoS Biol*, *6*(7), e159. https://doi.org/10.1371/journal.pbio.0060159

Hagmann, Patric. (2005). *From diffusion MRI to brain connectomics*. EPFL.

Haimovici, A., Tagliazucchi, E., Balenzuela, P., & Chialvo, D. R. (2013). Brain organization into resting state networks emerges at criticality on a model of the human connectome. *Physical Review Letters*, *110*(17), 178101. https://doi.org/10.1103/PhysRevLett.110.178101

Haken, H. (1975). Cooperative phenomena in systems far from thermal equilibrium and in nonphysical systems. *Reviews of Modern Physics*. https://doi.org/10.1103/RevModPhys.47.67

Halberstadt, A. L. (2015). Recent advances in the neuropsychopharmacology of serotonergic hallucinogens. *Behavioural Brain Research*. https://doi.org/10.1016/j.bbr.2014.07.016

Hamamé, C. M., Alario, F.-X., Llorens, A., Liégeois-Chauvel, C., & Trébuchon-Da Fonseca, A. (2014). High frequency gamma activity in the left hippocampus predicts visual object naming performance. *Brain and Language*, *135*, 104–114.

Hansen, E. C. A. A., Battaglia, D., Spiegler, A., Deco, G., & Jirsa, V. K. (2015). Functional connectivity dynamics: Modeling the switching behavior of the resting state. *NeuroImage*, *105*, 525–535. https://doi.org/10.1016/j.neuroimage.2014.11.001

Hanslmayr, S., Staresina, B. P., & Bowman, H. (2016). Oscillations and episodic memory: addressing the synchronization/desynchronization conundrum. *Trends in Neurosciences*, *39*(1), 16–25.

Hanslmayr, S., & Staudigl, T. (2014). How brain oscillations form memories—a processing based perspective on oscillatory

subsequent memory effects. *Neuroimage*, *85*, 648–655.

Hanslmayr, S., Volberg, G., Wimber, M., Raabe, M., Greenlee, M. W., & Bäuml, K. H. T. (2011). The relationship between brain oscillations and BOLD signal during memory formation: A combined EEG-fMRI study. *Journal of Neuroscience*. https://doi.org/10.1523/JNEUROSCI.3140-11.2011

Haque, R. U., Wittig Jr., J. H., Damera, S. R., Inati, S. K., & Zaghloul, K. A. (2015). Cortical Low-Frequency Power and Progressive Phase Synchrony Precede Successful Memory Encoding. *J Neurosci*, *35*(40), 13577–13586. https://doi.org/10.1523/JNEUROSCI.0687-15.2015

Hasselmo, M. E. (2005). What is the function of hippocampal theta rhythm? - Linking bahavioral data to phasic properties of field potential and unit recording data. *Hippocampus*. https://doi.org/10.1002/hipo.20116

Hasselmo, M. E., Bodelón, C., & Wyble, B. P. (2002). A proposed function for hippocampal theta rhythm: Separate phases of encoding and retrieval enhance reversal of prior learning. *Neural Computation*. https://doi.org/10.1162/089976602317318965

Hebb, D. O. (1949). *The Organization of Behavior, McGill University*. John Wiley & Sons, New York, USA.

Herweg, N. A., Apitz, T., Leicht, G., Mulert, C., Fuentemilla, L., & Bunzeck, N. (2016). Theta-alpha oscillations bind the hippocampus, prefrontal cortex, and striatum during recollection: Evidence from simultaneous EEG–fMRI. *Journal of Neuroscience*. https://doi.org/10.1523/JNEUROSCI.3629-15.2016

Herweg, N. A., Solomon, E. A., & Kahana, M. J. (2020). Theta Oscillations in Human Memory. *Trends in Cognitive Sciences*.

Hindriks, R., van Putten, M. J. A. M., & Deco, G. (2014). Intra-cortical propagation of EEG alpha oscillations. *NeuroImage*.

https://doi.org/10.1016/j.neuroimage.2014.08.027

Hollister, L. E., & Hartman, A. M. (1962). Mescaline, lysergic acid diethylamide and psilocybin: Comparison of clinical syndromes, effects on color perception and biochemical measures. *Comprehensive Psychiatry*. https://doi.org/10.1016/S0010-440X(62)80024-8

Hollister, L. E., & Sjoberg, B. M. (1964). Clinical syndromes and biochemical alterations following mescaline, lysergic acid diethylamide, psilocybin and a combination of the three psychotomimetic drugs. *Comprehensive Psychiatry*. https://doi.org/10.1016/S0010-440X(64)80030-4

Holtzheimer, P. E., & Mayberg, H. S. (2011). Stuck in a rut: Rethinking depression and its treatment. *Trends in Neurosciences*. https://doi.org/10.1016/j.tins.2010.10.004

Honey, C. J., Sporns, O., Cammoun, L., Gigandet, X., Thiran, J. P., Meuli, R., & Hagmann, P. (2009). Predicting human resting-state functional connectivity from structural connectivity. *Proceedings of the National Academy of Sciences of the United States of America*. https://doi.org/10.1073/pnas.0811168106

Honey, Christopher J., Kötter, R., Breakspear, M., & Sporns, O. (2007). Network structure of cerebral cortex shapes functional connectivity on multiple time scales. *Proceedings of the National Academy of Sciences of the United States of America*. https://doi.org/10.1073/pnas.0701519104

Howard, M. W., Rizzuto, D. S., Caplan, J. B., Madsen, J. R., Lisman, J., Aschenbrenner-Scheibe, R., … Kahana, M. J. (2003). Gamma oscillations correlate with working memory load in humans. *Cereb Cortex*, *13*(12), 1369–1374. Retrieved from https://www.ncbi.nlm.nih.gov/pubmed/14615302

Huerta, P. T., & Lisman, J. E. (1995). Bidirectional synaptic plasticity induced by a single burst during cholinergic theta oscillation in CA1 in vitro. *Neuron*. https://doi.org/10.1016/0896-6273(95)90094-2

Hurlstone, M. J., Hitch, G. J., & Baddeley, A. D. (2014). Memory for serial order across domains: An overview of the literature and directions for future research. *Psychological Bulletin*, *140*(2), 339.

Hutchison, R. M., Womelsdorf, T., Allen, E. A., Bandettini, P. A., Calhoun, V. D., Corbetta, M., … Chang, C. (2013). Dynamic functional connectivity: Promise, issues, and interpretations. *NeuroImage*. https://doi.org/10.1016/j.neuroimage.2013.05.079

Hyman, J. M., Wyble, B. P., Goyal, V., Rossi, C. A., & Hasselmo, M. E. (2003). Stimulation in Hippocampal Region CA1 in Behaving Rats Yields Long-Term Potentiation when Delivered to the Peak of Theta and Long-Term Depression when Delivered to the Trough. *Journal of Neuroscience*. https://doi.org/10.1523/jneurosci.23-37-11725.2003

Jacobs, B. L., & Azmitia, E. C. (1992). Structure and function of the brain serotonin system. *Physiological Reviews*. https://doi.org/10.1152/physrev.1992.72.1.165

Jenkinson, M., Bannister, P., Brady, M., & Smith, S. (2002). Improved optimization for the robust and accurate linear registration and motion correction of brain images. *Neuroimage*, *17*(2), 825–841. https://doi.org/10.1016/S1053-8119(02)91132-8

Jensen, O., Gelfand, J., Kounios, J., & Lisman, J. E. (2002). Oscillations in the alpha band (9–12 Hz) increase with memory load during retention in a short-term memory task. *Cerebral Cortex*, *12*(8), 877–882.

Jerbi, K., Ossandón, T., Hamame, C. M., Senova, S., Dalal, S. S., Jung, J., … Kahane, P. (2009). Task-related gamma-band dynamics from an intracerebral perspective: Review and implications for surface EEG and MEG. *Human Brain Mapping*, *30*(6), 1758–1771.

Johnson, M. W., Garcia-Romeu, A., Cosimano, M. P., & Griffiths, R. R. (2014). Pilot study of the 5-HT2AR agonist psilocybin in

the treatment of tobacco addiction. *Journal of Psychopharmacology*. https://doi.org/10.1177/0269881114548296

Jones, M. W., & Wilson, M. A. (2005). Theta rhythms coordinate hippocampal–prefrontal interactions in a spatial memory task. *PLoS Biology*, *3*(12), e402.

Jovicich, J., Czanner, S., Greve, D., Haley, E., Van Der Kouwe, A., Gollub, R., … Dale, A. (2006). Reliability in multi-site structural MRI studies: effects of gradient non-linearity correction on phantom and human data. *Neuroimage*, *30*(2), 436–443. https://doi.org/10.1016/j.neuroimage.2005.09.046

Jutras, M. J., Fries, P., & Buffalo, E. A. (2009). Gamma-band synchronization in the macaque hippocampus and memory formation. *Journal of Neuroscience*, *29*(40), 12521–12531.

Kaelen, M., Barrett, F. S., Roseman, L., Lorenz, R., Family, N., Bolstridge, M., … Carhart-Harris, R. L. (2015). LSD enhances the emotional response to music. *Psychopharmacology*. https://doi.org/10.1007/s00213-015-4014-y

Kaelen, Mendel, Lorenz, R., Barrett, F. S., Roseman, L., Orban, C., Santos-Ribeiro, A., … Muthukumaraswamy, S. (2017). Effects of LSD on music-evoked brain activity. *BioRxiv*.

Kahana, Michael J. (2006). The cognitive correlates of human brain oscillations. *Journal of Neuroscience*, *26*(6), 1669–1672.

Kahana, Michael Jacob. (2012). *Foundations of human memory*. OUP USA.

Kapur, S., Phillips, A. G., & Insel, T. R. (2012). Why has it taken so long for biological psychiatry to develop clinical tests and what to do about it. *Molecular Psychiatry*. https://doi.org/10.1038/mp.2012.105

Khader, P. H., Jost, K., Ranganath, C., & Rösler, F. (2010). Theta and alpha oscillations during working-memory maintenance

predict successful long-term memory encoding. *Neuroscience Letters*, *468*(3), 339–343.

Kim, H. (2011). Neural activity that predicts subsequent memory and forgetting: a meta-analysis of 74 fMRI studies. *Neuroimage*, *54*(3), 2446–2461.

King, M. V., Marsden, C. A., & Fone, K. C. F. (2008). A role for the 5-HT1A, 5-HT4 and 5-HT6 receptors in learning and memory. *Trends in Pharmacological Sciences*. https://doi.org/10.1016/j.tips.2008.07.001

Kingyon, J., Behroozmand, R., Kelley, R., Oya, H., Kawasaki, H., Narayanan, N. S., & Greenlee, J. D. W. (2015). High-gamma band fronto-temporal coherence as a measure of functional connectivity in speech motor control. *Neuroscience*, *305*, 15–25.

Kinnison, J., Padmala, S., Choi, J.-M., & Pessoa, L. (2012). Network analysis reveals increased integration during emotional and motivational processing. *Journal of Neuroscience*, *32*(24), 8361–8372.

Kirchhoff, B. A., Wagner, A. D., Maril, A., & Stern, C. E. (2000). Prefrontal–temporal circuitry for episodic encoding and subsequent memory. *Journal of Neuroscience*, *20*(16), 6173–6180.

Kirsch, I., Deacon, B. J., Huedo-Medina, T. B., Scoboria, A., Moore, T. J., & Johnson, B. T. (2008). Initial severity and antidepressant benefits: A meta-analysis of data submitted to the food and drug administration. *PLoS Medicine*. https://doi.org/10.1371/journal.pmed.0050045

Kitzbichler, M. G., Henson, R. N. A., Smith, M. L., Nathan, P. J., & Bullmore, E. T. (2011). Cognitive effort drives workspace configuration of human brain functional networks. *Journal of Neuroscience*, *31*(22), 8259–8270.

Kleiner, M., Brainard, D., Pelli, D., Ingling, A., Murray, R., &

Broussard, C. (2007). What's new in Psychtoolbox-3. *Perception*, *36*(14), 1.

Klimesch, W., Doppelmayr, M., Pachinger, T., & Ripper, B. (1997). Brain oscillations and human memory: EEG correlates in the upper alpha and theta band. *Neuroscience Letters*. https://doi.org/10.1016/S0304-3940(97)00771-4

Klimesch, W., Doppelmayr, M., Röhm, D., Pöllhuber, D., & Stadler, W. (2000). Simultaneous desynchronization and synchronization of different alpha responses in the human electroencephalograph: A neglected paradox? *Neuroscience Letters*. https://doi.org/10.1016/S0304-3940(00)00985-X

Klimesch, W, & Doppelmayr, M. (1996). Theta band power in the human scalp EEG and the encoding of new information. *Neuroreport*, *7*, 1235–1240.

Klimesch, W, Sauseng, P., & Hanslmayr, S. (2007). EEG alpha oscillations: the inhibition-timing hypothesis. *Brain Res Rev*, *53*(1), 63–88. https://doi.org/10.1016/j.brainresrev.2006.06.003

Klimesch, Wolfgang. (1999). EEG alpha and theta oscillations reflect cognitive and memory performance: a review and analysis. *Brain Research Reviews*, *29*(2–3), 169–195.

Klimesch, Wolfgang, Freunberger, R., Sauseng, P., & Gruber, W. (2008). A short review of slow phase synchronization and memory: Evidence for control processes in different memory systems? *Brain Research*. https://doi.org/10.1016/j.brainres.2008.06.049

Knudsen, G. M., Jensen, P. S., Erritzoe, D., Baaré, W. F. C., Ettrup, A., Fisher, P. M., … Hasselbalch, S. G. (2016). The center for integrated molecular brain imaging (Cimbi) database. *Neuroimage*, *124*, 1213–1219.

Koch, K. W., & Fuster, J. M. (1989). Unit activity in monkey parietal cortex related to haptic perception and temporary memory. *Experimental Brain Research*, *76*(2), 292–306.

https://doi.org/10.1007/BF00247889

Krichmar, J. L. (2013). A neurorobotic platform to test the influence of neuromodulatory signaling on anxious and curious behavior. *Frontiers in Neurorobotics*. https://doi.org/10.3389/fnbot.2013.00001

Krienen, F. M., Thomas Yeo, B. T., & Buckner, R. L. (2014). Reconfigurable task-dependent functional coupling modes cluster around a core functional architecture. *Philosophical Transactions of the Royal Society B: Biological Sciences*. https://doi.org/10.1098/rstb.2013.0526

Kringelbach, M. L., McIntosh, A. R., Ritter, P., Jirsa, V. K., & Deco, G. (2015). The rediscovery of slowness: exploring the timing of cognition. *Trends in Cognitive Sciences*, *19*(10), 616–628.

Kucewicz, M. T., Cimbalnik, J., Matsumoto, J. Y., Brinkmann, B. H., Bower, M. R., Vasoli, V., … Stead, S. M. (2014). High frequency oscillations are associated with cognitive processing in human recognition memory. *Brain*, *137*(8), 2231–2244.

Lachaux, J. Ph, Rudrauf, D., & Kahane, P. (2003). Intracranial EEG and human brain mapping. *Journal of Physiology-Paris*, *97*(4–6), 613–628. https://doi.org/10.1016/j.jphysparis.2004.01.018

Lachaux, J P, Rodriguez, E., Martinerie, J., & Varela, F. J. (1999). Measuring phase synchrony in brain signals. *Hum Brain Mapp*, *8*(4), 194–208. Retrieved from https://www.ncbi.nlm.nih.gov/pubmed/10619414

Lachaux, Jean Philippe, Axmacher, N., Mormann, F., Halgren, E., & Crone, N. E. (2012). High-frequency neural activity and human cognition: Past, present and possible future of intracranial EEG research. *Progress in Neurobiology*. https://doi.org/10.1016/j.pneurobio.2012.06.008

Lakatos, P., O'Connell, M. N., Barczak, A., Mills, A., Javitt, D. C., & Schroeder, C. E. (2009). The leading sense: supramodal control of neurophysiological context by attention. *Neuron*,

64(3), 419–430. https://doi.org/10.1016/j.neuron.2009.10.014

Lakatos, P., Shah, A. S., Knuth, K. H., Ulbert, I., Karmos, G., & Schroeder, C. E. (2005). An oscillatory hierarchy controlling neuronal excitability and stimulus processing in the auditory cortex. *J Neurophysiol*, *94*(3), 1904–1911. https://doi.org/10.1152/jn.00263.2005

Landén, M., & Thase, M. E. (2006). A model to explain the therapeutic effects of serotonin reuptake inhibitors: the role of 5-HT2 receptors. *Psychopharmacology Bulletin*.

Lega, B. C., Jacobs, J., & Kahana, M. (2012). Human hippocampal theta oscillations and the formation of episodic memories. *Hippocampus*, *22*(4), 748–761.

Lewis, D. E., Pearson, J., & Khuu, S. K. (2013). The color "fruit": object memories defined by color. *PloS One*, *8*(5), e64960.

Liang, X., Zou, Q., He, Y., & Yang, Y. (2015). Topologically reorganized connectivity architecture of default-mode, executive-control, and salience networks across working memory task loads. *Cerebral Cortex*, *26*(4), 1501–1511. https://doi.org/10.1093/cercor/bhu316

Licata, F., Li Volsi, G., Maugeri, G., Ciranna, L., & Santangelo, F. (1993). Serotonin-evoked modifications of the neuronal firing rate in the superior vestibular nucleus: A microiontophoretic study in the rat. *Neuroscience*. https://doi.org/10.1016/0306-4522(93)90541-M

Licata, Flora, Li Volsi, G., Maugeri, G., & Santangelo, F. (1995). Neuronal responses to 5-hydroxytryptamine in the red nucleus of rats. *Experimental Brain Research*. https://doi.org/10.1007/BF00230043

Licata, Flora, Volsi, G. L., Maugeri, G., & Santangelo, F. (1993). Excitatory and inhibitory effects of 5-hydroxytryptamine on the firing rate of medial vestibular nucleus neurons in the rat. *Neuroscience Letters*. https://doi.org/10.1016/0304-

3940(93)90205-Y

Long, N. M., Burke, J. F., & Kahana, M. J. (2014). Subsequent memory effect in intracranial and scalp EEG. *Neuroimage*, *84*, 488–494. https://doi.org/10.1016/j.neuroimage.2013.08.052

Lord, L. D., Expert, P., Atasoy, S., Roseman, L., Rapuano, K., Lambiotte, R., … Cabral, J. (2019). Dynamical exploration of the repertoire of brain networks at rest is modulated by psilocybin. *NeuroImage*. https://doi.org/10.1016/j.neuroimage.2019.05.060

Lord, L. D., Stevner, A. B., Deco, G., & Kringelbach, M. L. (2017). Understanding principles of integration and segregation using whole-brain computational connectomics: Implications for neuropsychiatric disorders. *Philosophical Transactions of the Royal Society A: Mathematical, Physical and Engineering Sciences*. https://doi.org/10.1098/rsta.2016.0283

MacKay, W. A. (1997). Synchronized neuronal oscillations and their role in motor processes. *Trends in Cognitive Sciences*. https://doi.org/10.1016/S1364-6613(97)01059-0

Marder, E. (2012). Neuromodulation of Neuronal Circuits: Back to the Future. *Neuron*. https://doi.org/10.1016/j.neuron.2012.09.010

Marinazzo, D., Pellicoro, M., Wu, G., Angelini, L., Cortés, J. M., & Stramaglia, S. (2014). Information transfer and criticality in the ising model on the human connectome. *PLoS ONE*. https://doi.org/10.1371/journal.pone.0093616

Mathewson, K. E., Gratton, G., Fabiani, M., Beck, D. M., & Ro, T. (2009). To see or not to see: prestimulus alpha phase predicts visual awareness. *J Neurosci*, *29*(9), 2725–2732. https://doi.org/10.1523/JNEUROSCI.3963-08.2009

Mazaheri, A., Nieuwenhuis, I. L. C., Van Dijk, H., & Jensen, O. (2009). Prestimulus alpha and mu activity predicts failure to inhibit motor responses. *Human Brain Mapping*, *30*(6), 1791–

1800.

McIntosh, A. R. (2000). Towards a network theory of cognition. *Neural Networks*. https://doi.org/10.1016/S0893-6080(00)00059-9

Mennes, M., Kelly, C., Colcombe, S., Xavier Castellanos, F., & Milham, M. P. (2013). The extrinsic and intrinsic functional architectures of the human brain are not equivalent. *Cerebral Cortex*. https://doi.org/10.1093/cercor/bhs010

Mercier, M. R., Molholm, S., Fiebelkorn, I. C., Butler, J. S., Schwartz, T. H., & Foxe, J. J. (2015). Neuro-oscillatory phase alignment drives speeded multisensory response times: an electro-corticographic investigation. *J Neurosci*, *35*(22), 8546–8557. https://doi.org/10.1523/JNEUROSCI.4527-14.2015

Merkow, M. B., Burke, J. F., Stein, J. M., & Kahana, M. J. (2014). Prestimulus theta in the human hippocampus predicts subsequent recognition but not recall. *Hippocampus*, *24*(12), 1562–1569. https://doi.org/10.1002/hipo.22335

Mesulam, M. -M. (1990). Large-scale neurocognitive networks and distributed processing for attention, language, and memory. *Annals of Neurology*. https://doi.org/10.1002/ana.410280502

Michelmann, S., Bowman, H., & Hanslmayr, S. (2018). Replay of stimulus-specific temporal patterns during associative memory formation. *Journal of Cognitive Neuroscience*. https://doi.org/10.1162/jocn_a_01304

Mizuhara, H., & Yamaguchi, Y. (2007). Human cortical circuits for central executive function emerge by theta phase synchronization. *NeuroImage*. https://doi.org/10.1016/j.neuroimage.2007.02.026

Moran, R. J., Campo, P., Symmonds, M., Stephan, K. E., Dolan, R. J., & Friston, K. J. (2013). Free energy, precision and learning: The role of cholinergic neuromodulation. *Journal of Neuroscience*. https://doi.org/10.1523/JNEUROSCI.4255-

12.2013

Moratti, S., Clementz, B. A., Gao, Y., Ortiz, T., & Keil, A. (2007). Neural mechanisms of evoked oscillations: stability and interaction with transient events. *Human Brain Mapping*, *28*(12), 1318–1333.

Moreno, F. A., Wiegand, C. B., Taitano, E. K., & Delgado, P. L. (2006). Safety, tolerability, and efficacy of psilocybin in 9 patients with obsessive-compulsive disorder. *Journal of Clinical Psychiatry*. https://doi.org/10.4088/JCP.v67n1110

Mormann, F., Lehnertz, K., David, P., & E. Elger, C. (2000). Mean phase coherence as a measure for phase synchronization and its application to the EEG of epilepsy patients. *Physica D: Nonlinear Phenomena*. https://doi.org/10.1016/S0167-2789(00)00087-7

Mountcastle, V. (1978). An organizing principle for cerebral function: the unit model and the distributed system. *The Mindful Brain*.

Müller, F., Lenz, C., Dolder, P., Lang, U., Schmidt, A., Liechti, M., & Borgwardt, S. (2017). Increased thalamic resting-state connectivity as a core driver of LSD-induced hallucinations. *Acta Psychiatrica Scandinavica*. https://doi.org/10.1111/acps.12818

Müller, Felix, Dolder, P. C., Schmidt, A., Liechti, M. E., & Borgwardt, S. (2018). Altered network hub connectivity after acute LSD administration. *NeuroImage: Clinical*. https://doi.org/10.1016/j.nicl.2018.03.005

Murdock Jr, B. B. (1962). The serial position effect of free recall. *Journal of Experimental Psychology*, *64*(5), 482.

Murray, R. J., Brosch, T., & Sander, D. (2014). The functional profile of the human amygdala in affective processing: Insights from intracranial recordings. *Cortex*. https://doi.org/10.1016/j.cortex.2014.06.010

Müsch, K., Hamamé, C. M., Perrone-Bertolotti, M., Minotti, L., Kahane, P., Engel, A. K., … Schneider, T. R. (2014). Selective attention modulates high-frequency activity in the face-processing network. *Cortex*. https://doi.org/10.1016/j.cortex.2014.06.006

Naish, K. R., Vedelago, L., MacKillop, J., & Amlung, M. (2018). Effects of neuromodulation on cognitive performance in individuals exhibiting addictive behaviors: A systematic review. *Drug and Alcohol Dependence*. https://doi.org/10.1016/j.drugalcdep.2018.08.018

Nakagawa, T. T., Jirsa, V. K., Spiegler, A., McIntosh, A. R., & Deco, G. (2013). Bottom up modeling of the connectome: Linking structure and function in the resting brain and their changes in aging. *NeuroImage*. https://doi.org/10.1016/j.neuroimage.2013.04.055

Nenert, R., Viswanathan, S., Dubuc, D. M., & Visscher, K. M. (2012). Modulations of ongoing alpha oscillations predict successful short-term visual memory encoding. *Frontiers in Human Neuroscience*, *6*, 127.

Newman, M. E. J. (2006). Modularit and community structure in networks. *Proceedings of the National Academy of Sciences*.

Nichols, D E. (2016). Psychedelics. *Pharmacol Rev*, *68*(2), 264–355. https://doi.org/10.1124/pr.115.011478

Nichols, David E. (2018). Chemistry and structure–Activity relationships of psychedelics. In *Current Topics in Behavioral Neurosciences*. https://doi.org/10.1007/7854_2017_475

Nir, Y., Mukamel, R., Dinstein, I., Privman, E., Harel, M., Fisch, L., … Malach, R. (2008). Interhemispheric correlations of slow spontaneous neuronal fluctuations revealed in human sensory cortex. *Nature Neuroscience*. https://doi.org/10.1038/nn.2177

O'Connell, R. G., Dockree, P. M., Robertson, I. H., Bellgrove, M. A., Foxe, J. J., & Kelly, S. P. (2009). Uncovering the neural

signature of lapsing attention: electrophysiological signals predict errors up to 20 s before they occur. *Journal of Neuroscience*, *29*(26), 8604–8611.

Olesen, O. V., Sibomana, M., Keller, S. H., Andersen, F., Jensen, J., Holm, S., … Højgaard, L. (2009). Spatial resolution of the HRRT PET scanner using 3D-OSEM PSF reconstruction. *Nuclear Science Symposium Conference Record (NSS/MIC), 2009 IEEE*, 3789–3790. https://doi.org/10.1109/NSSMIC.2009.5401892

Oostenveld, R., Fries, P., Maris, E., & Schoffelen, J. M. (2011). FieldTrip: Open source software for advanced analysis of MEG, EEG, and invasive electrophysiological data. *Comput Intell Neurosci*, *2011*, 156869. https://doi.org/10.1155/2011/156869

Osipova, D., Takashima, A., Oostenveld, R., Fernandez, G., Maris, E., & Jensen, O. (2006). Theta and gamma oscillations predict encoding and retrieval of declarative memory. *J Neurosci*, *26*(28), 7523–7531. https://doi.org/10.1523/JNEUROSCI.1948-06.2006

Ossandón, T., Vidal, J. R., Ciumas, C., Jerbi, K., Hamamé, C. M., Dalal, S. S., … Lachaux, J. P. (2012). Efficient "pop-out" visual search elicits sustained broadband gamma activity in the dorsal attention network. *Journal of Neuroscience*. https://doi.org/10.1523/JNEUROSCI.6048-11.2012

Otten, L. J., Quayle, A. H., Akram, S., Ditewig, T. A., & Rugg, M. D. (2006). Brain activity before an event predicts later recollection. *Nature Neuroscience*, *9*(4), 489.

Otten, L. J., Quayle, A. H., & Puvaneswaran, B. (2010). Prestimulus subsequent memory effects for auditory and visual events. *Journal of Cognitive Neuroscience*, *22*(6), 1212–1223.

Paller, K. A., Kutas, M., & Mayes, A. R. (1987). Neural correlates of encoding in an incidental learning paradigm. *Electroencephalography and Clinical Neurophysiology*, *67*(4), 360–371.

Paller, K. A., & Wagner, A. D. (2002). Observing the transformation of experience into memory. *Trends in Cognitive Sciences*, *6*(2), 93–102. https://doi.org/10.1016/S1364-6613(00)01845-3

Palva, S, & Palva, J. M. (2007). New vistas for alpha-frequency band oscillations. *Trends Neurosci*, *30*(4), 150–158. https://doi.org/10.1016/j.tins.2007.02.001

Palva, Satu, Monto, S., & Palva, J. M. (2010). Graph properties of synchronized cortical networks during visual working memory maintenance. *NeuroImage*. https://doi.org/10.1016/j.neuroimage.2009.11.031

Park, H. J., & Friston, K. (2013). Structural and functional brain networks: From connections to cognition. *Science*. https://doi.org/10.1126/science.1238411

Park, H., & Rugg, M. D. (2010). Prestimulus hippocampal activity predicts later recollection. *Hippocampus*, *20*(1), 24–28.

Park, H., & Rugg, M. D. (2011). Neural correlates of encoding within- and across-domain inter-item associations. *Journal of Cognitive Neuroscience*. https://doi.org/10.1162/jocn.2011.21611

Pavlides, C., Greenstein, Y. J., Grudman, M., & Winson, J. (1988). Long-term potentiation in the dentate gyrus is induced preferentially on the positive phase of θ-rhythm. *Brain Research*. https://doi.org/10.1016/0006-8993(88)91499-0

Perez, O., Mukamel, R., Tankus, A., Rosenblatt, J. D., Yeshurun, Y., & Fried, I. (2015). Preconscious prediction of a driver's decision using intracranial recordings. *Journal of Cognitive Neuroscience*. https://doi.org/10.1162/jocn_a_00799

Petersen, S. E., & Sporns, O. (2015). Brain Networks and Cognitive Architectures. *Neuron*. https://doi.org/10.1016/j.neuron.2015.09.027

Pillai, A. S., & Jirsa, V. K. (2017). Symmetry Breaking in Space-

Time Hierarchies Shapes Brain Dynamics and Behavior. *Neuron*. https://doi.org/10.1016/j.neuron.2017.05.013

Poldrack, R. A., & Yarkoni, T. (2016). From Brain Maps to Cognitive Ontologies: Informatics and the Search for Mental Structure. *Annual Review of Psychology*. https://doi.org/10.1146/annurev-psych-122414-033729

Ponce-Alvarez, A., Deco, G., Hagmann, P., Romani, G. L. L., Mantini, D., & Corbetta, M. (2015). Resting-State Temporal Synchronization Networks Emerge from Connectivity Topology and Heterogeneity. *PLoS Computational Biology*. https://doi.org/10.1371/journal.pcbi.1004100

Postelnicu, G., Zollei, L., & Fischl, B. (2009). Combined volumetric and surface registration. *IEEE Transactions on Medical Imaging*, *28*(4), 508–522. https://doi.org/10.1109/TMI.2008.2004426

Power, J. D., Cohen, A. L., Nelson, S. M., Wig, G. S., Barnes, K. A., Church, J. A., … Petersen, S. E. (2011). Functional network organization of the human brain. *Neuron*, *72*(4), 665–678. https://doi.org/10.1016/j.neuron.2011.09.006

Preller, K. H., Burt, J. B., Ji, J. L., Schleifer, C. H., Adkinson, B. D., Stämpfli, P., … Anticevic, A. (2018). Changes in global and thalamic brain connectivity in LSD-induced altered states of consciousness are attributable to the 5-HT2A receptor. *ELife*. https://doi.org/10.7554/eLife.35082

Preller, K. H., Herdener, M., Pokorny, T., Planzer, A., Kraehenmann, R., Stämpfli, P., … Vollenweider, F. X. (2017). The Fabric of Meaning and Subjective Effects in LSD-Induced States Depend on Serotonin 2A Receptor Activation. *Current Biology*. https://doi.org/10.1016/j.cub.2016.12.030

Price, C. J. (2000). The anatomy of language: Contributions from functional neuroimaging. *Journal of Anatomy*. https://doi.org/10.1017/S0021878299006901

Puig, M. V., Gulledge, A. T., Lambe, E. K., & Gonzalez-Burgos, G. (2015). Editorial: Neuromodulation of executive circuits. *Frontiers in Neural Circuits*. https://doi.org/10.3389/fncir.2015.00058

Raichle, M. E., MacLeod, A. M., Snyder, A. Z., Powers, W. J., Gusnard, D. A., & Shulman, G. L. (2001). A default mode of brain function. *Proceedings of the National Academy of Sciences of the United States of America*. https://doi.org/10.1073/pnas.98.2.676

Razi, A., Seghier, M. L., Zhou, Y., McColgan, P., Zeidman, P., Park, H. J., … Friston, K. J. (2017). Large-scale DCMs for resting-state fMRI. *Network Neuroscience*. https://doi.org/10.1162/netn_a_00015

Remington, G. (2008). Alterations of dopamine and serotonin transmission in schizophrenia. *Progress in Brain Research*. https://doi.org/10.1016/S0079-6123(08)00906-0

Rizzuto, D. S., Madsen, J. R., Bromfield, E. B., Schulze-Bonhage, A., Seelig, D., Aschenbrenner-Scheibe, R., & Kahana, M. J. (2003). Reset of human neocortical oscillations during a working memory task. *Proc Natl Acad Sci U S A*, *100*(13), 7931–7936. https://doi.org/10.1073/pnas.0732061100

Robbins, T. W., & Arnsten, A. F. T. (2009). The Neuropsychopharmacology of Fronto-Executive Function: Monoaminergic Modulation. *Annual Review of Neuroscience*. https://doi.org/10.1146/annurev.neuro.051508.135535

Roelfsema, P. R., Engel, A. K., König, P., & Singer, W. (1997). Visuomotor integration is associated with zero time-lag synchronization among cortical areas. *Nature*. https://doi.org/10.1038/385157a0

Roseman, L., Leech, R., Feilding, A., Nutt, D. J., & Carhart-Harris, R. L. (2014). The effects of psilocybin and MDMA on between-network resting state functional connectivity in healthy volunteers. *Frontiers in Human Neuroscience*.

https://doi.org/10.3389/fnhum.2014.00204

Ross, S., Bossis, A., Guss, J., Agin-Liebes, G., Malone, T., Cohen, B., … Schmidt, B. L. (2016). Rapid and sustained symptom reduction following psilocybin treatment for anxiety and depression in patients with life-threatening cancer: A randomized controlled trial. *Journal of Psychopharmacology*. https://doi.org/10.1177/0269881116675512

Rubinov, M., & Sporns, O. (2011). Weight-conserving characterization of complex functional brain networks. *NeuroImage*. https://doi.org/10.1016/j.neuroimage.2011.03.069

Rucker, J. J. H., Iliff, J., & Nutt, D. J. (2018). Psychiatry & the psychedelic drugs. Past, present & future. *Neuropharmacology*. https://doi.org/10.1016/j.neuropharm.2017.12.040

Rutishauser, U., Ross, I. B., Mamelak, A. N., & Schuman, E. M. (2010). Human memory strength is predicted by theta-frequency phase-locking of single neurons. *Nature*, *464*(7290), 903.

Ruzzoli, M., Torralba, M., Fernández, L. M., & Soto-Faraco, S. (2019). The relevance of alpha phase in human perception. *Cortex*.

Sahin, N. T., Pinker, S., Cash, S. S., Schomer, D., & Halgren, E. (2009). Sequential processing of lexical, grammatical, and phonological information within broca's area. *Science*. https://doi.org/10.1126/science.1174481

Sanz-Leon, P., Knock, S. A., Spiegler, A., & Jirsa, V. K. (2015). Mathematical framework for large-scale brain network modeling in The Virtual Brain. *NeuroImage*. https://doi.org/10.1016/j.neuroimage.2015.01.002

Sato, N., & Yamaguchi, Y. (2007). Theta synchronization networks emerge during human object-place memory encoding. *NeuroReport*. https://doi.org/10.1097/WNR.0b013e3280586760

Sauseng, P., Hoppe, J., Klimesch, W., Gerloff, C., & Hummel, F. C. (2007). Dissociation of sustained attention from central executive functions: Local activity and interregional connectivity in the theta range. *European Journal of Neuroscience*. https://doi.org/10.1111/j.1460-9568.2006.05286.x

Sauseng, Paul, Klimesch, W., Doppelmayr, M., Hanslmayr, S., Schabus, M., & Gruber, W. R. (2004). Theta coupling in the human electroencephalogram during a working memory task. *Neuroscience Letters*. https://doi.org/10.1016/j.neulet.2003.10.002

Schack, B., Vath, N., Petsche, H., Geissler, H. G., & Möller, E. (2002). Phase-coupling of theta-gamma EEG rhythms during short-term memory processing. *International Journal of Psychophysiology*. https://doi.org/10.1016/S0167-8760(01)00199-4

Schultz, W. (1997). Dopamine neurons and their role in reward mechanisms. *Current Opinion in Neurobiology*. https://doi.org/10.1016/S0959-4388(97)80007-4

Seager, M. A., Johnson, L. D., Chabot, E. S., Asaka, Y., & Berry, S. D. (2002). Oscillatory brain states and learning: Impact of hippocampal theta-contingent training. *Proceedings of the National Academy of Sciences of the United States of America*. https://doi.org/10.1073/pnas.032662099

Sederberg, P B, Kahana, M. J., Howard, M. W., Donner, E. J., & Madsen, J. R. (2003). Theta and gamma oscillations during encoding predict subsequent recall. *J Neurosci*, *23*(34), 10809–10814. Retrieved from https://www.ncbi.nlm.nih.gov/pubmed/14645473

Sederberg, Per B., Gauthier, L. V., Terushkin, V., Miller, J. F., Barnathan, J. A., & Kahana, M. J. (2006). Oscillatory correlates of the primacy effect in episodic memory. *NeuroImage*. https://doi.org/10.1016/j.neuroimage.2006.04.223

Sekuler, R., & Kahana, M. J. (2007). A stimulus-oriented approach to memory. *Current Directions in Psychological Science*, *16*(6), 305–310.

Serletis, D., Bulacio, J., Bingaman, W., Najm, I., & González-Martínez, J. (2014). The stereotactic approach for mapping epileptic networks: A prospective study of 200 patients. *Journal of Neurosurgery*. https://doi.org/10.3171/2014.7.JNS132306

Serretti, A., Calati, R., Mandelli, L., & De Ronchi, D. (2006). Serotonin Transporter Gene Variants and Behavior: A Comprehensive Review. *Current Drug Targets*. https://doi.org/10.2174/138945006779025419

Shadlen, M. N., & Newsome, W. T. (1998). The variable discharge of cortical neurons: implications for connectivity, computation, and information coding. *Journal of Neuroscience*, *18*(10), 3870–3896. https://doi.org/10.1523/jneurosci.18-10-03870.1998

Shatz, C. J. (1992). The developing brain. *Scientific American*. https://doi.org/10.4324/9781351035187-6

Shine, J. M., Aburn, M. J., Breakspear, M., & Poldrack, R. A. (2018). The modulation of neural gain facilitates a transition between functional segregation and integration in the brain. *ELife*. https://doi.org/10.7554/eLife.31130

Shine, J. M., Bissett, P. G., Bell, P. T., Koyejo, O., Balsters, J. H., Gorgolewski, K. J., … Poldrack, R. A. (2016). The Dynamics of Functional Brain Networks: Integrated Network States during Cognitive Task Performance. *Neuron*. https://doi.org/10.1016/j.neuron.2016.09.018

Shine, J. M., Koyejo, O., & Poldrack, R. A. (2016). Temporal metastates are associated with differential patterns of time-resolved connectivity, network topology, and attention. *Proceedings of the National Academy of Sciences of the United States of America*. https://doi.org/10.1073/pnas.1604898113

Smythies, J. (2005). Section V. Serotonin system. *International Review of Neurobiology*, *64*, 217–268.

Snodgrass, J. G., & Vanderwart, M. (1980). A standardized set of 260 pictures: Norms for name agreement, image agreement, familiarity, and visual complexity. *Journal of Experimental Psychology: Human Learning and Memory*. https://doi.org/10.1037/0278-7393.6.2.174

Softky, W. R., & Koch, C. (1993). The highly irregular firing of cortical cells is inconsistent with temporal integration of random EPSPs. *Journal of Neuroscience*, *13*(1), 334–350. https://doi.org/10.1523/jneurosci.13-01-00334.1993

Solomon, E. A., Stein, J. M., Das, S., Gorniak, R., Sperling, M. R., Worrell, G., … Kahana, M. J. (2019). Dynamic Theta Networks in the Human Medial Temporal Lobe Support Episodic Memory. *Curr Biol*, *29*(7), 1100-1111 e4. https://doi.org/10.1016/j.cub.2019.02.020

Sperling, M. R. (1997). Clinical Challenges in Invasive Monitoring in Epilepsy Surgery. *Epilepsia*. https://doi.org/10.1111/j.1528-1157.1997.tb04541.x

Sporns, O. (2010). *Networks of the Brain*. MIT Press.

Sporns, O. (2013). Network attributes for segregation and integration in the human brain. *Current Opinion in Neurobiology*. https://doi.org/10.1016/j.conb.2012.11.015

Sporns, O., & Betzel, R. F. (2016). Modular Brain Networks. *Annual Review of Psychology*. https://doi.org/10.1146/annurev-psych-122414-033634

Sporns, O., Chialvo, D. R., Kaiser, M., & Hilgetag, C. C. (2004). Organization, development and function of complex brain networks. *Trends in Cognitive Sciences*. https://doi.org/10.1016/j.tics.2004.07.008

Sporns, O., Tononi, G., & Kötter, R. (2005). The human connectome:

A structural description of the human brain. *PLoS Computational Biology*. https://doi.org/10.1371/journal.pcbi.0010042

Starcevic, V., & Brakoulias, V. (2008). Symptom subtypes of obsessive-compulsive disorder: Are they relevant for treatment? *Australian and New Zealand Journal of Psychiatry*. https://doi.org/10.1080/00048670802203442

Staudigl, T., & Hanslmayr, S. (2013). Theta oscillations at encoding mediate the context-dependent nature of human episodic memory. *Current Biology*, *23*(12), 1101–1106.

Stephan, K. E., & Friston, K. J. (2009). Functional Connectivity. In *Encyclopedia of Neuroscience*. https://doi.org/10.1016/B978-008045046-9.00308-9

Stephan, Klaas E., Bach, D. R., Fletcher, P. C., Flint, J., Frank, M. J., Friston, K. J., … Breakspear, M. (2016). Charting the landscape of priority problems in psychiatry, part 1: Classification and diagnosis. *The Lancet Psychiatry*. https://doi.org/10.1016/S2215-0366(15)00361-2

Stephan, Klaas E., Binder, E. B., Breakspear, M., Dayan, P., Johnstone, E. C., Meyer-Lindenberg, A., … Friston, K. J. (2016). Charting the landscape of priority problems in psychiatry, part 2: Pathogenesis and aetiology. *The Lancet Psychiatry*. https://doi.org/10.1016/S2215-0366(15)00360-0

Stephan, Klaas Enno, Weiskopf, N., Drysdale, P. M., Robinson, P. A., & Friston, K. J. (2007). Comparing hemodynamic models with DCM. *Neuroimage*, *38*(3), 387–401. https://doi.org/10.1016/j.neuroimage.2007.07.040

Štrac, D. Š., Pivac, N., & Mück-Šeler, D. (2016). The serotonergic system and cognitive function. *Translational Neuroscience*. https://doi.org/10.1515/tnsci-2016-0007

Strange, B. A., Otten, L. J., Josephs, O., Rugg, M. D., & Dolan, R. J. (2002). Dissociable human perirhinal, hippocampal, and

parahippocampal roles during verbal encoding. *Journal of Neuroscience*, *22*(2), 523–528.

Strunk, J., & Duarte, A. (2019). Prestimulus and poststimulus oscillatory activity predicts successful episodic encoding for both young and older adults. *Neurobiology of Aging*. https://doi.org/10.1016/j.neurobiolaging.2019.01.005

Summerfield, C., & Mangels, J. A. (2005). Coherent theta-band EEG activity predicts item-context binding during encoding. *NeuroImage*. https://doi.org/10.1016/j.neuroimage.2004.09.012

Sureau, F. C., Reader, A. J., Comtat, C., Leroy, C., Ribeiro, M.-J. J., Buvat, I. I., & Trébossen, R. (2008). Impact of image-space resolution modeling for studies with the high-resolution research tomograph. *Journal of Nuclear Medicine*, *49*(6), 1000–1008. https://doi.org/10.2967/jnumed.107.045351

Tagliazucchi, E., Roseman, L., Kaelen, M., Orban, C., Muthukumaraswamy, S. D., Murphy, K., … Carhart-Harris, R. (2016). Increased Global Functional Connectivity Correlates with LSD-Induced Ego Dissolution. *Current Biology*. https://doi.org/10.1016/j.cub.2016.02.010

Thiele, A., & Bellgrove, M. A. (2018). Neuromodulation of Attention. *Neuron*. https://doi.org/10.1016/j.neuron.2018.01.008

Thomsen, K. R., Whybrow, P. C., & Kringelbach, M. L. (2015). Reconceptualizing anhedonia: Novel perspectives on balancing the pleasure networks in the human brain. *Frontiers in Behavioral Neuroscience*. https://doi.org/10.3389/fnbeh.2015.00049

Thut, G., Nietzel, A., Brandt, S. A., & Pascual-Leone, A. (2006). α-Band electroencephalographic activity over occipital cortex indexes visuospatial attention bias and predicts visual target detection. *Journal of Neuroscience*, *26*(37), 9494–9502.

Tononi, G., Sporns, O., & Edelman, G. M. (1994). A measure for

brain complexity: relating functional segregation and integration in the nervous system. *Proceedings of the National Academy of Sciences*, *91*(11), 5033–5037. https://doi.org/10.1073/pnas.91.11.5033

Trusheim, M. R., Berndt, E. R., & Douglas, F. L. (2007). Stratified medicine: Strategic and economic implications of combining drugs and clinical biomarkers. *Nature Reviews Drug Discovery*. https://doi.org/10.1038/nrd2251

Tzourio-Mazoyer, N., Landeau, B., Papathanassiou, D., Crivello, F., Etard, O., Delcroix, N., … Joliot, M. (2002). Automated anatomical labeling of activations in SPM using a macroscopic anatomical parcellation of the MNI MRI single-subject brain. *Neuroimage*, *15*(1), 273–289. https://doi.org/10.1006/nimg.2001.0978

Valencia, M., Martinerie, J., Dupont, S., & Chavez, M. (2008). Dynamic small-world behavior in functional brain networks unveiled by an event-related networks approach. *Physical Review E - Statistical, Nonlinear, and Soft Matter Physics*. https://doi.org/10.1103/PhysRevE.77.050905

VanRullen, R., Busch, N. A., Drewes, J., & Dubois, J. (2011). Ongoing EEG phase as a trial-by-trial predictor of perceptual and attentional variability. *Frontiers in Psychology*. https://doi.org/10.3389/fpsyg.2011.00060

VanRullen, R. (2016). Perceptual Cycles. *Trends Cogn Sci*, *20*(10), 723–735. https://doi.org/10.1016/j.tics.2016.07.006

VanRullen, Rufin. (2016). How to evaluate phase differences between trial groups in ongoing electrophysiological signals. *Frontiers in Neuroscience*, *10*, 426.

Varela, F., Lachaux, J. P., Rodriguez, E., & Martinerie, J. (2001). The brainweb: Phase synchronization and large-scale integration. *Nature Reviews Neuroscience*. https://doi.org/10.1038/35067550

Vatansever, D., Menon, D. K., Manktelow, A. E., Sahakian, B. J., & Stamatakis, E. A. (2015). Default mode dynamics for global functional integration. *Journal of Neuroscience*. https://doi.org/10.1523/JNEUROSCI.2135-15.2015

Vinck, M., van Wingerden, M., Womelsdorf, T., Fries, P., & Pennartz, C. M. A. (2010). The pairwise phase consistency: a bias-free measure of rhythmic neuronal synchronization. *Neuroimage*, *51*(1), 112–122.

Wagner, A. D. (1999). Working memory contributions to human learning and remembering. *Neuron*. https://doi.org/10.1016/S0896-6273(00)80674-1

Wagner, A. D., Schacter, D. L., Rotte, M., Koutstaal, W., Maril, A., Dale, A. M., … Buckner, R. L. (1998). Building memories: remembering and forgetting of verbal experiences as predicted by brain activity. *Science*, *281*(5380), 1188–1191.

Wang, X., Zhen, Z., Song, Y., Huang, L., Kong, X., & Liu, J. (2016). The hierarchical structure of the face network revealed by its functional connectivity pattern. *Journal of Neuroscience*. https://doi.org/10.1523/JNEUROSCI.2789-15.2016

Weiss, S., & Rappelsberger, P. (2000). Long-range EEG synchronization during word encoding correlates with successful memory performance. *Cognitive Brain Research*. https://doi.org/10.1016/S0926-6410(00)00011-2

Wernicke, C. (1874). Der aphasische Symptomencomplex. Eine psychologische Studie auf anatomischer Basis. [The aphasia symptom complex. A psychological study on an anatomical basis]. In *Wernicke's work on aphasia*.

White, T. P., Jansen, M., Doege, K., Mullinger, K. J., Park, S. B., Liddle, E. B., … Liddle, P. F. (2013). Theta power during encoding predicts subsequent-memory performance and default mode network deactivation. *Hum Brain Mapp*, *34*(11), 2929–2943. https://doi.org/10.1002/hbm.22114

Wilson, M. A., & Molliver, M. E. (1991). The organization of serotonergic projections to cerebral cortex in primates: Retrograde transport studies. *Neuroscience*. https://doi.org/10.1016/0306-4522(91)90077-2

Wimber, M., Heinze, H.-J., & Richardson-Klavehn, A. (2010). Distinct frontoparietal networks set the stage for later perceptual identification priming and episodic recognition memory. *Journal of Neuroscience*, *30*(40), 13272–13280.

Winkler, A. M., Ridgway, G. R., Webster, M. A., Smith, S. M., & Nichols, T. E. (2014). Permutation inference for the general linear model. *NeuroImage*. https://doi.org/10.1016/j.neuroimage.2014.01.060

Womelsdorf, T., Fries, P., Mitra, P. P., & Desimone, R. (2006). Gamma-band synchronization in visual cortex predicts speed of change detection. *Nature*. https://doi.org/10.1038/nature04258

Wong, K.-F., & Wang, X.-J. (2006). A recurrent network mechanism of time integration in perceptual decisions. *Journal of Neuroscience*, *26*(4), 1314–1328.

Woods, R. P., Cherry, S. R., & Mazziotta, J. C. (1992). Rapid automated algorithm for aligning and reslicing PET images. *Journal of Computer Assisted Tomography*, *16*(4), 620–633. https://doi.org/10.1097/00004728-199207000-00024

Zangen, A., Nakash, R., Overstreet, D. H., & Yadid, G. (2001). Association between depressive behavior and absence of serotonin-dopamine interaction in the nucleus accumbens. *Psychopharmacology*. https://doi.org/10.1007/s002130100746

Zheng, J., Anderson, K. L., Leal, S. L., Shestyuk, A., Gulsen, G., Mnatsakanyan, L., … Lin, J. J. (2017). Amygdala-hippocampal dynamics during salient information processing. *Nature Communications*. https://doi.org/10.1038/ncomms14413